UNIVERSITY OF MISKOLC
FACULTY OF MATERIALS AND CHEMICAL ENGINEERING
ANTAL KERPELY DOCTORAL SCHOOL OF MATERIAL SCIENCE AND TECHNOLOGY
INSTITUTE OF ENERGY, CERAMICS AND POLYMER TECHNOLOGY

INVESTIGATION OF MULTI-STAGE COAL GASIFICATION FOR ENHANCED CONTROL OF SYNTHESIS GAS COMPOSITION

A PhD Dissertation

By

Thuan Duc Mai

Supervisor:

Dr. András Arnold Kállay

Head of the Doctoral School:

Prof. Dr. Valéria Mertinger

June 2023

Acknowledgement

I would first like to thank my supervisor Dr András Arnold Kállay for giving me the opportunity to work in his group and for his guidance and encouragement throughout my PhD. I will be always grateful for his support during this project and for his unique enthusiasm which has always been highly motivating.

I also express my thankful feelings to my colleagues in the Institute of Energy, Ceramics and Polymer Technology, University of Miskolc for all their support, as well as for sharing their extensive and valuable practical skills and knowledge with me.

I would also like to express my deepest appreciation to all the Antal Kerpely Doctoral School of Materials Science and Technology staff members at the University of Miskolc, for their advice, technical support, and continual assistance.

I would like to acknowledge the Hungarian government and the University of Miskolc for their financial support during the period of my PhD study.

Finally, I am forever thankful for the unconditional love and support of my wife, my son, and my family.

Table of Contents

Abbreviation

BET	Brunauer-Emmett Teller technique	
CCT	Clean coal technology	
DTG	Derivative thermogravimetry	
ECD	Electron capture detector	
LRC	Low-rank coal	
NDIR	Non-dispersive infrared sensor	
OECD	Organisation for Economic Co-operation and Development	
PID	Proportional–integral–derivative controller	
PLC	Programmable logic controller	
SNG	Synthetic natural gas	
TC	Thermocouple	
TCD	Thermal conductivity detector	
TG	Thermogravimetry	
WGS	Water gas shift reaction	
XRF	X-ray fluorescence	
CCE	Carbon conversion efficiency	%
CGE	Cold gas efficiency	%
HHV	Higher heating value	MJ/kg, MJ/Nm^3
LHV	Lower heating value	MJ/kg, MJ/Nm^3
LHV_{syngas}	Lower heating value of syngas	MJ/Nm^3
S/C	Steam per carbon ratio	mol/mol
Y	Dry syngas yield	Nm^3/kg_{coal}

1. Introduction

In 2018, the total primary energy consumption was 13864.9 million tonnes of oil equivalence (Mtoe) around the world [1]. It increased by 16.11% over ten years of the statistical period 2008-2018. In fact, the rapid development of population and urbanisation in the world leads to a high demand for global energy. In the energy scenarios to 2040 (Figure 1-1), the total energy consumption is expected to be 17983 Mtoe, which is 1.5 times as much as that in 2010 [2]. It is forecasted that energy consumption will grow up in China, India, and other Asia countries from 2020 to 2040. In comparison between the Organisation for Economic Co-operation and Development (OECD) and non-OECD countries, two-thirds of global energy will be consumed in non-OECD countries in 2040.

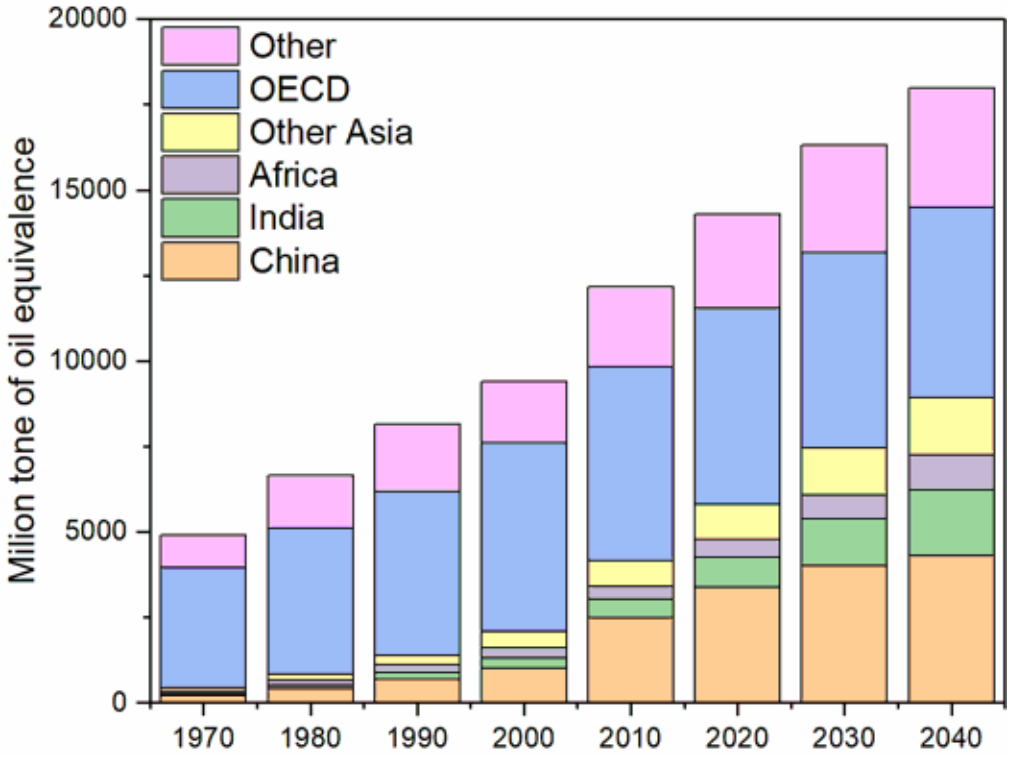

Figure 1-1. The global energy consumption by region and energy scenarios to 2040 **[2]**

Figure 1-2 presents the shares in global power generation by sources (coal, oil, gas, nuclear, hydro, and renewables) in the past and the scenarios for 2040 [2]. In the scenarios of power fabrication to 2040, fossil fuels will still be an indispensable source of human energy, with which coal will contribute approximately 28% of the total energy. Although the increase in renewables is a remarkable performance. The shares of non-fossil fuels (nuclear, hydro, and renewables) are expected to share 48% in 2040, in which the renewables are predicted to grow strongly, to one-fourth of total power generation in 2040.

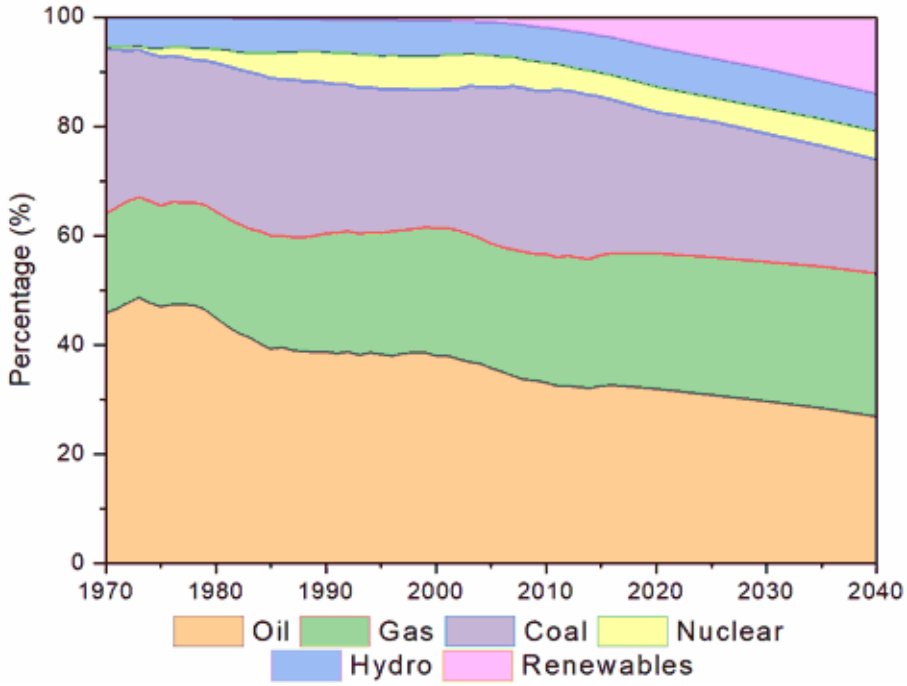

Figure 1-2. Global power generation by sources **[2]**

Today, coal is used mainly in the cement industry, iron and steel manufacturing, and electricity generation [3]. In 2018, the utilisation of coal accounted for the highest proportion of electrical generation, approximately 37.93% [4]. The proportion by sources in the electrical generation in 2018 is illustrated in Figure 1-3, nearly 65% from the fossil fuels. Still, now, the electricity generation from coal is the most important resource and couldn't be directly replaced by the other primary source of energy.

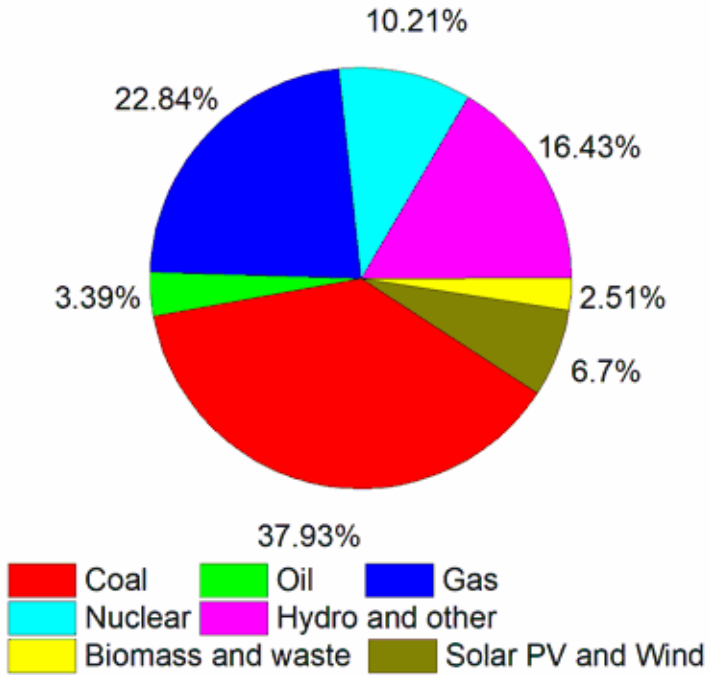

Figure 1-3. Electrical generation in 2018 **[4]**

In fact, the International Energy Agency's Global Energy and CO_2 status report showed that the global greenhouse gas (CO_2) emission reached a historic highest level in 2018, approximately 33.1 Gt CO_2, by 1.7 % higher than that of 2017 [4]. The main reason is the ever-increasing energy demand in developed and developing countries. Among the emission sources, the utilisation of coal in energy generation contributed the highest amount, nearly 44.1% of the total CO_2 emission, especially in coal-fired power generation. On one hand, it cannot be denied that electricity generation has been highly dependent on fossil fuels, like coal, at least until the half of this century. But on the other hand, the use of traditional technologies in coal power generation will lead to even higher emission levels. Clean coal technology (CCT) could be one of the solutions to this conflict.

The meaning of CCT is a broad term. Various combinations of CCTs depend on the way of definition and utilisation in each country around the world. Generally, CCT will cover one or more criteria in the following conditions: (i) the power plant is more efficient than a conventional coal-fired power plant through different operation parameters – temperature and pressure, or (ii) the plant has a facility that captures and stores carbon dioxide in the operation period, or (iii) the plant can reduce localised pollutants, as particulate matter (PM_{10}, $PM_{2.5}$), Nitrogen oxide NO_x, sulphur oxide SO_x, and heavy metals [5].

CCT could be grouped into two main categories (Figure 1-4), environmental protection and global warming [6]. Environmental protection includes NO_x combustion and flue gas treatment. Global warming is divided into high-efficiency cycle, CO_2 capture, and biomass co-combustion technology. Presently, the gasification of coal is considered the centre of CCTs.

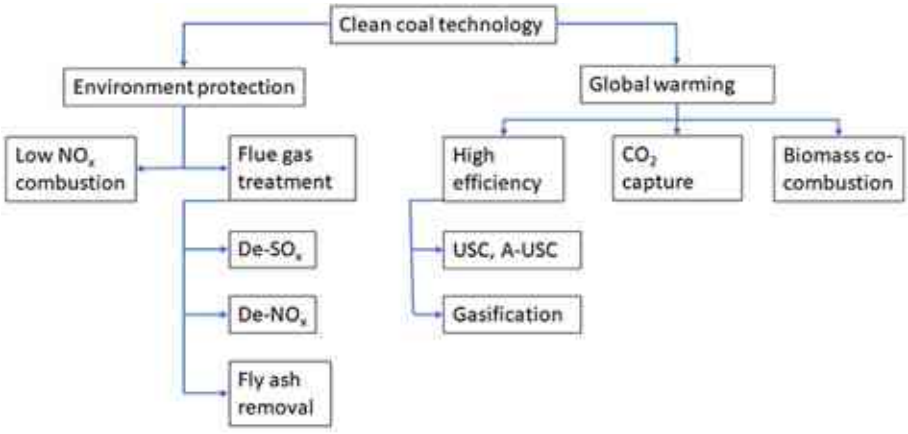

Figure 1-4. Clean coal technology **[6]**

Gasification is an incomplete combustion process of coal or another solid feedstock (biomass, municipal solid waste) [7]. The primary goals of gasification are, firstly, to convert the entire non-ash content of the feedstocks into gas, and to produce the gas with the highest

heating value as much as possible. The main products of the gasification process are gas, ash, and tar.

Gasification is one of the thermochemical conversion processes, besides the combustion and pyrolysis process. As previously stated, the gasification process occurs with the participation of reactants, such as air, steam, or CO_2, whereas pyrolysis takes place in an inert atmosphere or a vacuum. As shown in Figure 1-5, the different products are gained from the application of these processes. It is clear that the gasification and pyrolysis products have a higher flexibility for post-processing and use than the combustion process.

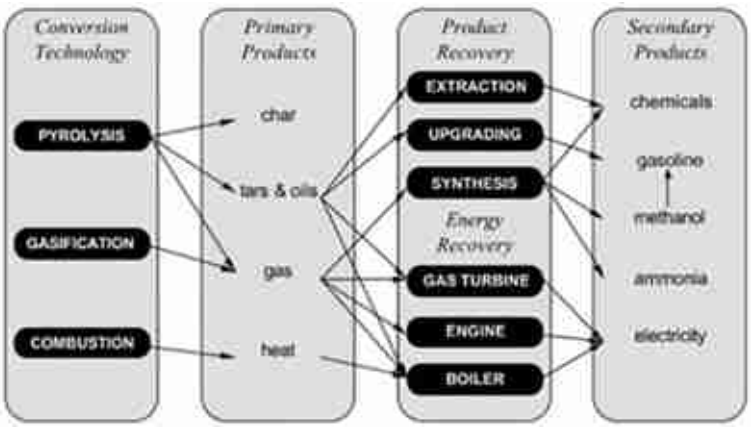

Figure 1-5. Thermochemical processes and products [8]

The gasification produced gas could be used either as a base material in chemical synthesis processes or as fuel in power generation [9]. The advantages of the gasification process can be listed as:

- The high flexibility of synthesis gas products (power and chemical) application
- The carbon dioxide emission rate is lower, even if the syngas is used as fuel in the further combustion process.
- The Sulphur released from steam gasification is in the form of H_2S rather than SO_2, which can be removed from the synthesis gas and can be used in Sulphur and Sulphur acid production, thus, producing a valuable product as a by-product.
- Nitrous oxides are primarily converted into ammonia, which can be removed from the synthesis gas at a lower cost.
- Emission rates of furan and dioxin are significantly lower compared to combustion.
- The total volume of gas that must be cleaned after gasification is lower than that of combustion.

2. Gasification process – Literature review

2.1. Principle of the gasification process

Generally, gasification is a thermochemical process, in which by using heat and gasification agents, carbon-based materials (coal, biomass, MSW, natural gas, natural oil…) can be converted into a combustible or synthesis gas. The gasification mechanism is illustrated in Figure 2-1.

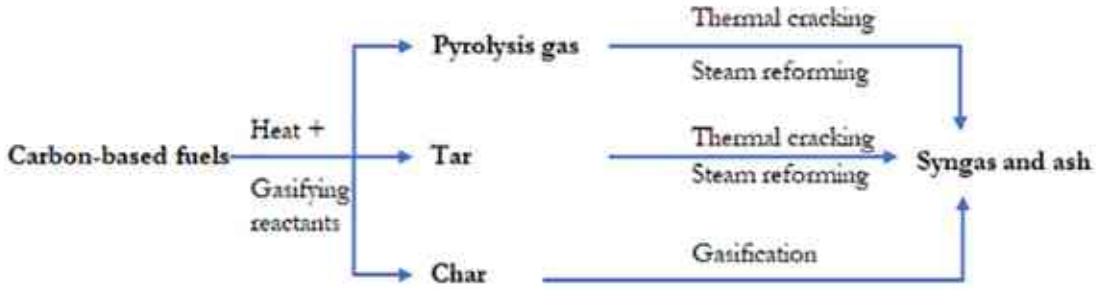

Figure 2-1. Gasification mechanism

During the gasification process, the principal chemical reactions may include species such as carbon, oxygen, carbon dioxide, carbon monoxide, hydrogen, steam, and methane. The main reaction of the gasification process can be listed as [8]:

Combustion reaction:

$$C + \frac{1}{2}O_2 \rightarrow CO \ (\Delta H_{298} = -111\ kJ/mol) \quad (2\text{-}1)$$

$$CO + \frac{1}{2}O_2 \rightarrow CO_2 \ (\Delta H_{298} = -283\ kJ/mol) \quad (2\text{-}2)$$

$$H_2 + \frac{1}{2}O_2 \rightarrow H_2O \ (\Delta H_{298} = -242\ kJ/mol) \quad (2\text{-}3)$$

Boudouard reaction:

$$C + CO_2 \leftrightarrow 2CO \ (\Delta H_{298} = 172\ kJ/mol) \quad (2\text{-}4)$$

Water-gas reaction:

$$C + H_2O \leftrightarrow CO + H_2 \ (\Delta H_{298} = 131\ kJ/mol) \quad (2\text{-}5)$$

Methane reaction:

$$C + 2H_2 \leftrightarrow CH_4 \ (\Delta H_{298} = -75\ kJ/mol) \quad (2\text{-}6)$$

Water-gas shift (WGS) reaction:

$$CO + H_2O \leftrightarrow CO_2 + H_2 \ (\Delta H_{298} = -41\ kJ/mol) \quad (2\text{-}7)$$

Steam methane reforming reaction:

$$CH_4 + H_2O \leftrightarrow CO + 3H_2 \ (\Delta H_{298} = 206\ kJ/mol) \quad (2\text{-}8)$$

Reactions (2-1), (2-4), (2-5), (2-6) describe how char is gasified by oxygen, carbon dioxide, steam, and hydrogen. The reactions, where the enthalpy change is a negative value, are exothermic reactions. While the reactions with the positive enthalpy value are endothermic reactions. The heat requirement for the endothermic reaction is supplied from the partial combustion of feedstocks, known as the direct gasification (autothermal gasification), or the external heat source – the indirect gasification (allothermal gasification).

Factors that affect the produced gas of the gasification process might be listed as feedstock types, operation parameters (e.g., gasification temperature, heating rate, pressure), gasifying reactants, and catalysts.

2.1.1. Effects of gasification temperatures

Temperature is a crucial operating parameter in the gasification process. It has significant effects on gas yield, produced gas composition, gasification efficiency, tar yield, and char yield also. The gasification temperature is controlled by the combustion of char indirect gasification. While it is adjusted by the external heat source in allothermal gasification. The increase of temperature in the gasifier depends on the gasifier's composition material, the concentration of volatile matter of fuel, the effects on ash fusion, and the by-products at high temperatures such as NO_x [10].

There are several researchers who reported that the higher gasification temperature led to an increase in gas yield, which resulted in:

- The higher gasification temperature helps the higher rate of thermal cracking of the pyrolysis gas [11–14].
- The enhancement of endothermic reactions at the higher gasification temperature [15–18].
- The higher gasification temperature promotes the thermal cracking and steam reforming of the tar [11,12,16,19,20].

The variations of gasification temperature have a significant effect on produced gas compositions (H_2, CO, CO_2, CH_4 etc.), and the results show some slight debate among researchers. According to Le Chatelier's principle, the higher temperature improves the product in the endothermic reactions and reactants in the exothermic reactions. The endothermic reactions in the gasification process can be listed as Boudouard reaction (2-4), Water gas reaction (2-5), Steam methane reforming reaction (2-8), Hydrocarbons reforming reaction (2-9), and Tar reforming reaction (2-10).

Hydrocarbon reforming reaction [11]:

$$C_nH_m + 2nH_2O \rightarrow nCO_2 + \left(2n + \frac{m}{2}\right)H_2 \ (\Delta H_{298} > 0) \quad (2\text{-}9)$$

Tar reforming reaction [11]:

$$Tar + n_1H_2O \rightarrow n_2CO_2 + n_3H_2 \ (\Delta H_{298} > 0) \quad (2\text{-}10)$$

The increase in gasification temperature favoured the production of H_2 in endothermic reactions [21–26]. In addition, the devolatilization (or decomposition) and the thermal cracking of tar were intensified with the increase in temperature, which also led to a higher concentration of H_2 [21,27]. However, when the temperature rose further, the H_2 content decreased, as a result of the combustion of hydrogen when using air as the gasifying agent [22,23]. Furthermore, it was claimed that the reaction rate of the WGS reaction (2-7) decreased at the higher temperature and the reverse WGS reaction when the temperature exceeded the equilibrium temperature [15,17,28,29]. They led to the H_2 content decreased. In addition, Wenni Li et al. [29] studied that the enlargement of gas volume in the gasifier by the excess temperature led to the reduction of residence time for a secondary reaction, which resulted in the decrease of H_2 content also.

Several types of research illustrated that the higher gasification temperature promoted the endothermic reactions, therefore more CO production and CO_2 consumption [12,23,26,30–36]. In addition, the reverse WGS reaction at higher temperatures resulted in increasing CO content and decreasing CO_2 content [37,38]. At higher temperatures in the reactor, the devolatilization and thermal cracking in the pyrolysis process also promoted the CO content [23]. However, Ge Pu et al. [22] used an air-fixed bed gasifier for pine sawdust material, the temperature performed from 650 to 950 at 100 °C. The CO concentration increased sharply from 650 °C to 750 °C and then decreased at 950 °C. In the research of Yonghong Niu et al. [15], the steam-fixed bed gasifier for biomass material was used and the temperature was adjusted from 700 to 950 in 50 °C steps. From 700 °C to 850 °C, the CO content increased, but it decreased if the temperature was further increased.

There was a high agreement among researchers about the variation of CH_4 content, it decreased with increasing temperature [11,12,15,21,29,36,39–41]. The main reason was the increasing reactivity of the steam methane reforming reaction at the higher temperature, hence, more CH_4 were consumed. Furthermore, Adam Smolinski et al. [42] studied that the reaction of CH_4 with CO_2 at high temperatures resulted in a decrease in CH_4 content also. The effects of gasification temperature in several research articles are showed in Table 2-1.

Table 2-1. The effects of gasification temperature and steam ratio in several research articles

References	Type of gasifier	Material types and moving/non-moving material	Temperature range (°C)	S/C (mol/mol or mass/mass) or S/M (mass/mass) ratio	Main results
[11]	Fixed bed	Biomass/non-moving	600-900	S/M: 0-2.8	- The positive effect of an increase in gasification temperature was lower when increasing from 800 to 900 °C. - The highest gas yield was at an S/M ratio of 1.43
[12]	Fixed bed	Municipal solid waste/non-moving	700-900	S/C: 0-2.41	- The gas yield increased with an increase in gasification temperature. - The H_2/CO ratio reached 0.96 and 2.03 at the S/C ratio of 0.84 and 1.52
[13]	Fixed bed	Sewage sludge/moving	700-900		- The gas yield increased when the gasification temperature increased from 700 to 900 °C, and the H_2/CO increased from 0.93 to 1.23 at the same gasification temperature conditions
[24]	Fixed bed	Coal/non-moving	600-800		- The carbon conversion efficiency increased as the gasification temperature increased from 600 to 800 °C
[25]	Fluidized bed	Coal/moving	660-750		- The H_2 concentration increased with a range of the experimental gasification temperatures.
[26]	Fixed bed at high pressure	Coal-biomass-petroleum coke/non-moving	850-1000	S/C: 1.47-4.03	- The H_2/CO ratio decreased from 4.4 at 850 °C to 2.1 at 1000 °C. - The H_2/CO ratio increased from 2.0 at the S/C ratio of 1.47 to 2.3 at at the S/C ratio of 4.03 at the gasification temperature of 950 °C.
[28]	Fixed bed	Biochar	750-1050	Steam flow rate: 6-25 ml/h	- An increase in the gasification temperature resulted in an increase in gas yield. The H_2 concentration decreased when the gasification temperature increased to 1050 °C. The H_2/CO ratio

References	Type of gasifier	Material types and moving/non-moving material	Temperature range (°C)	S/C (mol/mol or mass/mass) or S/M (mass/mass) ratio	Main results
					decreased from 8.3 to 4.06 when the gasification temperature increased from 750 to 1050 °C. - The H_2 concentration decreased slightly when the steam flow rate rose from 6 to 25 ml/h and the H_2/CO ratio decreased from 5.00 to 4.51 when the steam flow rate increased from 6 to 25 ml/h.
[36]	Fixed bed	Low-rank coal	700-900		- The H_2/CO ratio of the experiments of low-rank coals decreased with temperature, from 16-22 at 700 °C to around 5 at 800 °C
[43]	Fixed bed	Coal	700-900	Steam flow rate: 0.21 ml/h	- An increase in gasification temperature resulted in an increase in the H_2 and CO concentrations. However, the increasing rate of H_2 concentration was lower when the gasification temperature increased from 800 to 900 °C
[39]	Fixed bed	Coal	750-850	S/C: 0.2-2.2	- With an increase in gasification temperature, the dry gas yield increased significantly. At the same conditions, the H_2 concentration showed a little change and the CO concentration increased slightly. The H_2/CO ratio achieved around 5 at 850 °C.
[40]	Fluidized bed	Coal/moving	830-970	S/C: 0-0.4 within E/R: 0.1	- The dry gas yield increased when the S/C ratio increased from 0 to 0.3. Further raising the S/C ratio, the gas yield changed little. - An increase in gasification temperature resulted in an increase in H_2 and CO concentration. Due to using the reactant as a mixing of oxygen and steam, therefore, the CO concentration was dominant in the synthesis gas.

References	Type of gasifier	Material types and moving/non-moving material	Temperature range (°C)	S/C (mol/mol or mass/mass) or S/M (mass/mass) ratio	Main results
[37]	Fixed bed	Coal/non-moving	700-900	0.21 ml/min	- The H_2 and CO concentration increased as the gasification temperature increased from 700 to 900 °C. But the increase rate was lower when the gasification temperature was from 800 to 900 °C in the case of H_2 concentration.
[38]	Pressurized fixed bed	Coal	700-800		- The syngas yield showed a decreasing trend when the gasification temperature increased from 700 to 800 °C. The H_2 concentration decreased slightly, while the CO concentration increased with the increase of gasification temperature.
[44]	Fluidized bed	Coal	700-850	S/C:0.25-1.5	- The syngas yield increased significantly when the S/C ratio increased from 0.25 to 1.00, but no significant change when the S/C grew further to 1.5. The H_2/CO ratio reached around 2 at an S/C ratio of 1.00. - The synthesis gas yields were relatively the same at the gasification temperatures of 800 and 850 °C. While the H_2/CO ratio decreased as the gasification temperature increased from 700 to 850 °C. The H_2/CO ratio reached around 2 at 850 °C and the S/C ratio of 1.00.

2.1.2. Effect of steam ratio

In the gasification process, air, steam, oxygen, or their combination can be used as gasifying agents. The selectivity of the gasification reactions varies with different gasifying agents, thus affecting the composition and LHV of produced gas [45]. Air is the most popular media used in large-scale gasification systems. It is the cheapest option, although the produced gas will have a high concentration of nitrogen, thus significantly decreasing the heating value of the gas as well as limiting the option of further use in chemical processes. Using oxygen leads to high operational costs and safety risks. Using steam as a gasifying agent requires separate heat introduction in the system, as the main reactions within the process are endothermic. Therefore, the utilisation of an external heat source or partial combustion process is necessary. In general, the mixture of steam and air/oxygen is the most commonly used. The effects of steam ratio are summerized in Table 2-1.

Regarding the quantity of syngas in the gasification process, it was mainly claimed that the gas yield increased firstly with increasing steam ratio [11,12,21,39,40,46–50], but it is decreased when the addition of steam grew further. The increase in steam ratio improved all steam reforming and char gasification reactions, this resulted in an increase in gas yield and carbon conversion efficiency. In addition, the presence of steam enhanced the heat transfer efficiency in the gasifier by the increasing thermal conduction. However, the excess steam at low temperatures led to a decrease in the temperature of the gasifier, and consequently, the gas yield degraded.

There are many researchers, who claimed that the H_2 concentration increased with increasing steam ratio [25,33,39,40,44,47,49–52] because the introduction of steam enhanced the Water-gas reaction (2-5), Water gas shift reaction (2-7), and steam reforming reaction (2-8) (2-9) (2-10). However, the excess steam ratio led to reducing the H_2 content [47,50,51]. The excess steam lowered the local gasification temperature, it reduced the gasification rate.

The higher steam quantity favoured the Water-gas shift reaction (2-7), which resulted in more CO consumption and CO_2 producing [39,40,44,47,49]. In the meantime, the CH_4 declined as a result of the higher reaction rate of the steam methane reforming reaction (2-8).

2.2. Types of gasifiers

The feedstocks differ highly in their chemical, physical and morphological properties. Therefore, the universal gasifier that is able to handle all or most feedstock types, does not

exist, and may not exist in the foreseeable future [53]. In the gasifier, all the gasification reactions take place at high temperatures and normal pressure (ambient pressure) or high pressure. The high-pressure operation is associated with the introduction of the feedstocks into the reactor [53]. To select a gasifier, the properties need to be considered in order to ensure stability, gas quality, efficiency, and pressure losses only within certain ranges of the fuel characteristics, which are [53]: (i) energy content, (ii) moisture content, (iii) volatile matter production, (iv) mineral matter content – ash forming propensity, (v) ash chemical composition and reactivity, (vi) feedstock reactivity, (vii) feedstock size and size distribution, (viii) bulk density of the feedstock, and (ix) feedstock propensity for char formation.

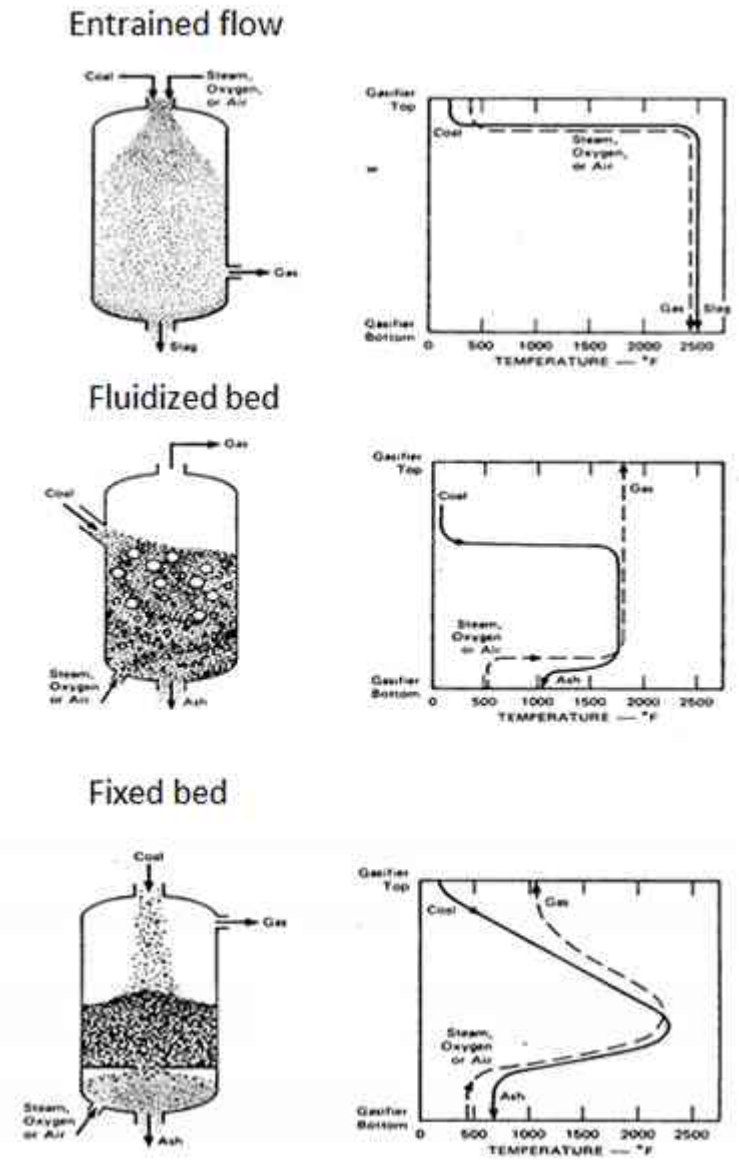

Figure 2-2. Gasification technologies [54]

In general, the gasifier can be classified into three principal configurations, entrained flow, fluidized bed, and fixed bed gasifier (moving bed). Figure 2-2 presents the configuration of gasifier types in the transportation of gas and particles, and the temperature also [54]. In the entrained flow gasifier, the fuels and gasifying agents are fed into the gasifier from the top at elevated pressure. This gasifier type has the largest capacity, but the requirements of feeding particle size and operating temperature are very high, therefore the input energy is higher than that of other types. In a fluidized bed gasifier, the fuels-gas mixing is suspended in the reaction zone, but it leads to carbon conversion problems. This gasifier type is highly recommended for biomass due to the low average tar production [55]. The main problem of biomass gasification is the tar production in fixed bed gasifiers, in contrast, there are many advantages of fixed bed gasifiers over the other types, such as low investment and operation cost, simple and reliable operation, high carbon conversion and thermal efficiency.

An updraft fixed bed gasifier is a vertical reactor where the movement of fuel and syngas is opposite (Figure 2-3). The fuel is fed from the top of the gasifier, whereas the oxidizers come from the bottom, and the fuel gas is collected at the top of the gasifier also. The gasifying agents enter at the bottom of the gasifier through a grate, it contacts firstly with the hot ash and oxidant zone above the grate, and then to the reduction zone. The heat requirement for the pyrolysis and drying process is supplied from the hot production gas. Therefore, the syngas composition contains the water vapour from the drying process, tar, and by-products from the pyrolysis process. All of them do not travel through the gasification for thermal cracking, so it needs to pay more energy in the separating system [56]. In addition, the high temperature in the ash outlet can lead to problems of fusion in solid equipment.

In the downdraft moving bed gasifier (Figure 2-3), the fuel is fed at the top of the reactor and the gasifying agent is injected in the oxidation zone while the produced gas is collected at the bottom of the gasifier. The pyrolysis gas passes co-currently through the oxidation and gasification zones, so this leads to the lower content of tar, but the reduction of the heating value of syngas also [57]. The other drawback of this gasifier type is the fuel gas leaves the reactor at an elevated temperature then the efficiency of the gasification process will be decreased [56].

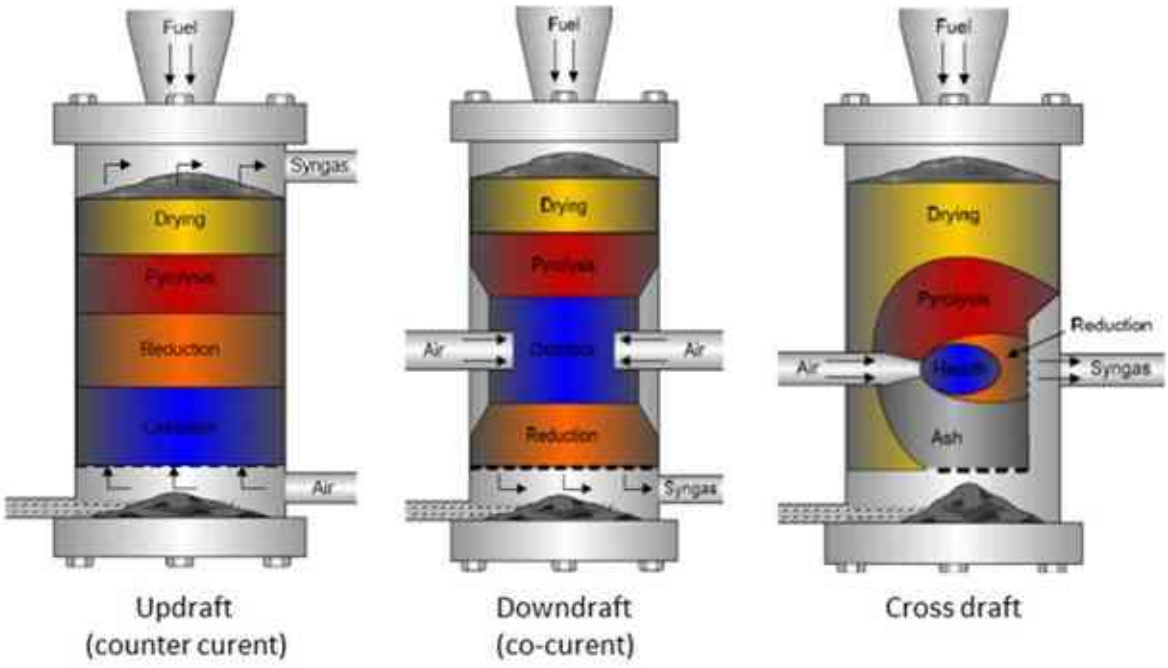

Figure 2-3. Fixed bed gasifier [56]

The gasifying agent is entered at the middle of the reactor and the syngas outlet is built on the opposite side in the cross-draft fixed bed gasifier (Figure 2-3). There are several limitations of this gasifier type, such as low produced gas quality, high level of tar content, high level of CO_2 concentration, and high temperature of gas exit [56].

2.3. End-use of produced gas

The produced gasification gas composition is the most important role in the application of produced gas. The composition of gasification produced gas depends on various factors, including feedstock, gasifier type, and gasification operation parameters (e.g., temperature, pressure, reactant type, etc.). The produced gas can be listed as low Btu gas, medium Btu gas, high Btu gas, and synthesis gas [53]:

- Low-heating gas (produced gas) is a gaseous product of the gasification process, in which air is used as a reactant. Typically, the heat content of Low heating gas varies in a range of 5.59÷11.18 MJ/m^3. Using air as a reactant, the nitrogen content presents from less than 33 V/V% to slightly more than 50 V/V%. The produced gas is suitable for the combustion process.
- Medium-heating gas produces typically by steam gasification. Its heating value ranges from 11.18÷20.49 MJ/m^3. Medium heat-content gas is considerably more versatile than low heat-content gas. It can burn directly in the boiler and use in the combined power cycle. But medium heat content gas is especially amenable

to synthesising methane (by methanation), higher hydrocarbon derivatives (by Fischer-Tropsch synthesis), methanol, and a variety of synthetic chemicals.

- High-heating gas is also known as synthetic natural gas or substitute natural gas (SNG). It is essentially pure methane content.
- Synthesis gas (syngas) is a mixture of carbon monoxide (CO) and hydrogen (H_2), which is the product of high-temperature gasification with reactants such as steam or oxygen. After cleaning, syngas can be used to produce organic molecules such as synthetic natural gas (SNG-methane (CH_4)) or liquid biofuels such as synthetic diesel (via Fischer-Tropsch synthesis).

Generally, gasification gas is more efficient in production than the original fuel in combustion characteristic for electrical generation, especially in combined heat and power plants [58–60]. In addition, the high flexibility of utilisation of produced gas is presented in the fuel cell application [61–63]. Within the chemical industry, the required ratio of H_2/CO, as represented in Table 2-2, is determined by the final product of the chemical synthesis.

Table 2-2. Synthesized final products and the required H_2/CO ratios for the synthesis [64–67]

Product	**Basic chemical reactions**	**H_2/CO ratio**
FT liquid fuels	$2n\ H_2 + n\ CO \rightarrow C_nH_{2n} + n\ H_2O$ $(2n+1)\ H_2 + n\ CO \rightarrow C_nH_{2n+1} + n\ H_2O$	2.0 2.1
Methanol	$2\ H_2 + CO \rightarrow CH_3OH$	2.0
Ethanol	$2\ CO + 4\ H_2 \rightarrow C_2H_5OH + H_2O$	2.0
Higher alcohols	$n\ CO + 2n\ H_2 \rightarrow C_nH_{2n+1}OH + (n-1)\ H_2O$	2.0
Dimethyl ether	$2\ CO + 4\ H_2 \rightarrow CH_3OCH_3 + H_2O$	2.0
Acetic acid	$2\ CO + 2\ H_2 \rightarrow CH_3COOH$	1.0
Ethylene	$2\ CO + 4\ H_2 \rightarrow C_2H_4 + 2\ H_2O$	2.0
Ethylene glycol	$2\ CO + 3\ H_2 \rightarrow C_2H_6O_2$	1.5
Acetic anhydride	$4\ CO + 4\ H_2 \rightarrow (CH_3CO)_2O + H_2O$	1.0
Ethyl acetate	$4\ CO + 6\ H_2 \rightarrow CH_3COOC_2H_5 + 2\ H_2O$	1.5
Vinyl acetate	$4\ CO + 5\ H_2 \rightarrow CH_3COOCHCH_2 + 2\ H_2O$	1.25

2.4. Synthesis gas clean-up

In the gasification process, the raw synthesis gas of various feeding fuels is similar [68]. The gasification process generates not only useful gaseous products but also the by-products or pollutants, such as tar, fly ash, NO_x, H_2S, SO_x, and alkali metals [68,69]. The requirement in fuel gas quality from the downstream applications is listed in Table 2-3.

Table 2-3. Produced gas requirement

Gas quality		IC engine [70–73]	Gas turbine [70,74–76]	F-T synthesis [77–79]
Tar (mg/Nm^3)		< 100.00	< 5.00 (in vapour	< 1.00 (ppmV)
PM (mg/Nm^3)		<50.00	phase)	0
Particle size, µm		< 10.00	< 20.00	-
Min. LHV (MJ/Nm^3)	-		< 0.10	-
Min. H_2 content (V/V%)	-		4-6	-
Max. alkali content, ppb	-		10-20	< 10.00
S component, ppm	-		20-1000	< 1.00
N component, ppb	-		< 1.00	< 20.00
HCl, ppm	-		-	< 0.10
Alkali metals, ppb	-		< 0.50	< 10.00
			< 50.00	

2.4.1. Particulate removal

Particle content requirement depends on the end-use application of the produced gas, as shown in Table 2-3. The particulate matter in synthesis gas can lead to many critical issues, such as the particles depositing in the nozzle and other places and blocking the system. For gas turbine applications the particles affect the turbine blade due to the abrasion effect. The particles also affect the anode of the solid oxide fuel cell and deactivate the catalyst for the Fischer−Tropsch synthesis [80].

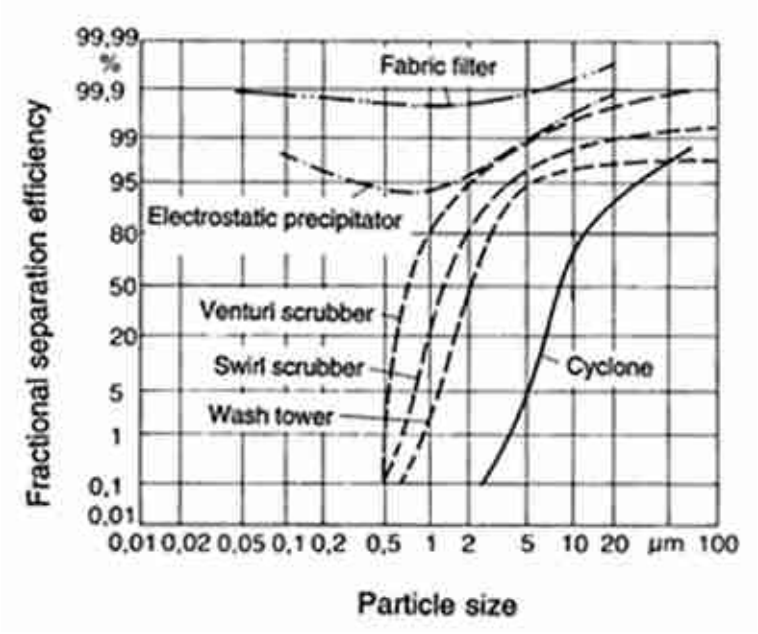

Figure 2-4. The particle removal efficiency of conventional filter types [71]

There are several ways to reduce the particulate matter in synthesis gas, such as cyclone, barrier filter, electrostatic precipitator, and wet scrubber. Figure 2-4 shows the general behaviour for particle collection of conventional filter types. In wet scrubbers,

particles are collected by collision with liquid droplets and accumulated in a demister. Generally, the scrubbing liquid is water. The scrubbing liquid should stay in liquid phase, well below its boiling point. As consequently, the synthesis gas will be cooled well below 100 °C where the washing liquid is water. Wet scrubbers are used primarily to remove tars content rather than particulates. Removing the particulates separately can avoid the condensation of the sticky tars on the particulate surface. As consequently, it prevents fouling and plugging of filter surfaces. The working temperature range and pressure drop of each filter type are presented in Table 2-4, in which, cyclon, fibrous ceramic filter, metallic foam filter, and granular bed filter can be applied in the case of the high temperature of synthesis gas.

Table 2-4. The working temperature range and pressure drop of particulate filters [81]

Particulate filter	Temperature range (°C)	Pressure drop (kPa)
Cyclone	100-900	<10.00
Fabric bag filter	60-250	1-25.00
Wet scrubber	20-100	5-20.00
Fibrous ceramic filter	200-800	1-5.00
Metallic foam filter	200-800	<1.00
Granular bed filter	200-800	<10.00

2.4.2. Tar and tar reduction

Tar is defined as the formed aromatic organics under thermal or partial-oxidation regimes (gasification) of any organic material [70]. In the thermochemical decomposition process of solid fuels, tar exists in the liquid state at room temperature and in vapour form at high temperature. Tar is not only an inevitable matter in pyrolysis processes but is also present in the gasification process. The effect of tar can be listed as blocking the pipeline of the gasification system at low temperatures, corrosion the downstream, deactivating the catalyst in the downstream synthetic process, reducing the thermal efficiency of the gasification system, producing phenol-containing wastewater, and degrading the production environment in the plant [82].

A widely accepted definition of tar proposed by the Directorate-General for Energy of the European Commission is that tar is all hydrocarbons with a molecular weight higher than benzene [83]. There are two widespread ways to classify the tar composition (Table 2-5) [70,82,83]. The first one described the process condition, and the other is based on the physical properties of tar, such as solubility and condensability of tar, and the number of rings in the tar components.

As shown in Figure 2-5, there are three main technologies for the tar removal process, biological method, physical method, and chemical method [82]. The biological method uses the active biological enzyme for the tar removal process. However, this process is not scaled up at this time for industrial applications. The physical method is used to convert the tar content from the gas phase to the liquid phase by inertia collision, interception, diffusion, electrostatic force, and gravity in the cleaning gas system. But the drawbacks of this method are the limitation in tar energy utilisation, the secondary pollution from wastewater, and the high energy demand. The third method is the chemical process, in which, using thermal chemical cracking reactions and/or reforming reactions to convert tar content into non-condensable gas components. This method can be performed in-situ gasification process or post-gasification process.

Table 2-5. Tar classification

Milne method		**ECN-TNO-UT method**	
Name	Property and typical compound	**Name**	Property and typical compound
Primary products	Characterized by cellulose-derived, hemicellulose-derived and lignin-derived products	**GC-undetectable tar**	- Very heavy tars, cannot be detected by GC; - Determined by subtracting the GC-detectable tar fraction from the total gravimetric tar;
Second products	Characterized by phenolics and olefins	**Heterocyclic**	- Tar containing hetero atoms, highly water-soluble compounds; - Pyridine, phenol, cresols, quinolone, isoquinoline, dibenzo phenol;
Alkyl tertiary products	Mainly methyl derivatives of aromatic compound	**Light aromatic (1 ring)**	- Usually light hydrocarbons with single ring; do not pose a problem regarding condensability and solubility;
Condensed tertiary products	PAH series without substituent	**Light PAH compounds (2–3 rings)**	- 2 and 3 rings compounds; condense at low temperatures even at very low concentrations; - Indene, naphthalene, methylnaphthalene, biphenyl, acenaphtylene, fluorene, phenanthrene, anthracene;
		Heavy PAH compounds (4–7 rings)	- High-temperatures at low concentrations; Fluoranthene, pyrene, chrysene, perylene, coronene, benzopyrene, benzo fluoranthene;

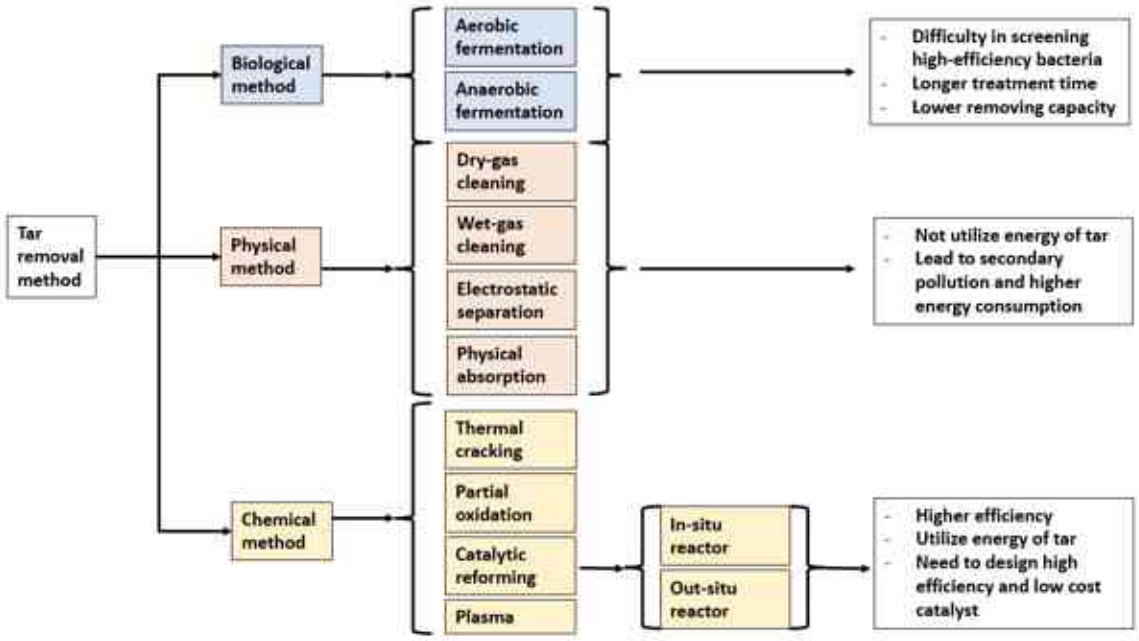

Figure 2-5. Tar removal methods [82]

2.4.3. Sulphur removal

For the gasification process of low-rank fuels such as brown coal (lignite), the sulphur content is quite high. It is formed mainly in hydrogen sulphide (H_2S), and acidic products in combination with water vapour in the synthesis gas [53]. It results in the corrosion of the system. In addition, a small amount of sulphur can lead to the poisoning of catalysts that are used in the synthesis gas cleaning or upgrading for not only the gasification process but also for the chemical synthesis process [81]. When the gasification gas is combusted, the sulphur content is converted to sulphur dioxide, as a regulated air pollutant.

Typically, H_2S removal can carry out with many specific methods. They can be categorised depending on the temperature of synthesis gas (hot and cold gas desulfurisation), adsorption and/or absorption methods, or sorbent state (solid or liquid types). Table 2-6 shows the properties of dry and wet sulphur removal methods.

Table 2-6. Hydrogen sulphide removal [84,85]

Feature	**Dry sulphur removal method**	**Wet sulphur removal method**
Sorbent state:	solid	liquid
Principle:	chemical absorption	chemical absorption, physical absorption
Material:	single or mixture of metal oxides	chemical solvents: e.g. alkanol amines, monoethanolamine,

Feature	Dry sulphur removal method	Wet sulphur removal method
	single metal oxides: e.g. Zn, Fe, Cu, Mn, Co, V oxides mixture metal oxides: e.g. Mn+V+Cu oxides, Zn+Cu oxides	diethanolamine, methyl diethanolamine Physical solvents: e.g. methanol and dimethyl
Temperature range:	hot gas; normal to high temperature (700 °C)	cold gas; sub-zero to normal temperature
Sulfur removal capacity:	mostly	partially
The concentration of H_2S in syngas:	low	high
Purifying effect:	fine	rough
Operation method:	intermittent and simple	continuous and complex
Cost:	low	high

2.5. Review of multi-stage fixed bed gasification process

As mentioned in section 2.3, the most valuable benefit of the gasification process is the great flexibility of synthesis gas utilisation, especially in the chemical process. Regarding the control of the H_2/CO ratio during the gasification process, there are several effective ways in changing the gasification parameters (temperature, pressure, etc.), the selection of reactant types and their ratio, the utilisation of catalysts, and the gasifier setup modification. The multi-stage gasification is well-known as a promising approach in the enhancement of process efficiency and quality of product gas as well. In the gasification process, the sub-processes include drying, devolatilization, partial oxidation, and reduction process. In multi-stage gasification, the separation or combination of these sub-processes is highly dependent on the fuel properties such as reactivity, ash content, sulphur content, and volatile content [86]. The multi-stage gasification can be commonly categorised as single-line and double-line process, are shown in Figure 2-6.

In the single-line process, there is only one stream of mass (solid and gas products) that go through several reactors in series or a reactor with multi-injection of reactant. In the double-line process, the mass stream will be separated into at least two partial lines which flow through several reactors in parallel. The double-line gasification process was commonly used in lab-scale experiments [19,87–90]. In which, the starting material was gasified in a reactor to produce syngas. Then the syngas flowed to the 2nd reactor for a thermal cracking process and/or reforming process with/without the presence of a catalyst. In other research, the double-line concept was developed with a combination of the

gasification process and the combustion process of char [86,91,92]. The scheme of a typical experimental apparatus is illustrated in Figure 2-7. The residual char from the gasification process is combusted in a circulating fluidized bed chamber. The hot solid bed materials act like heat carriers to transport heat from the combustor to the gasifier. The combustion chamber and gasifier are connected by a circulating solid char loop to separate the combustion flue gas and syngas of the gasification process.

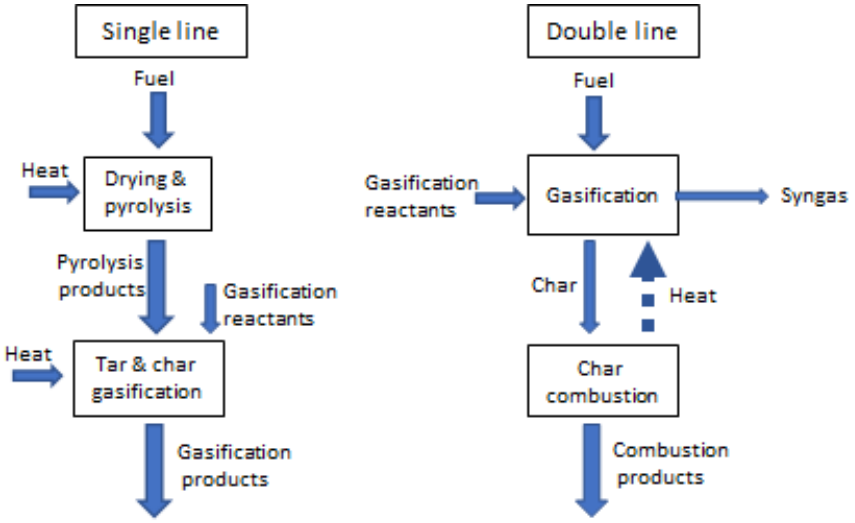

Figure 2-6. Single-line and double-line gasification process [86]

This section will be focusing on the progress of the single-line multi-stage fixed bed gasification process. Generally, there are two main methods in the single-line multi-stage gasification process, physical and non-physical modification. In which, the physical modification aims to separate and optimize the sub-processes (drying, devolatilization, combustion, and gasification) for higher gasification efficiency. While the non-physical method is carried out by the separation of air distribution during the gasification process. There are two or more air intakes used in the non-physical method, called as multi-air stages gasification process.

With the many benefits in the operation and efficiency of the process, the down-draft gasifier was used in several types of research in the multi-air stages gasification process. This research can be categorised into double air stages [93–99] (Figure 2-8-left) and three air stages (Figure 2-8-right) [100] autothermal gasification process. In most cases, one of the air intakes was used to hold the partial combustion in the double-air gasification process. The other air intake would be introduced in the pyrolysis and/or drying zone to increase the efficiency of the pyrolysis process by the partial oxidation of organic matter.

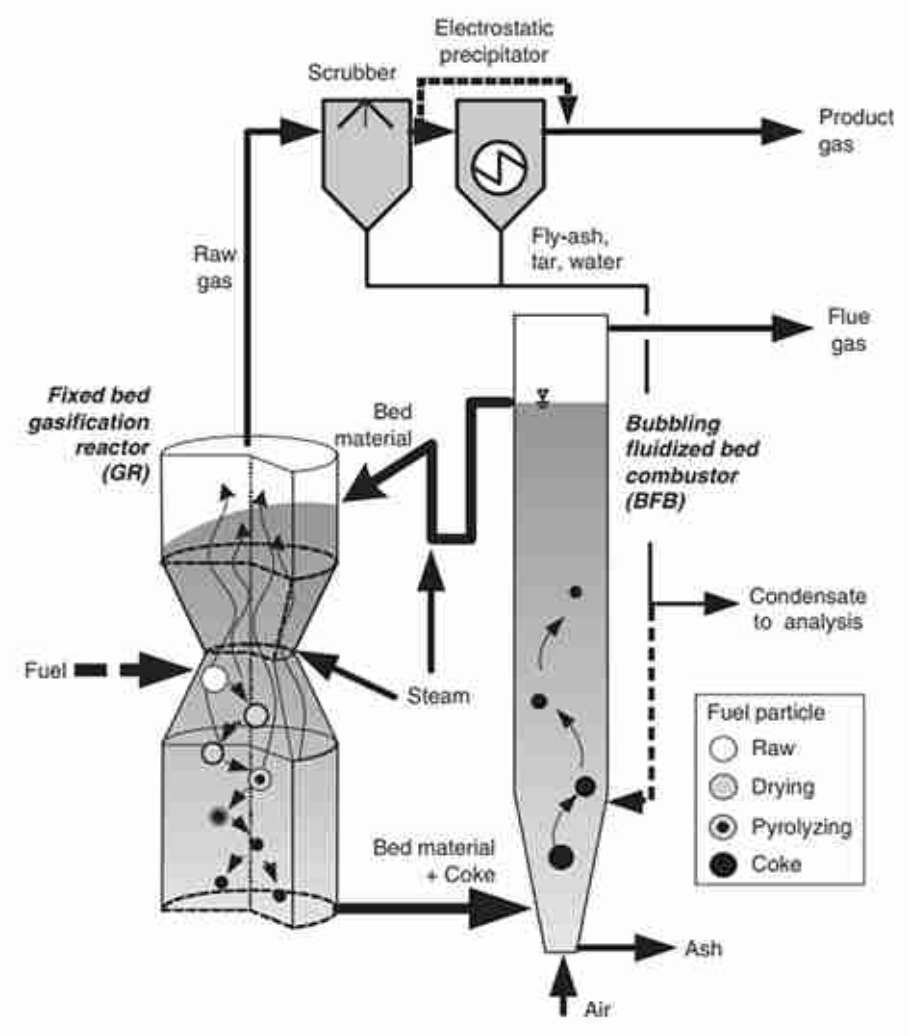

Figure 2-7. Double line concept with the char combustion [86]

T. Bui et al. examined the double-air stage in a down-draft throatless autothermal gasifier with biomass fuel [93]. Besides the main air inlet for the partial combustion zone, the other air inlet was established for a flaming pyrolysis process. This study indicated that the tar content in the double-air gasification process was about 40 times lower than that in single-stage air gasification. Regarding to the synthesis gas composition, the main components were carbon-based gases (CO and CO_2) due to using air as a reactant in the gasification process. The H_2/CO ratio were 0.64 and 0.61 in two-stage and single-stage, respectively. The effects of airflow rate and its distribution in air intakes were investigated in a down-draft gasification process of biomass with 0.3 m of internal diameter and 1.06 m of height [96,99]. With the airflow rate range of 16÷24 Nm^3/h and the air distribution at 0, 40, and 80 %, these investigations showed that the gasification efficiency was increased with the proper ratio of airflow rate and the air distribution as well. This could be clearly seen in the reduction of tar and particle content in synthesis gas. With an airflow rate of 20 Nm^3/h and the air supply for the pyrolysis stage at 80 % compared to the airflow rate for the partial

combustion stage, the tar content was from 54.25 to 102 mg/Nm^3 and particle content was 4 mg/Nm^3. While that were 418.95 of tar content and 146.03 mg/Nm^3 of particle content with 0 % of air distribution [96]. These researches also revealed that CO and H_2 were dominant components in synthesis gas, counting for around 19.04 and 16.78 V/V% [99]; 19.2 and 17.14 V/V% [96]. The mixture of the air/oxygen and steam in the double air-stage autothermal gasification process helped to increase the H_2 concentration, even though the steam used in the experiment was not superheated [95,97]. The mean value of H_2 concentration was in a range of 18.4 to 34.3 V/V% with the mixture reactants of air/oxygen and steam, while that was only 16.3 to 17.2 V/V% in the case of air gasification [95]. Saleh et al. examined the municipal solid waste gasification process in three air stages gasifier with an additional air stage in the reduction zone [100]. The air intake in the reduction zone increased the gasification performance compared to the single-stage condition. Regarding the synthesis gas composition, the CO and H_2 concentration firstly improved with an increase in air flow rate in the reduction zone. However, it was a reduction trend for the further increase in air flow rate in the reduction zone due to the higher combustion rate. In addition, the three-air stage also produced the synthesis gas with a lower tar content at 57.29 mg/Nm^3 compared to 146.98 mg/Nm^3 in single-air stage gasification.

Two-stage is a concept used as the physical modification in the single-line multi-stage gasification process [101–104] (Figure 2-9). In which, the sub-processes (such as drying, pyrolysis, partial combustion, and reduction) are mechanically separated to optimise each stage for higher efficiency in the whole gasification process. In the two-stage gasification process, the drying and pyrolysis processes are carried out in an allothermal auger reactor. The necessary heat for the pyrolysis process is provided by the flue gas of the combustion process (such as internal combustion engine or burner) of synthesis gas. The second stage is an autothermal fixed bed reactor, including partial combustion and reduction process. After the pyrolysis process, the partial combustion of pyrolysis gas and char takes place with the right selected ratio of reactant in the free space above the hot char bed. Finally, the produced gas is passed through the hot char bed at the bottom of the reactor for further reaction. Using air as a reactant for the biomass two-stage gasification process, Brandt et al. [101] studied the tar reduction in the gasification process for the application of synthesis gas in the internal combustion engine. It was presented that the tar content in produced gas was reduced to less than 15 mg/Nm^3 and none of which was heavy tar. Wang et al. [103] examined the two-stage biomass gasification process with oxygen-enriched air as a reactant. It was revealed that the oxygen concentration had a significant effect on the synthesis gas

composition, but less on the ratio of H_2/CO. The ratio of H_2/CO was around 1 in all experiments, although the concentration of H_2+CO increased from 30 V/V% to 70 V/V% at oxygen concentrations of 21 V/V% and 99.5 V/V%, respectively. The O_2-CO_2 was considered as a reactant in the research of biomass two-stage gasification process with a focus on tar, sulphur compounds, and synthesis gas composition as well [104]. It was demonstrated that the presence of CO_2 led to a reduction in H_2 concentration, but an increasing trend in CO_2 and CO concentration. In O_2-CO_2 operation, the synthesis gas had a high quality with tar and sulphur concentration. It led to higher flexibility in application.

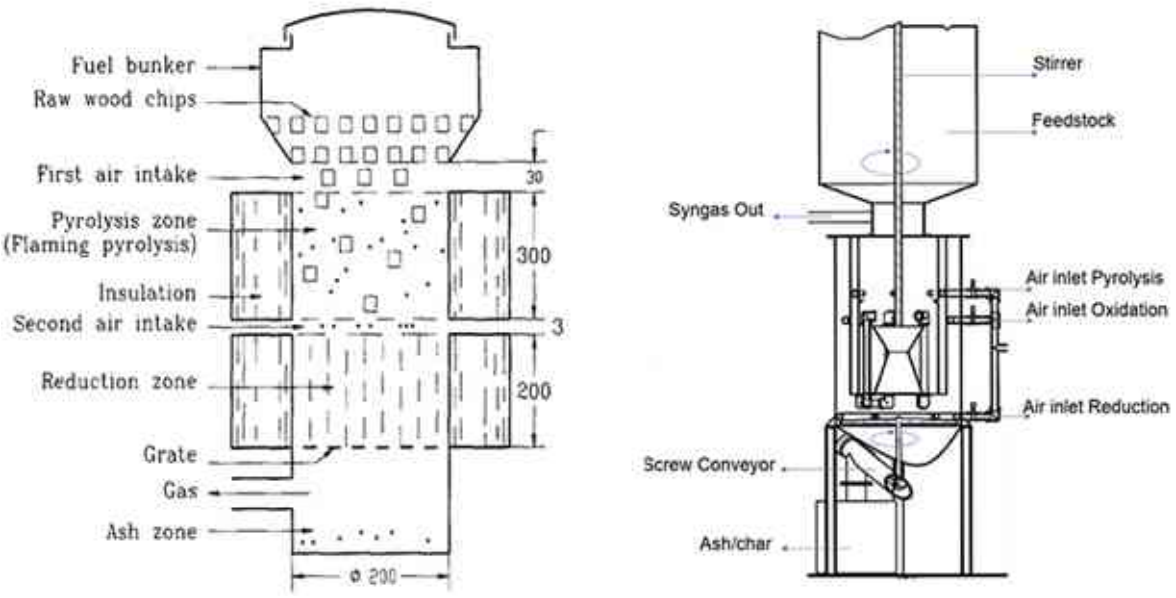

Figure 2-8. The multi-air stage gasification process [93,100]

Brynda et al. researched the biomass gasification unit (named GP750) to use a combination of physical and non-physical modification for the combined heat and power plant [105] (Figure 2-10). In this study, there were two air-stages used in a fixed bed gasifier. The first air intake was supplied for the partial combustion stage in the gasifier to produce the essential heat. The char and gas went down to the reduction zone. However, a ceramic cone separator was used between the combustion and reduction stages. This separator only split the gas compounds from the partial combustion zone. The second air intake was provided for partial oxidation of the volatile matter inside the separator. After that, the mixture of gases passed through the hot char bed for further reaction. During the long-term experiment with air as a reactant, the H_2 and CO concentration remained at around 23 and 25 V/V%, respectively. Especially, the lowest tar content was 4.1 mg/m^3, normally in a range of 5 to 50 mg/m^3.

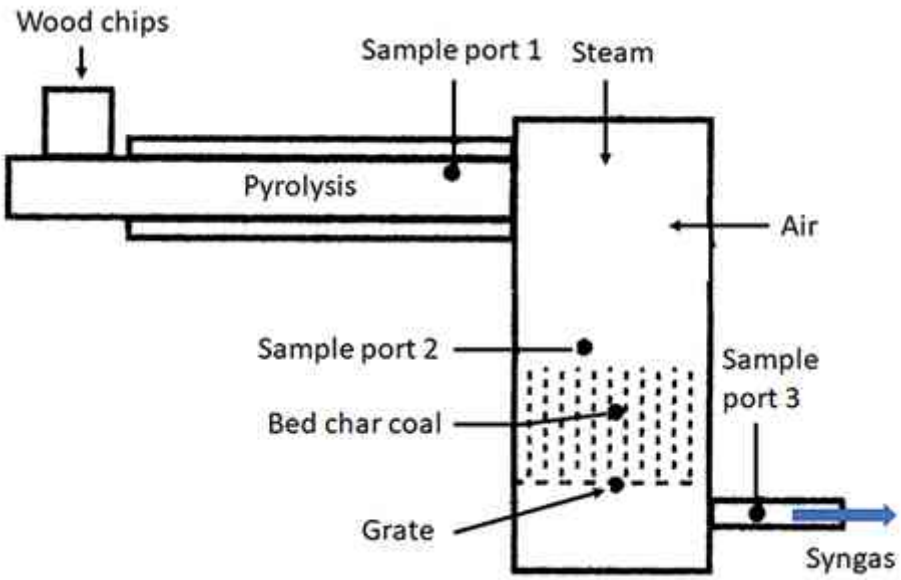

Figure 2-9. Two-stage gasification process [101]

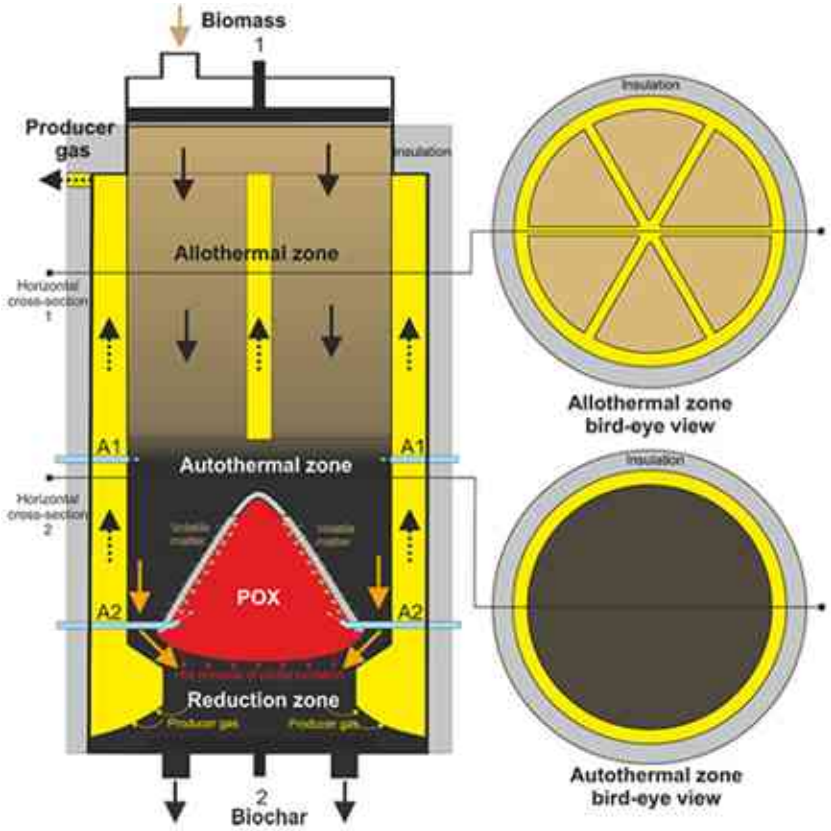

Figure 2-10. Scheme of the GP750 gasifier [105]

2.6. Low-rank coals and Hungarian low-rank coal gasification

Coal is known to be the most abundant and widespread among fossil fuel resources [106]. The range of coal can be classified from peat to anthracite, as shown in Table 2-7.

Table 2-7. Classification of coal by rank (ASTM D388)

		Fixed carbon limit, % (Dry, mineral-matter-free basis)		**Volatile matter limit, % (Dry, mineral-matter-free basis)**		**Calorific limit, MJ/kg (Moist, mineral-matter-free basis)**	
Class	**Group**	Equal or greater than	Less than	Greater than	Equal or less than	Equal or greater than	Less than
I. Anthracitic	1. Meta-anthracite	98.00	-	-	2.00	-	
	2. Anthracite	92.00	98.00	2.00	8.00	-	
	3. Semi-anthracite	86.00	92.00	8.00	14.00	-	
II. Bituminous	1. Low volatile bituminous coal	78.00	86.00	14.00	22.00	-	
	2. Medium volatile bituminous coal	69.00	78.00	22.00	31.00	-	
	3. High volatile A bituminous coal	-	69.00	31.00	-	32.56	
	4. High volatile B bituminous coal	-	-	-	-	30.24	32.56
	5. High volatile C bituminous coal	-	-	-	-	26.75	30.24
III. Sub-Bituminous	1. Subbituminous A coal	-	-	-	-	24.42	26.75
	2. Subbituminous B coal	-	-	-	-	24.42	26.75
	3. Subbituminous C coal	-	-	-	-	22.10	24.42
IV. Lignite	1. Lignite A	-	-	-	-	19.31	22.10
	2. Lignite B	-	-	-	-	-	19.31

Basically, the low-rank coals (LRCs) comprise of sub-bituminous coal and lignite (brown coal), well-known from the early-stage formation of coalification. These coal types constitute about one-third of the global proven coal reservoir [107,108], mainly in the United States of America, European countries, Australia, and several Asian countries. LRCs are characterised as lighter, with higher moisture content, and lower heating value than that of

high-rank coals (bituminous and anthracite) [109]. The higher moisture content leads to a higher challenge level in the application of LRCs. The high moisture content results in lower heating value, which leads to lower thermal efficiency of the plant, higher CO_2 emission, as well as higher construction and operation cost [110–112]. Furthermore, the cost of long transportation and storage of LRCs would be increased due to their high moisture content. On the other hand, the LRCs have a strong tendency for self-ignition during the hauling and storage period as a result of the high oxygen functional group [113,114]. The other disadvantage of LRCs is the higher ash content, it also increases the cost of operation in the post-treatment processing [115].

However, the LRCs have certain advantages compared to other high-rank coals. It can be seen clearly that the first one is the lower cost of open-cut LRCs mining and the inexpensive energy source [112,116]. Moreover, the higher inherent contents of volatile, alkali and alkaline earth metals make the higher reactivity for the LRCs [24,117,118]. It leads to the better application of LRCs in the pyrolysis and gasification process. Currently, the LRCs are mainly used in thermal power plants for local electricity generation [119]. However, coal utilization is growing as a key in chemical industries, as raw material for coking, methanol, ammonia, dimethyl ether, olefin, etc [120].

The total Hungarian coal proved reservoir has been about 2909 million tonnes, till the end of 2019 [107]. From which, the LRCs are accounted for nearly 90.5% of the total Hungarian coal reservoir. These coal types (brown coal and sub-bituminous) are distributed mainly in Trans-Danubian and North-East coal basins in Hungary [121]. The properties of these LRCs are very high sulphur and moisture content, as well as a very low heating value [122].

In Hungary, coal is used mainly in the energy sector, sharing 17% of the national gross electricity generation in 2010 [123]. However, the investigation into the gasification of Hungarian low-rank coal is an attractive field in terms of the multi-purpose transformation for cleaner production in recent years. A. Pettinau et al. [122] carried out experiments on Hungarian low-rank coal in both lab-scale and pilot-scale gasifiers. In this study, the brown coal was collected in the North-East coal basin in Hungary, with 13.78÷20.48 MJ/kg of lower heating value (LHV) and 31.1÷38 %wt. of carbon content in the dry basis sample. The lab-scale gasifier was made of resistant steel pipe within 80 mm of inner diameter and 1200 mm of effective length at the University of Miskolc. The gasifier temperature was set at 800 °C by an external electrical heater. The steam flow rate was supplied at the rate of 5.2

g/min and pressure at 0.3 MPa after the drying and devolatilization process. In each experiment, there was 2.5 kg of coal fed into the gasifier. During the steam gasification period, the average gas production was 0.3 m^3/h. The H_2 content varied from 60 to 70 V/V%., while the CO and CO_2 content were below 20% in gasification time. With the mixing of oxygen and steam, the oxygen was fed from the bottom of the gasifier with a flow rate of 300÷350 dm^3/min. It was observed that the CO content was dominant between 35 and 40 V/V% and followed by H_2 at around 35 V/V%. Regarding the pilot gasification process, it was carried out in the Sotacarbo pilot platform, in Italy. With the experiments in air blown up-draft gasifier, there were about 24-25 kg/g of raw synthesis gas produced within the feeding rate at 11 kg/h of raw Hungarian low-rank coal. The LHV of syngas was 3.55 MJ/kg. The results observed that the cold gas and hot gas efficiency reached a high level, approximately 95-99 % of cold gas efficiency and 93-97 % of hot gas efficiency. Furthermore, this research noted that the fixed bed gasifier is more suitable for the Hungarian low-rank coal type in the energetic term.

L. Bokányi and Á. Pintér-Móricz [121] investigated the plasma gasification conditions with/without air addition. The gasifier has 38 cm of inner diameter and 52 cm of height with a capacity of 30 kVA. The Borsod brown coal was used in these experiments, with very high moisture content at 27 wt%. and the LHV at 15.44 MJ/kg. The results were presented that the H_2 and CO content was higher in the case of using O_2 addition than that without O_2. It led to the higher heating value of the synthesis gas when the O_2 was used as a reactant in a plasma gasifier. It was also noted that there was a possibility to convert 97.2 % of the carbon content into carbon monoxide in the synthesis gas. This study concluded that the Borsod brown coal can be efficiently transformed into the synthesis gas within the plasma gasifier with O_2 addition. It can clearly be seen that there is a gap in the detail of the gasification experiments of Hungarian low-rank coal. The effects of gasification operation conditions, reactants, as well as optimisation conditions in the gasification process for the specific application of synthesis gas need to be investigated in greater depth.

2.7. Scientific gaps and objects of research

The previous studies on the gasification process of Hungarian low-rank coals have identified a scientific gap in investigating the synergy effects of gasification temperature and steam-to-carbon (S/C [mol/mol]) ratio on both the gasification products and syngas composition.

Although several concepts of single-line multi-stage gasification processes have been developed since the 1990s, these studies primarily focused on reducing tar formation during biomass gasification in multi-stage reactors. The produced gas was predominantly used for combined heat and power systems. Consequently, the existing knowledge gap is the performance of the multi-stage gasification process for low-rank coals, specifically in achieving the desired H_2/CO ratio suitable for chemical applications. The general objective of this study is to increase the knowledge of a new advanced process of multi-stage fixed bed gasification using steam as the reactant.

Specific objectives are:

- Full demonstration of multi-stage fixed bed gasification with the continuous fuel line.
- To study the effects of gasification temperature on the multi-stage gasification process, such as gasification products, syngas quality, carbon conversion, as well as gasification efficiency.
- To study the effects of steam flow rate on the multi-stage gasification process, such as gas quality, tar content, carbon conversion, as well as gasification efficiency.
- To generate the optimisation conditions of the operation parameters for H_2/CO ratio.
- To examine the gasification performance of coal samples from gravity separation process.

3. Material and experimental apparatuses

In this chapter, the coal sample preparation and general analysis are first described. It is followed by the depiction of a single-line multi-stage gasification process in detail. Methods of sampling, analysis, and data processing are also introduced in this chapter.

3.1. Determination of the characteristics of starting material

3.1.1. Sampling method

In this study, the raw Hungarian low-rank coal was supplied by the Ormosszén Zrt. from their mining site in Felsőnyárád, Hungary. The diameter of the coal particle was 10-20 mm. Initially, the coal sample was dried for 7 days at ambient temperatures. After that, they were stored in different packages for further experiments. The coal sample is exhibited in Figure 3-1.

Figure 3-1. Hungarian low-rank coal sample

3 kg of raw coal particles were randomly collected from the coal packages for general analysis. The raw coal particles were crushed into small size coarse particles with a size distribution between 1 to 3 mm and manually blended into a relatively homogeneous mixture. In order to reduce a large amount of coarse coal sample to a suitable volume for pulverising process, in this case, the quartering method was used for the sub-sampling process. The large volume of coarse coal sample was poured into the cone shape, which was then flattened to form a disc (Figure 3-2). Then, the sample was divided into four quarters,

from which two opposite quarters were removed. The quartering method can be repeated until the sample reaches the desired sample mass.

For the general analysis, such as heating value analysis, elemental analysis, and thermal analysis, the requirement of particle size is under 212 μm. The coal samples were milled by a planetary ball pulveriser (the Planetary Mono Mill PULVERISETTE 6) at 300 RPM within 3 minutes and separated with a 0.2 mm mesh size sieve. The ball milling equipment is illustrated in Figure 3-3.

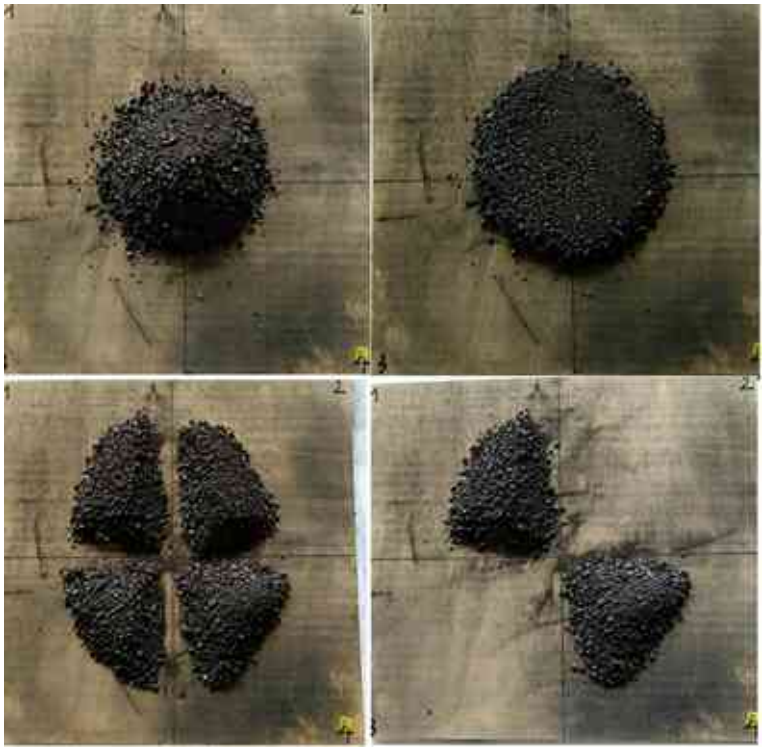

Figure 3-2. Sampling process for general analysis

Figure 3-3. Planetary ball pulveriser- Fritsch

3.1.2. Heating value analysis

Heating value is an important characteristic of fuels in the energy conversion process, it is the amount of heat released in the complete combustion process of a unit quantity of fuel and its products. High heating value (HHV) or gross calorific value (GCV), is a type of heating value, determined by measuring the heat released when coal is burned in a constant volume calorimeter, with an initial oxygen pressure of 2 to 4 MPa, and when the combustion products are cooled to a final temperature between 20 and 35 ºC [124]. The high heating values of the brown coal samples were determined by a Parr 6200 Isoperibol Calorimeter type analyser (Figure 3-4), using the *ISO 1928:2009 - Solid mineral fuels - Determination of gross calorific value by the bomb calorimetric method and calculation of net calorific value* standard [125].

Figure 3-4. Isoperibol Calorimeter-Parr 6200

3.1.3. Elemental analysis

Elemental analysis (ultimate analysis) is the determination of the mass percentage of carbon, hydrogen, sulphur, nitrogen, and oxygen content. Carbon content should include organic carbon and any carbon as mineral carbonate. Hydrogen content is composed of the hydrogen in the organic material and moisture content within the coal. Sulphur content can be presented as organic sulphur, inorganic sulphides, and inorganic sulphates [126]. The moisture and ash contents also have to be measured to be able to refer to the appropriate

basis (ar – air dry, db – dry basis, and daf – dry and ash-free). In this scope, the elemental composition of coal was examined under a standard of *ISO 29541:2010 Solid mineral fuels - Determination of total carbon, hydrogen and nitrogen content - Instrumental method* [127] with a Carlo Erba EA 1108 elementalt analyser (Figure 3-5).

Figure 3-5. Elemental analyser-Carlo Erba EA 1108

3.1.4. Thermal analysis

The proximate analysis is one of general analysis, to describe the weight percentage of moisture, volatile, fixed carbon, and ash contents. An alternative less time-consuming method for proximate analysis is thermogravimetry. Thermogravimetry (TG) is a technique, in which the change in the sample mass is expressed in time or temperature when the furnace is heated up within an inert or an oxidant atmosphere. Derivative thermogravimetry (DTG) is a type of thermal analysis to illustrate the rate of change in the sample weight by temperature. In this research, thermal analysis is performed in a MOM Derivatograph-C type (Figure 3-6), with a maximum operating temperature of 1500 ºC. In this case, the oxidant and non-oxidant atmospheres are switched within the testing process. In the first stage moisture content release is heated up to a temperature of 110 ºC in a non-oxidant atmosphere where is held for up to 40 minutes. Then, the temperature is ramped to 900 ºC and held up for 40 minutes. The goal of this stage is the release of volatiles. This stage is followed by the switching of the atmosphere from inert to oxidant to burn out the fixed carbon content. After the completed combustion, the rest of the sample weight is the ash content.

Figure 3-6. Thermogravimetric analyser-MOM Derivatograph-C

3.1.5. Ash fusion temperature analysis

The ash fusion temperature analysis defines the temperature of the ash melting process when the ash sample transforms from the solid state to the liquid state. In this research, the ash fusion temperature analysis is conducted under a standard of *ISO 540:2008, Hard coal and coke — Determination of ash fusibility* [128], with an SYLAB IF-2000G analyser (Figure 3-7), the maximum operating temperature at 1550 ºC.

Figure 3-7. Ash fusion analyser-SYLAB IF-2000G

3.1.6. Specific surface area and X-ray fluorescence (XRF) analysis

The specific surface area of coal samples was determined based on the Brunauer-Emmett Teller (BET) technique, using a Micromeritics Tristar 3000 instrument at the

University of Miskolc. The oxide compositions of the sample were determined by an X-ray fluorescence spectrometer (Fischerscope X-ray XDAL spectrometer) at the University of Miskolc.

3.2. Gravity separation process

The primary objective of coal cleaning is to separate combustible organic materials from inorganic gangue minerals, which offers two benefits: (i) it enhances the quality of coal by increasing its heating value, and (ii) it curbs environmental emissions during combustion. Separation techniques can be broadly classified into gravity separation, flotation, and magnetic and electrical separation processes [129]. Among these, gravity separation is the most used method due to its simplicity, affordability, and high efficiency.

In this study, the separation process of the original low-rank coal sample was carried out with a laboratory-scale separator at the Faculty of Earth and Environmental Sciences and Engineering, University of Miskolc. The magnetite suspension fluid was utilized in this process to separate the coal samples into two distinct fractions. The lighter fraction had a density lower than 1.60 g/cm^3- marked as the C1 sample, while the heavier fraction had a density in the range of 1.60 to 1.80 g/cm^3- marked as the C2 sample. The schematic diagram of the separator is illustrated in Figure 3-8.

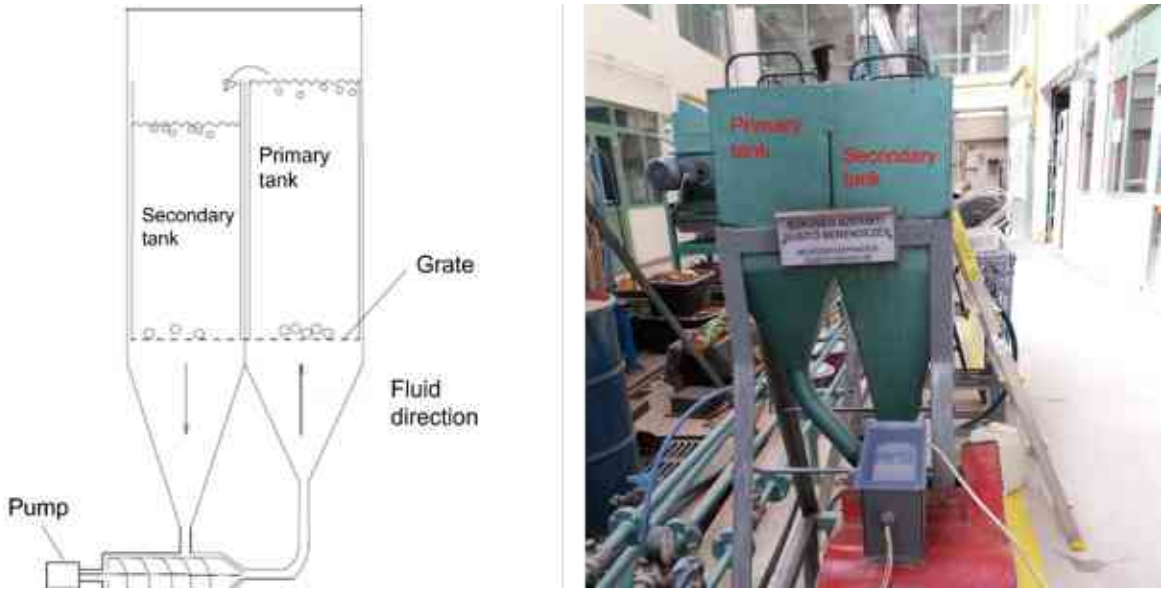

Figure 3-8. Gravity separation process

To initiate the separation process, 25 liters of magnetite suspension liquid, with a specific density of 1.60 g/cm^3, was poured into the separator while the circulation pump was operational. Subsequently, 1 kg of coal mixed with the suspension liquid was added to the primary tank of the separator. The process continued until no further lighter samples floated

up and flowed to the secondary tank. Once the lighter samples were successful separated, the separator was stopped, and the tanks were removed to collect the samples inside. At this stage of the separation process, the coal sample was separated into two fractions, the first fraction, denoted as C1, had a specific density below 1.6 g/cm^3, while the second fraction had a specific density higher than 1.6 g/cm^3. The second fraction was prepared for the second stage of the separation process with the specific density of suspension liquid of 1.8 g/cm^3. Similarly, after the completion of the second stage, two coal fractions were obtained: a fraction with a specific density between 1.6 g/cm^3 and 1.8 g/cm^3, referred to as C2, and another fraction with a specific density higher than 1.8 g/cm^3. The coal fraction with a specific density higher than 1.8 g/cm^3 was not utilized for the experiments as it likely contained rocks or shaling (gangue). Following separation, these samples (C1 and C2) were dried in an oven drier. The separation process was repeated until the required volume of sample was obtained. After separation process, the weight fractions of C1, C2, and gangue samples were 65, 15, and 20 wt%, respectively. The gangue sample with the ash content around 82 wt% did not examined further. Photographs of C1 and C2 samples are presented in Figure 3-9.

Figure 3-9. C1 and C2 samples

3.3. Multi-stage gasification apparatuses and experimental procedure

The design and construction of the single-line multi-stage gasifier started in 2020. The first trial operation was in September 2021. Both the construction and the operation of the multi-stage gasifier have required a large contribution from the people of the former Institute of Energy and Quality, University of Miskolc.

3.3.1. The single-line multi-stage gasification system

The whole system as shown in Figure 3-10 has been constructed at the University of Miskolc, and experiments have been performed by the former Institute of Energy and Quality.

Figure 3-10. Multi-stage gasification system at the University of Miskolc, Hungary

The schematic diagram of the single-line multi-stage gasification process is demonstrated in Figure 3-11. This system is installed in a 6 m^2 area and 3.40 m of height. The multi-stage gasification system can preliminarily be grouped into three parts, up-stream, down-stream, and control parts. The upstream part includes the fuel feeding system, reactors, electrical heaters, steam generator, and ash collecting system. The downstream part involves the tar collecting system, venturi washer, gas meter, and gas analyser. The control part is used for the automation of the gasification system, as well as the data logging during the gasification process. The main controlled devices are the motors, the steam generator, and the electrical heaters. While the main input parameters are the temperatures along with reactors, the synthesis gas flow rate, the synthesis gas pressure, the water flow rate and

pressure in the venturi scrubber, and the synthesis gas composition from the gas analyser. There are seven separate electrical heaters installed along the whole gasifier. This helps to operate at different temperatures at each segment of the reactor during the gasification process.

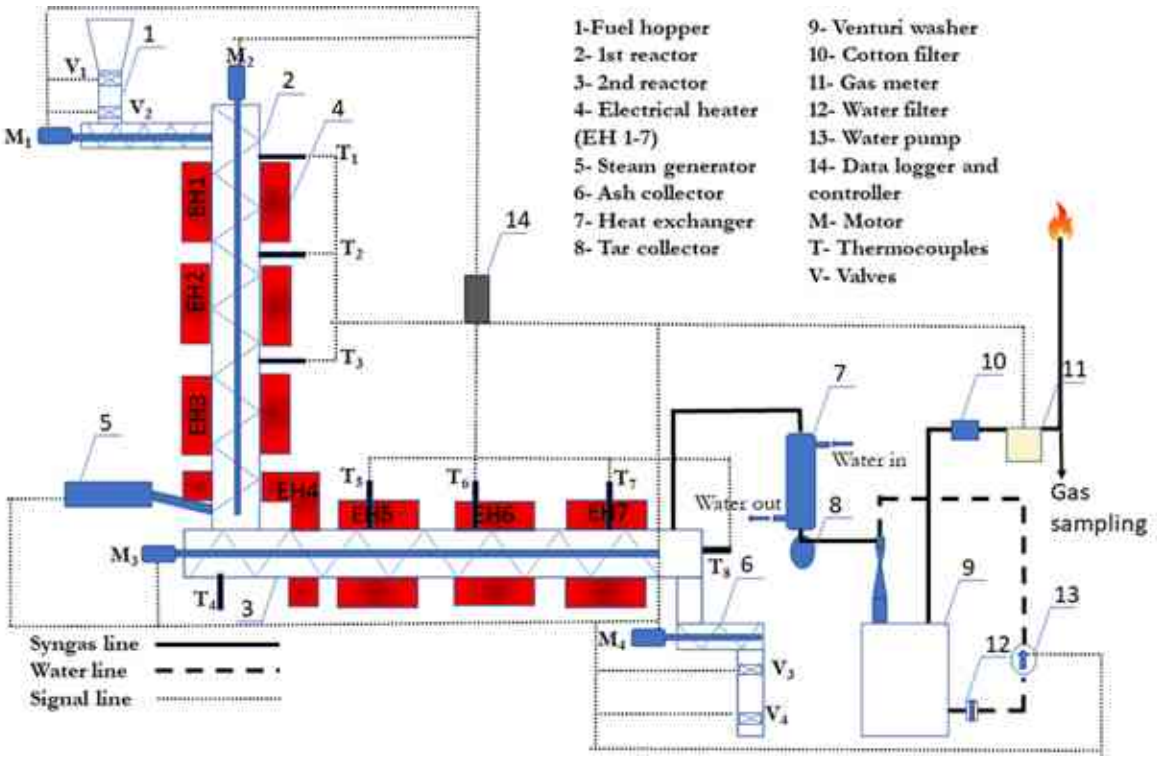

Figure 3-11. Schematic diagram of the multi-stage gasification system

3.3.2. Up-stream part

The up-stream part includes the fuel feeding system, reactors, electrical heaters, steam generator, and ash collecting system.

3.3.2.1. Fuel feeding system

The starting material is fed into a fuel hopper that is located on the top of the 1st reactor, as shown in Figure 3-12. The fuel hopper has a cone shape with 5.60 dm^3 of total capacity. The connecting pipe and fuel transport pipe is made of heat-resistant steel with 88 mm of outer diameter and 80 mm of inner diameter. The starting material will slowly be transported to the auger conveyor through a connecting pipe and fed into the 1st reactor. To separate the gasifier from the ambient environment (synthesis gas – ambient air) the feeding system was equipped with two pneumatic valves that operate in a defined sequence by a Programmable logic controller (PLC). In this multi-stage gasification system, the gasifier is a moving-bed type using auger conveyors (Figure 3-12-right). The rotation of the auger

conveyor is operated through individual electric motors, installed in the fuel feeding system, the 1st reactor, the 2nd reactor, and the ash handling system. The movement speed of the material is adjusted through the speed of motors, they are controlled through the main control panel.

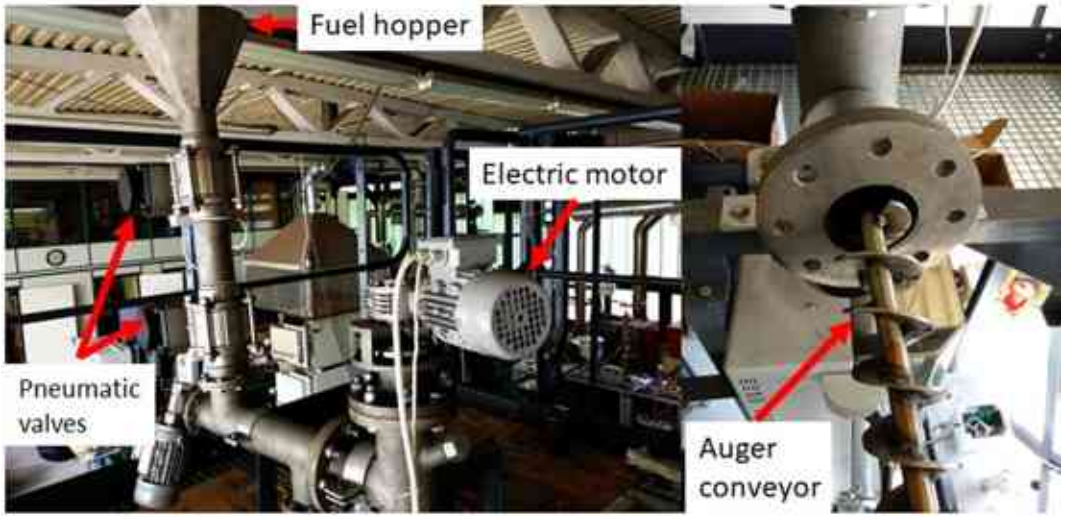

Figure 3-12. Fuel feeding system

3.3.2.2. Reactors and electrical heaters

In the multi-stage gasification system, the gasifier is individually separated into the pyrolysis stage and reduction stage. This will help to improve the gasification efficiency in each stage, as well as the fine-tuning of H_2/CO ratio during the gasification process. As shown in Figure 3-13, the gasifier is in an "L" shape. Where, the 1st and 2nd stages are for the pyrolysis and reduction processes, respectively. The 1st stage is placed in a vertical direction, while the second one is placed in a horizontal direction. The 1st and 2nd stages are connected by a flange. There is a steam inlet at the connection section for the gasification process (at the end of 1st reactor).

The gasifier is made of heat-resistant steel with 100 mm of outer diameter and 80 mm of inner diameter in both stages. The effective length is 1600 mm in each stage and is covered by the electrical heaters. The fuel is transported by the auger conveyor in both stages to prevent the blockage of fuel during the gasification process.

There are 7 electrical ceramic band heaters used to provide the heat required for the gasification process (both pyrolysis and reduction stages), as shown in Figure 3-14. These electrical heaters are individually controlled to reach the optimal temperature for each stage. This heater type has several benefits. Firstly, the diameter of the heater can be adjusted with the diameter of the reactor. It helps to reduce the heat loss during the experiments, as well

as the temperature difference at both ends of the heater. There are three individual heaters arranged along each reactor and one at the connecting section. This improves the flexibility in the initial temperature selection for the experiment. Additionally, the length of the heater can be customized to fit the specific area. Each electrical ceramic band heater is connected individually with a solid-state relay. A solid-state relay is regulated through a PID controller. These PID controllers are also communicated with the main PLC.

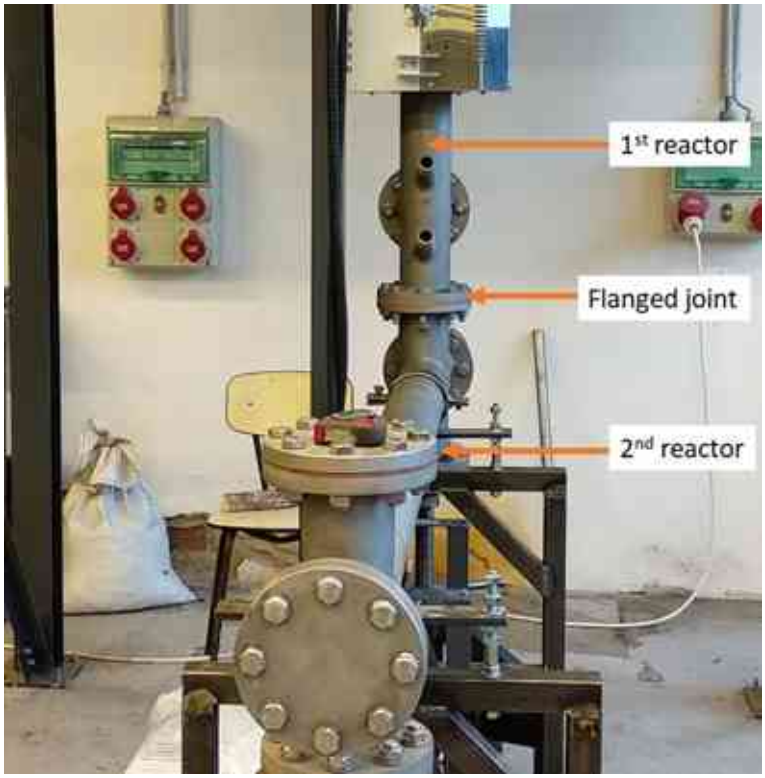

Figure 3-13. The 1st and 2nd reactors

Figure 3-14. Electrical ceramic band heaters

During the gasification process, the gasification temperature along the 1st and 2nd stages will be indicated in the main control screen through the main process controller. The

temperature data will be also recorded for further analysis. The temperatures are recorded using K-type thermocouples with 1.0 mm of 310 stainless steel sheath, as illustrated in Figure 3-15.

Figure 3-15. Thermocouple and mounting point

3.3.2.3. Steam generator

In the gasification process, there are several common gasification reactants used such as air, steam, oxygen, carbon dioxide, or their combination. With the in-situ control of H_2/CO ratio during the gasification process, the utilisation of steam is dominant compared to the other reactants. The steam generator is illustrated in Figure 3-16.

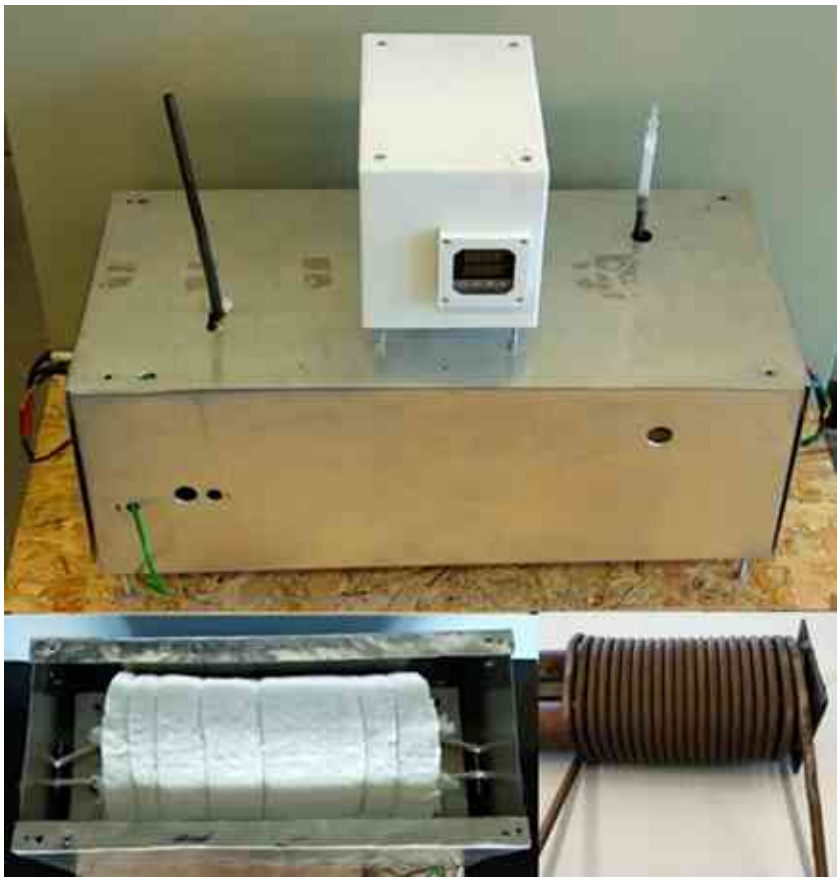

Figure 3-16. Steam generator

The schematic diagram of steam generator is described in Figure 3-17. The heat demand for the evaporation process is provided by three electrical resistance heaters, with 600 W of electrical power for each heater. The temperature of the heating coil is regulated through a PID controller. The distilled water is transported to the heating coil by a peristaltic pump, which is driven by a stepper motor. While the speed of the stepper motor is controlled by a stepper motor driver and the main control panel. The flow rate of steam varies from 1 to 20 g/min at ambient pressure. The temperature of steam can be retained at 300 °C during the experiment period.

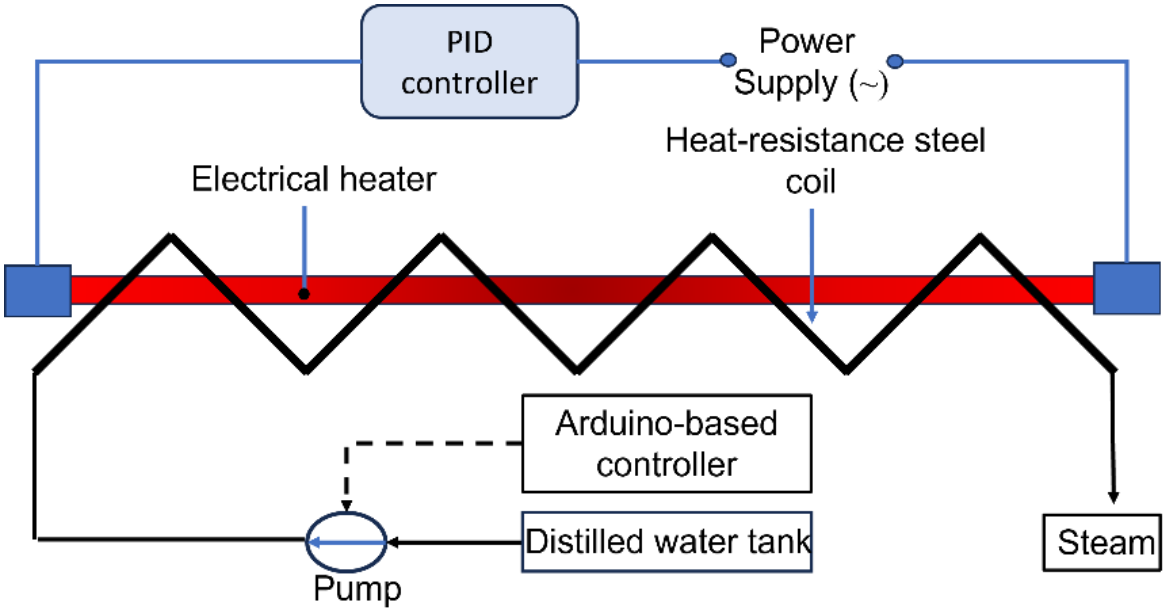

Figure 3-17. Schematic diagram of the steam generator

3.3.2.4. Ash collecting system

After the gasification process, the gasification char will be collected and weighted for further analysis. The gasification char collecting system is installed at the end of the 2nd stage gasifier, as demonstrated in Figure 3-18.

The gasification char will be transported by an auger conveyor to the char collector. At the char collector, there are two pneumatic valves installed in series to separate the gasifier from the ambient air. Like the fuel feeding system and gasifier, the body of the ash collecting system is also made from heat-resistant steel. The outer and inner diameters are 88 and 80 mm, respectively. The moving of the gasification char is indicated by the red dash-line.

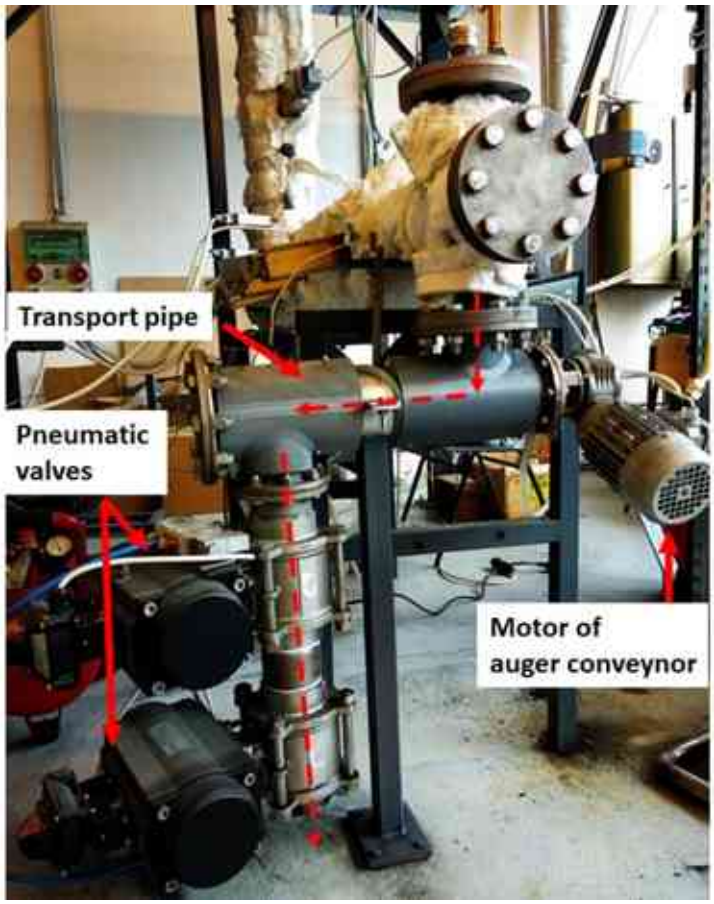

Figure 3-18. Ash collecting system

3.3.3. Down-stream system

The gasification products include the gasification char and the high temperature gasification gas. This gas is mainly composed of H_2, CO, CO_2, CH_4 and impurities. These impurities can be listed as fly ash and condensate ingredients (tar, steam) at low temperatures. After the gasification process in the 2^{nd} stage, the synthesis gas passes through the downstream system. The schematic diagram of the downstream system is described in Figure 3-19.

The heat exchanger is used to cool down the synthesis gas and remove the condensates like tar and steam and particle content. The condensates are collected in a small vessel located below the heat exchanger. And then, the synthesis gas passes through the venturi scrubber to remove the residual solid particles and tar content. In addition, the venturi scrubber also helps to retain a continuous stream of synthesis gas from the gasifier to the burner. The scrubbing liquid is water, that will be circled to create a close loop in the venturi scrubber. To prevent the impurities from the scrubbing liquid barrel from entering the nozzle, the scrubbing water will be filtered. Two parallel water filters are installed in the

system, that can be separately operated and changed if required during the gasification experiment. After the scrubbing process, the synthesis gas is passed through a cotton filter before entering the gas meter. After the gas meter is located a sampling stub for the gas analyser. Finally, the synthesis gas will be burned with a combustion torch.

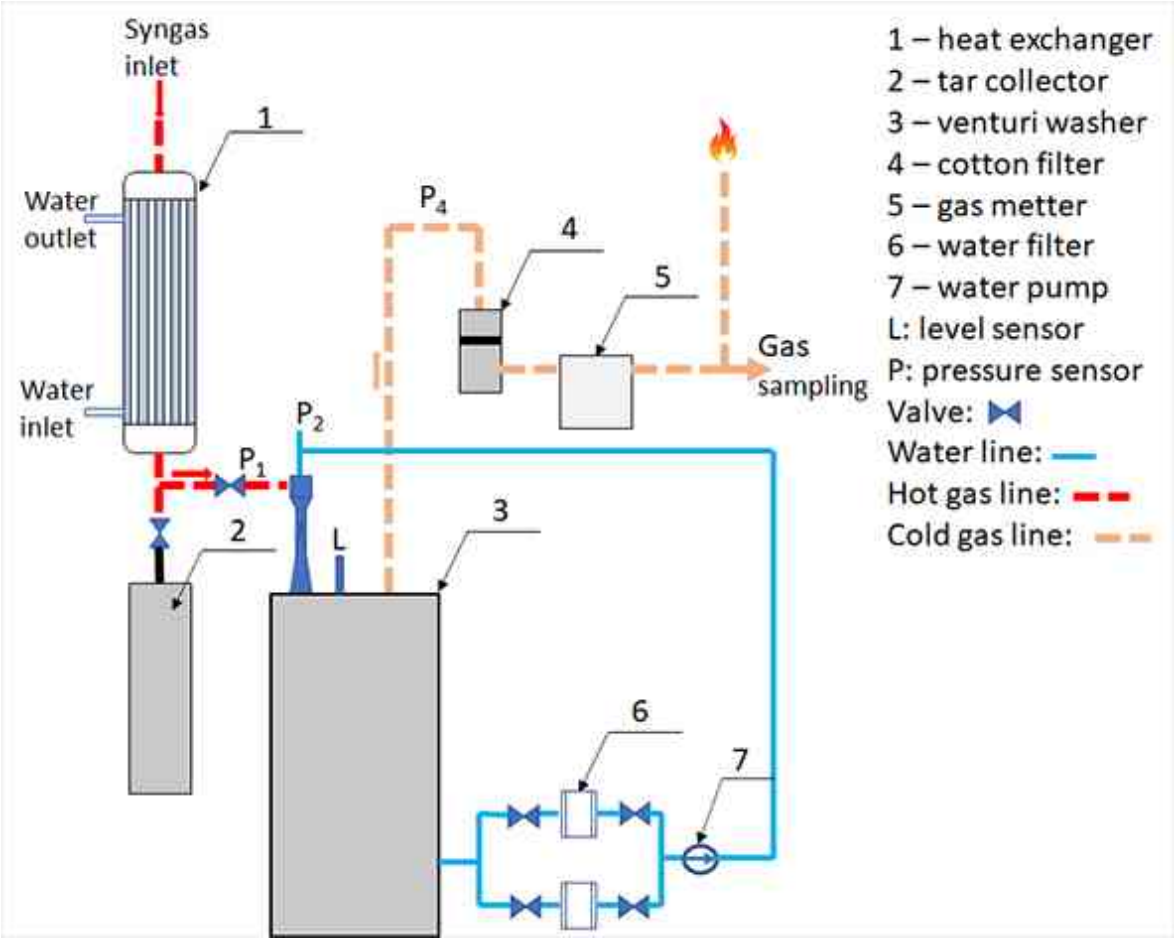

Figure 3-19. Schematic diagram of down-stream system

3.3.4. Programable logic controller

The gasification system is controlled by a programable logic controller. The PLC is responsible for the operation of the main components, as well as for the measurement and storage of operating data. The controlled objects can be listed as the motors, the electrical heaters, the steam generator, and the water pump. The gasification temperature, the syngas pressure, the syngas composition, the syngas volume, as well as the total energy consumption, will be indicated and saved during experiments. The main control system is illustrated in Figure 3-20.

In Figure 3-20, the left side presents the power supply switch, emergency switch, control screen, and seven PID controllers. While the electrical components are shown on the

right-hand side of the picture. The first row includes a 3-phase circuit breaker (Schneider-MCB C32) for the main power supply, a power meter (Tracon electric-TVOF37), and several 1-phase circuit breakers (the power supply for the electrical heater, motors, and other components; Schneider-MCB C25 and C6). In the second row (from the left to the right-hand side), it has a negative and ground terminal, 3 contactors for the control of electrical heaters and motors (Schneider LC1D32 and LC1D256), a 5 V DC supplier (Weidmüller CP SNT 25W), and 12 V DC supplier (Weidmüller Pro Eco 120W). In the 3rd row, there are a 24V DC supplier (Wago 787-732) and a PLC (Wago 750-8102).

Figure 3-20. Programable logic controller

In the 4th, 5th, and 6th rows, the electrical components are used for the operation of 4 motors in the gasification system. To prevent the overheating of motors during the experiments, there are 4 temperature monitoring relays installed in the 4th row (from the left-hand side) (ELKO EP-TER-7). There are 4 variable-frequency drives-VFD (Delta-VFD-EL)

and 4 manual motor starters (ABB-MS-116) assembled in the 5th and 6th row, respectively. The final row includes terminals for the power and control cables to the controlled objects, as well as the input data cables.

3.3.5. Experiment procedure and method of data processing.

3.3.5.1. Experiment procedure

In each experiment, the reactors were heated up to the desired temperature. When the reactor reached the set temperature, the starting material was fed from the fuel hopper to the first stage of the gasifier through a screw conveyor. In the first stage of the gasifier, the pyrolysis process was carried out. Following, the pyrolysis char and gas flowed through to the second stage of the gasifier. In the second stage, the steam was introduced into the gasifier for the reduction reactions. The ash produced from the gasification then was collected in the ash collector. After the gasification process took place, the synthesis gas entered the downstream section. In this section, the removal of tar and particle content took place within the heat exchanger and the venturi scrubber. In the heat exchanger, the synthesis gas was cooled down to collect the condensable components from the produced synthesis gas. The venturi scrubber was mainly used to control the flow rate of synthesis gas and to separate the remaining particles and volatiles from synthesis gas. In the venturi scrubber, the scrubbing water from the bottom of the water tank was pumped through a water filter to remove large size particles before entering the spaying nozzle. The high pressure ensures the atomizing of the washing liquid, which then is turbulently mixed at the throat section of the scrubber with the synthesis gas. In addition, the high-pressure spray of scrubbing liquid creates a vacuum at the gas inlet of the scrubber. Therefore, through the regulation of the liquid pressure in the venturi scrubber, we can set the pressure within the reactor. Finally, the dry synthesis gas passes through the gas meter and is combusted in a burner.

During the experiments, the condensate liquid and char yield was collected and weighed every hour for further analysis. During the gasification process, the temperature of the gasifier was independently regulated for the first and second stages by the controller. The steam flow rate was also controlled through the main control panel. While the temperature along the gasifier, as well as the volume flow rate of synthesis gas, were recorded and monitored by the PLC.

3.3.5.2. Syngas composition analysis

During the experiments, the synthesis gas composition was in-situ analysed with a GASBOARD- 3100P gas analyser, as shown in Figure 3-21.

Figure 3-21. Syngas analyser-GASBOARD-3100P

Table 3-1. Technical index of syngas analyser

Composition	Measur-ement range (%)	Resolution (%)	Linear error (%FS)	Repeatability (%)	Zero drift (%FS)	Span drift (%FS)	Response time (s)
CO	0÷100	0.01	±2	±1	±2	±2	≤15
CO_2	0÷100	0.01	±2	±1	±2	±2	≤15
CH_4	0÷40	0.01	±2	±1	±2	±2	≤15
C_nH_m	0÷20	0.01	±2	±1	±2	±2	≤15
H_2	0÷100	0.01	±3	±1	±3	±3	≤30
O_2	0÷25	0.01	±3	±1	±3	±3	≤60

The synthesis gas composition of CO, CO_2, CH_4 and C_nH_m was measured within a non-dispersive infrared sensor (NDIR sensor). The H_2 concentration was determined by a thermal conductivity detector (TCD sensor), while the O_2 concentration was evaluated by an electron capture detector (ECD sensor). The technical index of the syngas analyser is shown in Table 3-1. To prevent the moisture, particle, and tar contents from entering the syngas analyser, the syngas had to pass through a series of gas filters before entering the syngas analyser. The gas filters included a cotton filter, a silica gel filter, and an activated carbon fibre filter.

3.3.5.3. Data processing

Based on the measured flow rate of synthesis gas, synthesis gas composition and characteristics of starting material, the following factors that influence the performance of the gasification process were calculated:

- Dry syngas yield- Y (Nm^3/kg_{coal})
- The low heating value of syngas- LHV_{syngas} (MJ/Nm^3)
- Carbon conversion efficiency- CCE (%)
- Cold gas efficiency- CGE (%)

Dry syngas yield- Y (Nm^3/kg_{coal})

The volume flow rate of dry syngas ($\dot{Y}$-Nm^3/h) was measured by a gas meter. The dry syngas yield was calculated by dividing the volume flow rate of dry syngas by the mass flow rate of starting material ($\dot{m}$-kg/h), as given in equation-(3-1):

$$Y = \frac{\dot{Y}}{\dot{m}} \left(\frac{Nm^3}{kg_{coal}} \right) \tag{3-1}$$

The low heating value of syngas- LHV_{syngas} (MJ/Nm^3)

The low heating value of dry syngas was determined using the following equation:

$$\mathrm{LHV_{syngas}} = \frac{(\mathrm{H_2} * 10.798 + \mathrm{CO} * 12.636 + \mathrm{CH_4} * 35.818)}{100} \left(\frac{\mathrm{MJ}}{\mathrm{Nm^3}} \right) \tag{3-2}$$

in which, H_2, CO and CH_4 are volume concentrations of components in synthesis gas (V/V%).

Carbon conversion efficiency- CCE (%)

The carbon conversion efficiency (CCE) of the gasification process was calculated by:

$$\mathrm{CCE}(\%) = \left(\frac{12 * \mathrm{Y} * (\mathrm{CO} + \mathrm{CO_2} + \mathrm{CH_4})}{22.40 * \mathrm{C}\%} \right) * 100 \tag{3-3}$$

where C% is the carbon content of the starting material (wt%).

Cold gas efficiency- CGE (%)

The cold gas efficiency (CGE) of the gasification process was determined by:

$$\mathrm{CGE}(\%) = \left(\frac{\mathrm{LHV_{syngas}} * \mathrm{Y}}{\mathrm{LHV_{coal}}} \right) * 100 \tag{3-4}$$

where LHV_{coal} is the low heating value of starting material (MJ/kg).

4. The effects of gasification temperature and steam-to-carbon (S/C) ratio on the multi-stage gasification process of low rank coal from Hungary

This chapter discusses the findings of experiments conducted on the multi-stage gasification of low rank coal from Felsőnyárád, Hungary using pure steam as a reactant. Specifically, it examines the impact of the gasification temperature in the 2nd stage and the S/C ratio on various aspects, including gasification products, syngas composition, gasification performance, and residual solid char characteristics.

4.1. Experimental parameters

The experiments involved varying the gasification temperatures and steam flow rates while maintaining a constant mass flow rate of coal. The pyrolysis temperatures were kept constant at 300 °C at the 1st electrical heater and 600 °C at the 2nd electrical heater. The steam flow rate was determined based on the S/C ratio, which is calculated by dividing the total number of water molecules by the total number of carbon molecules in the feed coal, excluding the carbon content that reacts with oxygen during the gasification process. The experimental conditions are summarized in Table 4-1.

Table 4-1. Experimental conditions for gasification of raw brown coal

Mass flow rate of coal	Gasification temperature	S/C ratio	Steam flow rate	Time of experiment
g/h	°C	mol/mol	g/min	days
		0.75	4.5	3
1084	700	1.00	6.7	3
		1.25	8.8	3
		0.75	4.5	3
1084	800	1.00	6.7	3
		1.25	8.8	3
		0.75	4.5	3
1084	900	1.00	6.7	3
		1.25	8.8	3

In the previous research, I conducted the gasification experiment in a non-moving fixed bed gasifier with the same type of coal. The experiment was carried out initially with 3 kg of coal at the gasification temperatures of 700, 800, and 900 °C and along with different steam flow rates of 5, 7.5, and 10 g/min. These steam flow rates corresponded to S/C ratios of 0.9, 1.3, and 1.8, respectively. After introduction of steam, the reduction process took approximately 200 to 250 minutes, approximately 60 to 80 minutes for 1000 g of coal if a linear reaction is approximated along the reactor tube. Therefore, for the subsequent multi-

stage gasification experiment, a desired mass flow rate was 1000 g/h. On the other hand, the feeding volume of fuel feeder is 1 L, and it took roughly 40 minutes to transport 1 L of fuel into the reactor. Considering that 1 L of the original coal weighed approximately 720 g, consequently, the calculated mass flow rate was around 1084 g/h. The results of the experiment revealed that the dry syngas yield increased slightly as the S/C ratio rose from 1.3 to 1.8. However, the volume fraction of H_2 decreased under the same conditions. Furthermore, the condensate liquid yields were significantly higher at a S/C ratio of 1.8. Therefore, the S/C ratios chosen for the experiment of the multi-stage gasification process in my research were indicated in Table 4-1

4.2. Characteristics of coal sample

The results of the proximate analysis were determined by the thermogravimetric analysis. The TG, DTG, and DTA curves as a function of temperature and time during thermogravimetric analysis are illustrated in Figure 4-1.

The initial weight loss was achieved during the first heating of the coal sample between 50 and 110 ℃, due to the evaporation of moisture content. It reflected in an intensive endothermic peak in the DTA profile at 101.94 ℃. The second weight loss was attributed to the devolatilization process that occurred after the evaporation process. The first exothermic peak in the DTA profile was observed at 837 ℃, and it was related to the self-combustion of the released gas during the devolatilization process. The final weight loss was attributed to the combustion process of the fixed carbon content when switching from an N_2 ambient to an air ambient. Based on the variation of the TG profile, the moisture, volatile, fixed carbon, and ash contents were calculated, and the results are shown in Table 4-2.

The properties of brown coal samples were characterized by elemental and proximate analyses, as well as heating values. The properties of brown coal samples were determined on an as-received basis, as reported in Table 4-2.

The most significant elemental component, carbon, accounted for 35.60 wt%, which is comparable to previous research on coal samples from the same coal basin, such as 35.80 wt% on a dry basis for coal samples from Borsod coal basin [130], and 24.43 and 31.75 wt% on the as-received basis for coal samples from the North-East brown coal basin [122]. The oxygen content in the brown coal sample was high, at 25.14 wt%, which contributed to its relatively low value of heating content. The low heating value of the coal sample was 14.02

MJ/kg. The sulphur, hydrogen, and nitrogen contents were 3.07, 3.39, and 0.72 wt%, respectively.

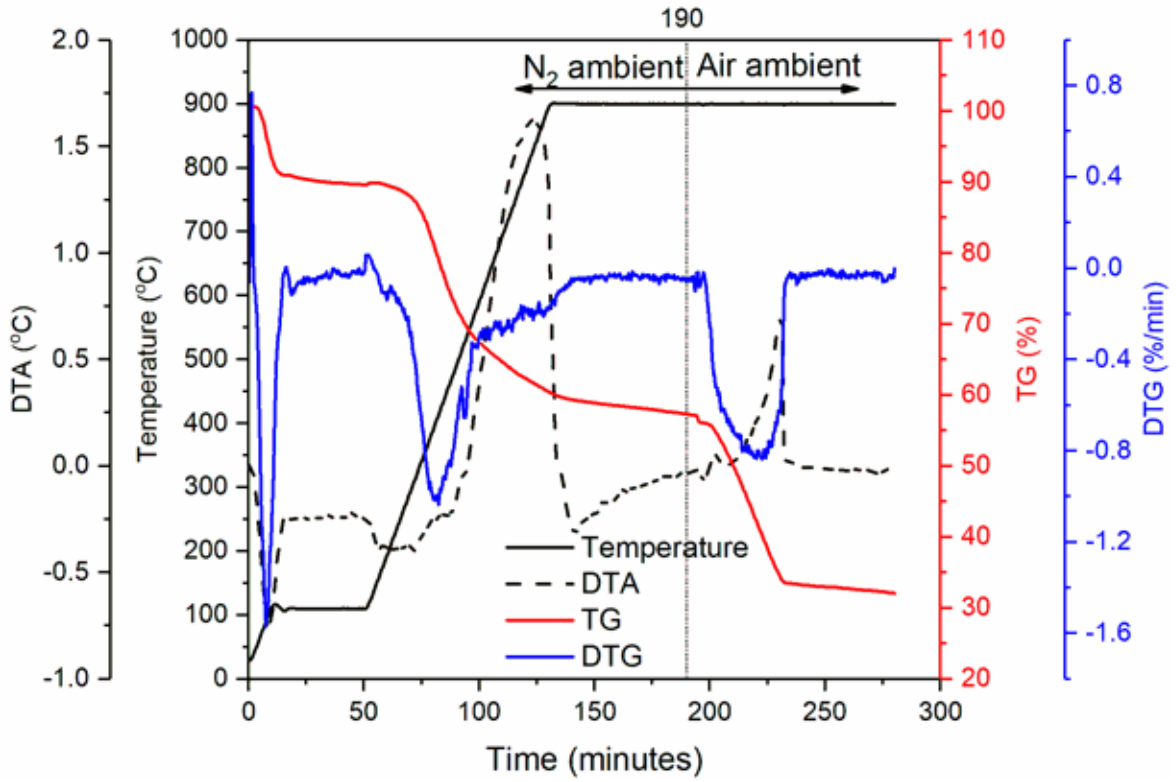

Figure 4-1. TG, DTG, and DTA profiles of low-rank coal sample

Table 4-2. Elemental, proximate and heating value analyses

Elemental analysis (as-received basis)			**Proximate analysis (as-received basis)**		
N	0.72		Moisture	10.37	
C	35.60		Volatile	32.33	
H	3.39	wt%	Fixed carbon	25.22	wt%
S	3.07		Ash	32.08	
O (by diif.)	25.14				
Heating value analysis					
Higher heating value	15.03	MJ/kg			
Lower heating value	14.02				

The results of ash fusion analysis are presented in Figure 4-2, which shows the different temperatures at which the sample shape changes. The initial deformation temperature is the temperature at which the rounding of the edges occurs. At the softening temperature, the sample shape forms a spherical lump. The hemispherical temperature is the temperature at which the sample shape fuses down to a hemispherical lump. Fluid temperature is the temperature at which the sample shape is spread out in a layer. In this

study, the initial deformation, softening, hemispherical, and fluid temperatures were determined to be 1170, 1280, 1320, and 1360 °C, respectively. With the initial deformation temperature of 1170 °C, the chosen gasification temperatures of 700, 800, and 900 °C were suitable for the gasification process under the chemical reaction control.

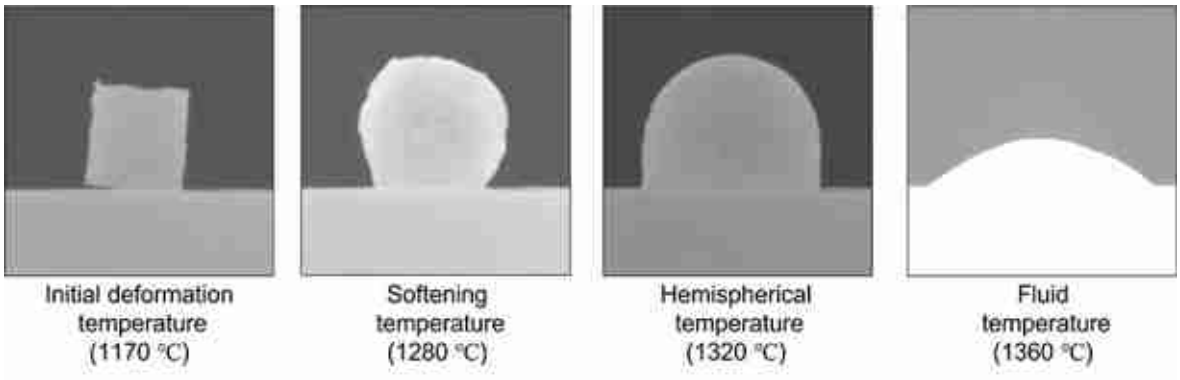

Figure 4-2. Ash fusion analysis of low-rank coal sample

4.3. Data monitoring of a typical experimental day

This section discusses the data for a typical experimental day on 30th, November 2022. In this experiment, the gasification temperature was at 900 °C and the S/C ratio was 1.25. Throughout the experiment, various parameters such as the inside temperature of the reactor, the scrubber water pressure, the suction pressure at the gas inlet of the venturi scrubber, the synthesis gas volume and the synthesis gas composition were continuously recorded in real-time.

The inside temperatures along the gasifier were depicted in Figure 4-3. Before the gasification period, the gasifier was heated up by the electrical heaters without the feeding of coal and steam. The heat required for the pyrolysis stage was supplied by the 1st and 2nd electrical heaters (Figure 3-11) and set at 300 and 600 °C, respectively. The inside temperatures along the pyrolysis stage were indicated by the 1st and 2nd thermocouples (TC1 and TC2). At the end of the heating-up period, TC1 and TC2 were around 230 and 575 °C, which were lower than the setting values of electrical heaters. This could be explained by the fact that the mounting points of TC1 and TC2 are at the ends of heaters, therefore, there was a difference between the temperature at the middle of the electrical heater and thermocouple.

The temperatures along the 2nd stage were designated by TC3, TC5, and TC6. The mounting point of TC3 is above the 3rd electrical heater, resulting in a temperature of around

880 ℃ instead of 900 ℃. In the meantime, the TC5 and TC6 showed 900 ℃. The temperature of the syngas before leaving the gasifier was recorded by TC8. After the feeding of coal and steam, there was a slight decrease in the temperature at TC1 and a steep increase in the temperature at TC8 due to the generation process of syngas. After 90 minutes following the steam introduction, the temperatures stabilized along the gasifier.

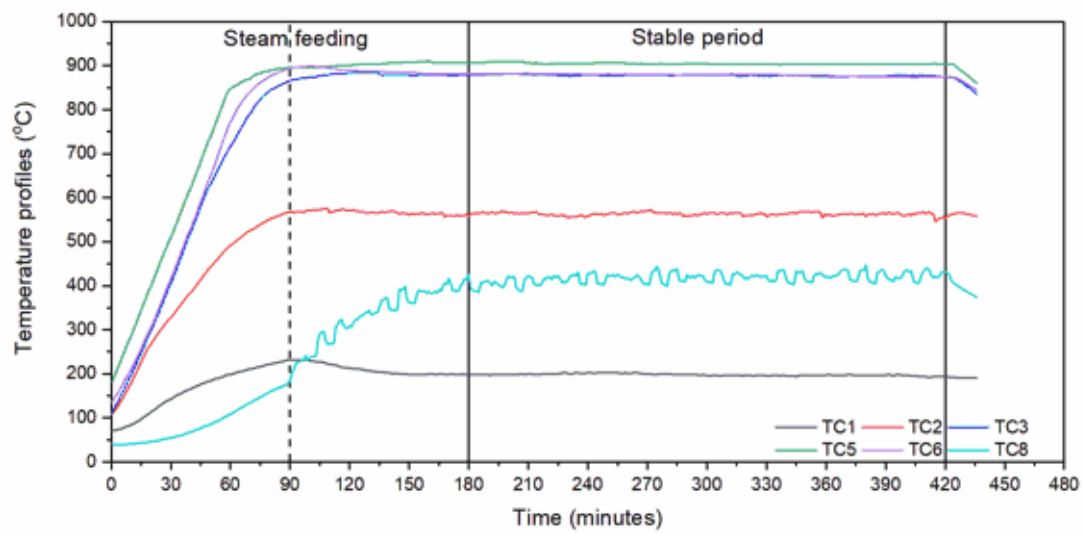

Figure 4-3. The inside temperature profiles along the gasifier

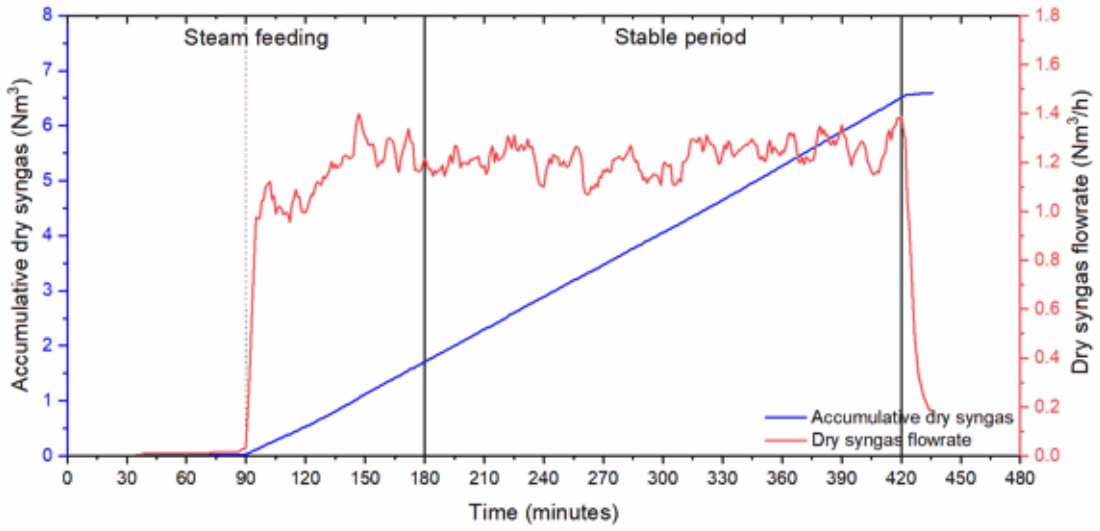

Figure 4-4. Accumulative volume and volume flow rate of dry syngas

The accumulative volume and volume flow rate of syngas are depicted in Figure 4-4. After the steam introduction, the dry syngas flow rate increased rapidly and then gradually until it reached a stable range. In all experiments, it took from 60 to 90 minutes to reach the steady state after the steam feeding. In this experiment, after the steam introduction, the stable period was selected for analysis from 90th minute to 330th minute (4 hours). The

average dry syngas flow rate during this stable period was 1.22 Nm^3/h. Additionally, the accumulation of dry syngas volume steadily increased during the stable period, indicating the presence of a consistent steam gasification process. The stable period was carried out for 4 hours, after that the introduction of steam and coal was stopped. Following, the dry syngas flow rate immediately showed a significant decrease, highlighting the importance of the steam in the gasification process.

Figure 4-5 presents the pressure at the gas inlet and scrubbing water of the venturi scrubber recorded throughout the experiment. During the experimental time, the scrubbing water pump was regulated by the PLC to maintain the suction pressure at the gas inlet of the venturi scrubber at -1 mbar. This ensured a continuous syngas flow from the gasifier to the burner, as well as providing sufficient residence time for syngas in the gasifier. Prior to the feeding of steam and coal, the pressure of scrubbing water was quite low due to the absence of syngas production. After the feeding of steam and coal, there was a significant increase in scrubbing water pressure to maintain the suction pressure at the gas inlet of the venturi scrubber. The pressure at the gas inlet of the venturi scrubber remained stable, averaging at -0.75 mbar without exceeding 0 mbar during the stable period.

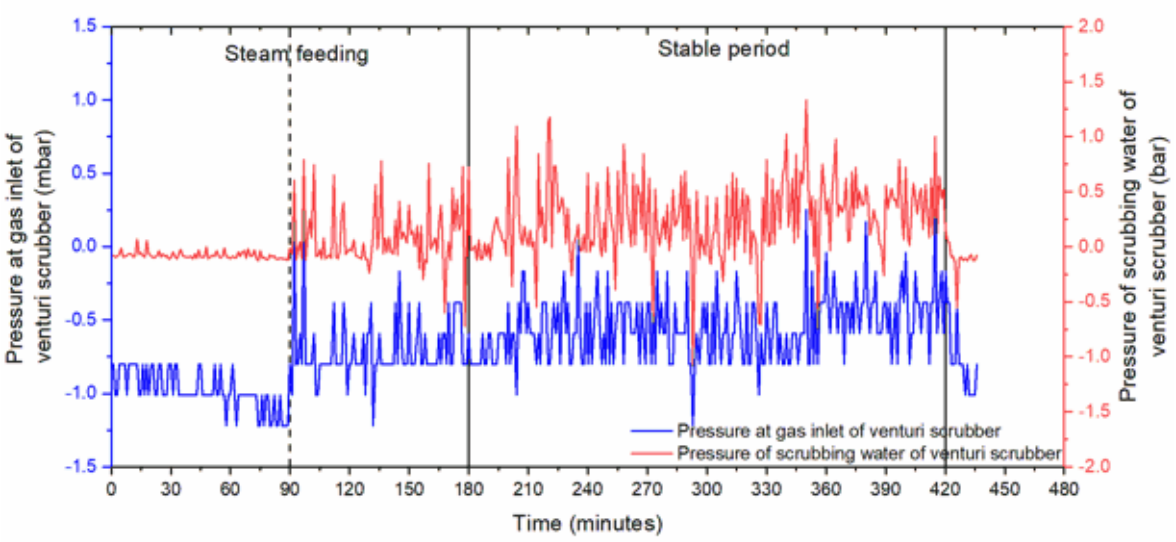

Figure 4-5. Pressure at gas inlet of venturi scrubber and pressure of scrubbing water

Figure 4-6 illustrates the volume fraction of syngas components, including carbon monoxide (CO), carbon dioxide (CO_2), methane (CH_4), long-chain hydrocarbons (C_nH_m), hydrogen (H_2), oxygen (O_2), and nitrogen (N_2) and other gas.

In the heating-up period, there was only a small amount of pyrolysis gas, hence the N_2 and O_2 were dominant components. Following the introduction of coal and steam, the concentrations of H_2, CO, and CO_2 increased significantly, while those of O_2 and N_2

decreased dramatically, almost to 0 V/V% in the case of O_2 and around 1.30 V/V% in the case of N_2 and other gas. After 90 minutes, the volume fractions of syngas reached a stable state. During the stable period, the concentrations of the long-chain hydrocarbon (C_nH_m) and O_2 in the produced gas were nearly unnoticed, which indicated the high reaction rate of the steam reforming reaction of the long-chain hydrocarbons in the steam gasification process. The N_2 and other gas concentrations were under 2% during the stable period. This N_2 content was mainly due to the air entering during the coal feeding process. H_2 was the most abundant gas compound, accounting for around 55.50 V/V% during the stable period. Other main gas components were CO and CO_2, around 27.55 and 13.70 V/V%, respectively. The produced gas also included a small amount of CH_4, lower than 4.00 V/V% in this case. The average volume fraction of H_2, CO, CO_2, and CH_4 reached approximately 98.54 V/V% in total. The graphs of syngas concentrations from other experiments can be found in Appendix 1-Graphs of syngas concentration.

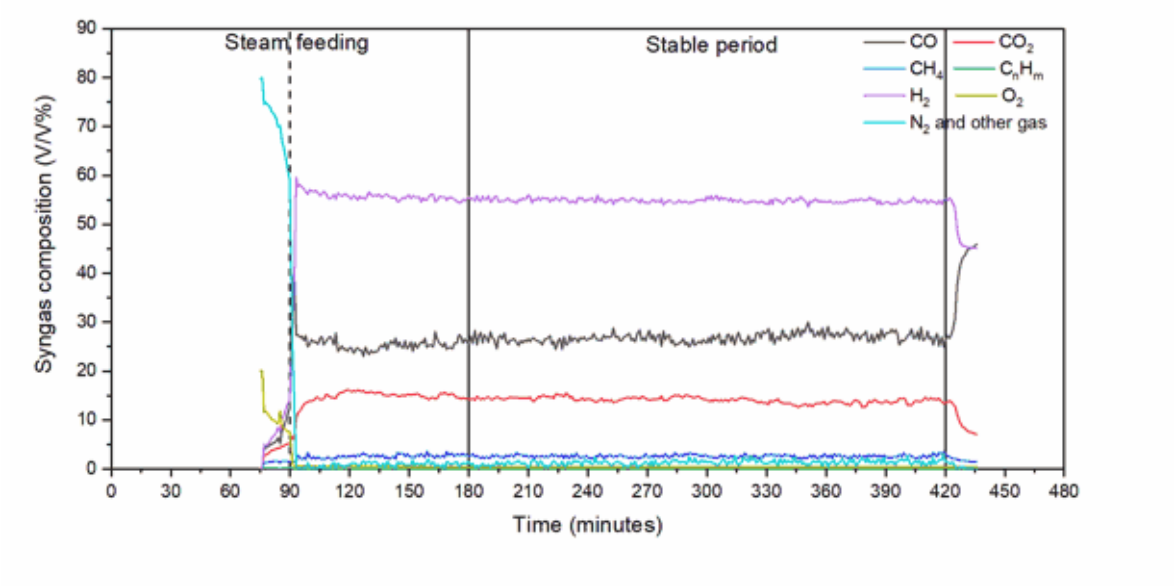

Figure 4-6. Syngas composition

The low heating value of syngas- LHV_{syngas} and H_2/CO ratio are shown in Figure 4-7. The LHV_{syngas} was primarily influenced by the major combustible syngas components, including H_2, CO, and CH_4, as expressed in equation (3-2). The LHV_{syngas} increased immediately after the feeding of coal and fuel, due to the increase in the H_2 and CO concentrations. Consequently, it decreased steadily and reached a stable value of 10.22 MJ/Nm^3. The H_2/CO ratio was governed by the molar fraction of H_2 and CO, which varied within a range of 2.29÷1.79. The trial average value of the H_2/CO ratio was 2.05 in this experiment.

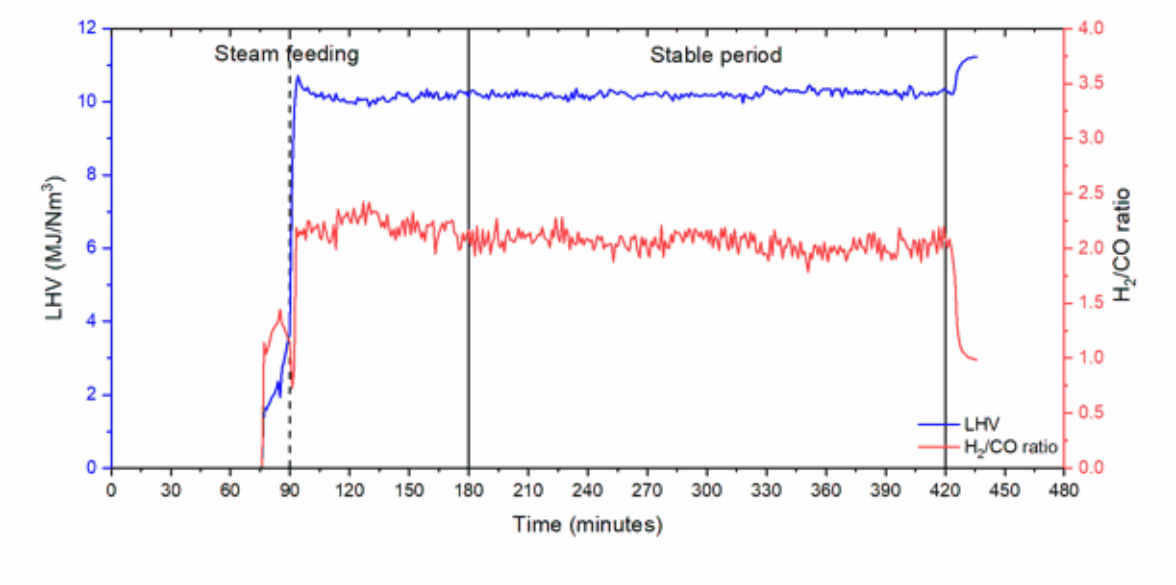

Figure 4-7. Low heating value of syngas and H_2/CO ratio

4.4. Effects of gasification temperatures and S/C ratio on gasification products

This section discusses the effects of gasification temperature and S/C ratio on gasification products, including char, liquid, and dry gas yield. The experiments were conducted at 700, 800, and 900 ℃ of the gasification temperature. The S/C ratio was studied at 0.75, 1.00, and 1.25 at each gasification temperature condition.

4.4.1. Effects of gasification temperatures and S/C ratio on char yield

At each gasification condition (temperature and S/C ratio), the experiment was conducted for at least 3 days. During the experiment, the char and condensate liquid yields were collected and weighed every hour for further analysis. Due to the continuous experiments and a slow movement of material, therefore the char and liquid yields were the mean value of char and condensate liquid collected during the last 3 hours on the last day at each experiment condition. The detail data of char and condensate liquid yields are presented in Appendix 2- Products of the experiments of the original coal sample. The mean value of char yield as a function of gasification temperature and S/C ratio is demonstrated in Figure 4-8.

The char yield showed a decreasing trend as the gasification temperature was increased from 700 to 900 ℃ across all S/C ratios. At 0.75 and 1.00 of the S/C ratios, the char yield declined slightly when the gasification temperature increased from 700 to 800 ℃, followed by a significant decrease when the gasification temperature was raised to 900 ℃. At an S/C ratio of 0.75, the char yield was 622.73 g/h at 700 ℃, 599.65 g/h at 800 ℃, and

488.27 g/h at 900℃. At 1.00 of the S/C ratio, the corresponding values were 580.87, 567.97, and 407.10 g/h, respectively. The lowest char yield reached 900 ℃ and 1.25 of the S/C ratio, approximately 373.03 g/h.

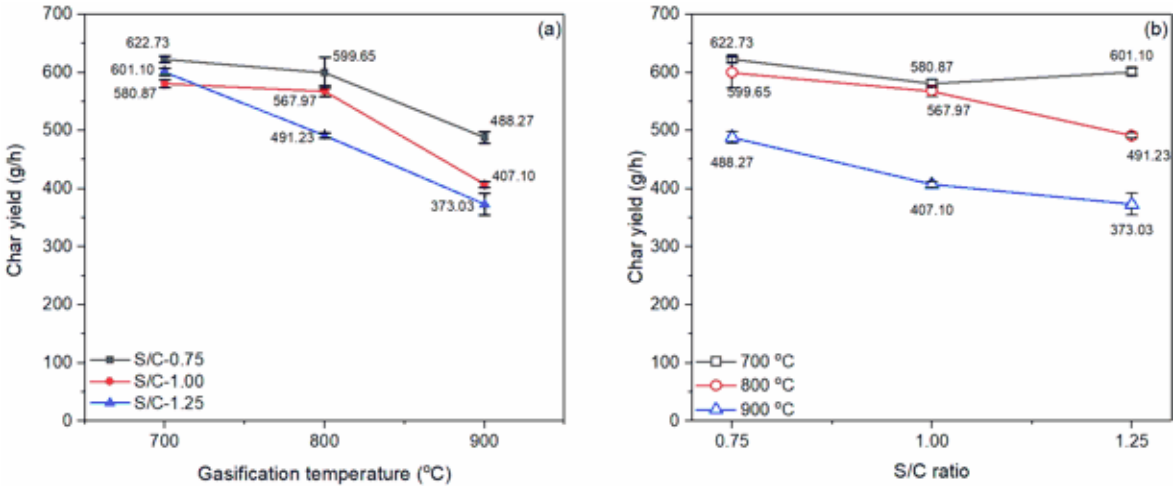

Figure 4-8. The effects of gasification temperature (a) and S/C ratio (b) on char yield

The char yield decreased when the S/C ratio increased from 0.75 to 1.25 under the same condition of gasification temperatures. However, in the case of 700 ℃, the char yield increased from 580.87 g/h to 601.10 g/h when the S/C ratio varied from 1.00 to 1.25. This could be attributed to the higher steam flow rate at low gasification temperature, which lowered the local temperature inside the gasifier, resulting in a lower conversion rate of char. Moreover, at higher gasification temperatures, the decrease in char yield was more prominent as the S/C ratio increased from 0.75 to 1.25. At 800 ℃ of gasification temperature, the char yield decreased by 18.08 % as the S/C ratio increased from 0.75 to 1.25, while at 900 ℃, the decrease was by 23.61 %.

4.4.2. Effects of gasification temperatures and S/C ratio on liquid yield

Figure 4-9 illustrates the effects of gasification temperature and S/C ratio on the mean value of condensate liquid yield.

The condensate liquid yield decreased significantly with the increase of the gasification temperature while maintaining the same S/C ratio. At an S/C ratio of 0.75, the amount of condensate liquid dropped from 327.9 g/h to 85.10 g/h at gasification temperatures of 700 and 900 ºC, respectively. The corresponding numbers for an S/C ratio of 1.25 were 432.5 g/h at 700 ºC and 269.2 g/h at 900 ºC. These findings clearly indicate a significant variation in the condensate liquid yield at each S/C ratio as the gasification

temperature increased from 700 to 900 °C, with a decrease of 74.05 % and 37.75 % observed at S/C ratios of 0.25 and 1.25, respectively.

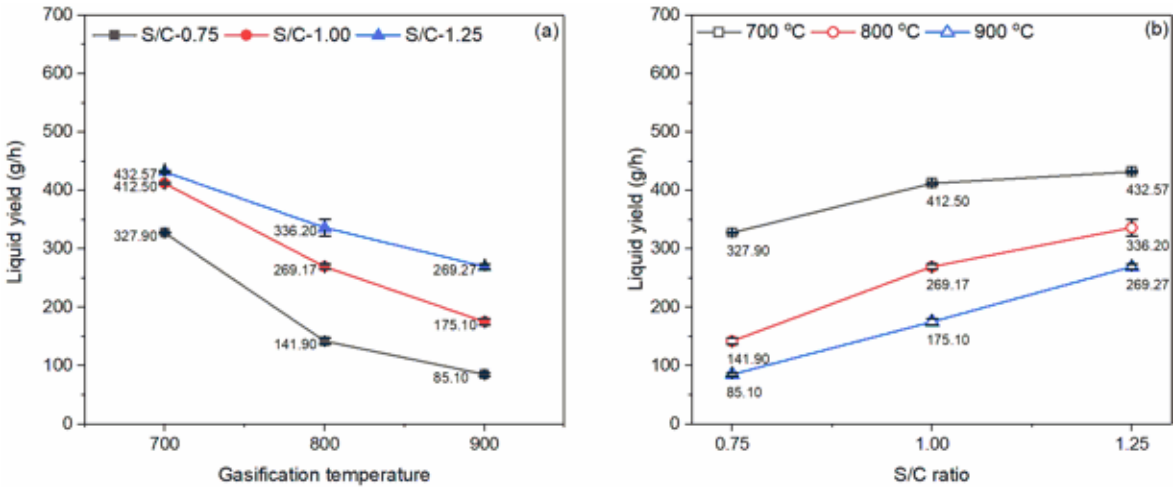

Figure 4-9. The effects of gasification temperature (a) and S/C ratio (b) on condensate liquid yield

At a constant gasification temperature, the greater S/C ratio resulted in a higher condensate liquid yield. This could be explained by the fact that a higher S/C ratio necessitated a greater introduction of steam quantity into the gasifier.

4.4.3. Effects of gasification temperatures and S/C ratio on dry gas yield

The effects of gasification temperature and S/C ratio on dry gas yield are illustrated in Figure 4-10. At a constant S/C ratio, the dry gas yield increased significantly with the increasing gasification temperature. For instance, at a gasification temperature of 700 °C and 0.75 S/C ratio, the dry gas yield was only 0.41 Nm^3/kg_{coal}. However, the dry gas yield increased approximately 2 times at 900 ºC of gasification temperature, reaching 0.85 Nm^3/kg_{coal}. The positive impact of increasing gasification temperature on dry gas yield was more remarkable at a higher S/C ratio. The dry gas yield generated at 900 ºC was 2.3 and 2.6 times higher than that at 700 ºC for the S/C ratios of 1.00 and 1.25, respectively. The increase in dry gas yield at higher gasification temperatures could be explained by two aspects. Firstly, the higher gasification temperature promoted the thermal cracking (equation-(4-1)) and steam reforming (equation-(2-10)) reactions of the tar content [12,19,20]. Secondly, the endothermic reactions (Boudouard reaction-(2-4), water gas reaction-(2-5)) were promoted by increasing gasification temperature [39,41].

$$Tar \rightarrow light\ hydrocarbons + gases \quad (4\text{-}1)$$

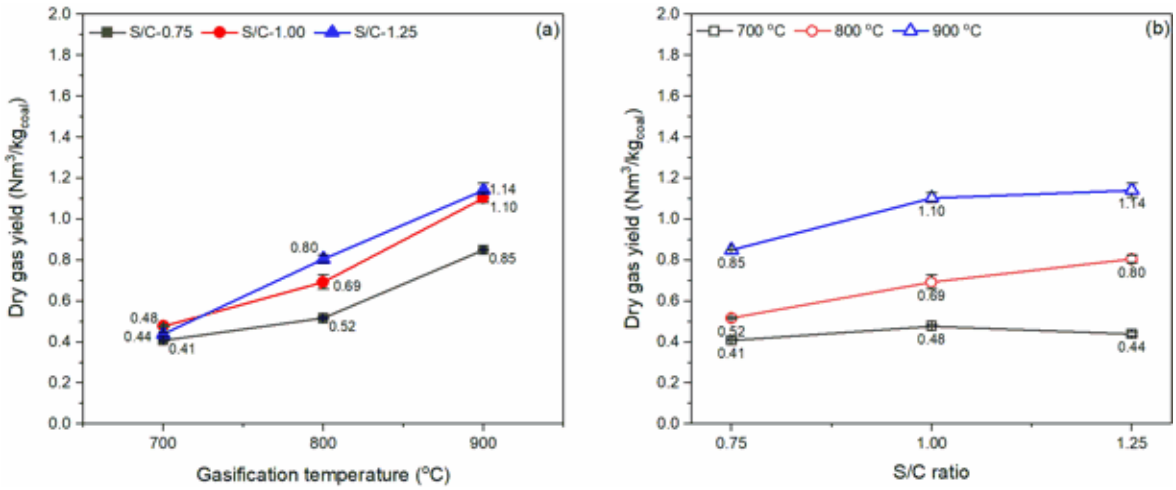

Figure 4-10. The effects of gasification temperature and S/C ratio on dry gas yield

At constant gasification temperature, the dry gas yield increased remarkably if the S/C ratio increased from 0.75 to 1.00 and they increased slowly if the S/C ratio increased further from 1.00 to 1.25. At 700 ºC, dry gas yield decreased slightly when the S/C ratio increased from 1.00 to 1.25, from 0.48 Nm^3/kg_{coal} to 0.44 Nm^3/kg_{coal}. This means that the positive effects of increasing the S/C ratio on char gasification were limited at this temperature below the 1.25 S/C ratio. The highest dry gas yield was 1.14 Nm^3/kg_{coal} at 900 ºC of gasification temperature and 1.25 of S/C ratio. An increase in the dry gas yield as an increasing S/C ratio could be explained mainly by the introduction of higher steam quantity, which improved the reaction rate of water gas reaction (equation-(2-5)) [39,48,49]. However, the excess steam at a low temperature (in the case of 700 °C) led to a decrease in the local temperature of the gasifier, consequently, the gas yield degraded [49,50].

4.5. Effects of gasification temperature and S/C ratio on syngas composition

This section discusses the effects of gasification temperature and S/C ratio on syngas composition, the low heating value of syngas, as well as H_2/CO ratio.

4.5.1. Syngas composition

In this study, the main components of syngas were CO, CO_2, CH_4, and H_2, accounting for an average of 95÷96.30 V/V% at 700 °C, 96.70÷97.30 V/V% at 800 °C, and above 98 V/V% at 900 °C. Therefore, the discussion focuses on these gas components in this section. The details of the syngas composition are summarised in Appendix 3- Average syngas concentration from the experiments of the original coal sample, with mean, maximum, minimum, and standard deviation values.

Figure 4-11 shows the effect of gasification temperature on the volume fraction of H_2 at various S/C ratios. At a constant S/C ratio, the changes in H_2 concentration did not appear monotonic trend when the gasification temperature increased from 700 to 900 °C. Initially, it increased first and then slightly decreased. It is evident from Figure 4-11 that the influence of gasification temperature on H_2 concentration was greater at lower S/C ratios compared to higher ones. For instance, at 0.75 of the S/C ratio the H_2 concentration increased from 52.96 V/V% at 700 °C to 55.04 V/V% at 800 °C and subsequently decreased to 54.03 V/V% at 900 °C. At 1.25 of the S/C ratio, the corresponding values were 54.29, 55.57, and 54.76 V/V%, respectively. At a constant gasification temperature, a slight increasing trend in the H_2 concentration was observed when the S/C ratio increased from 0.75 to 1.25 at a constant gasification temperature. At 700 °C of gasification temperature, the H_2 concentration increased from 52.96 V/V% at 0.75 to 54.29 V/V% at 1.25 of the S/C ratio. In the meantime, the increases in H_2 concentration were only by 0.53 V/V% at 800 °C and by 0.73 V/V% at 900 °C (as shown in Figure 4-11).

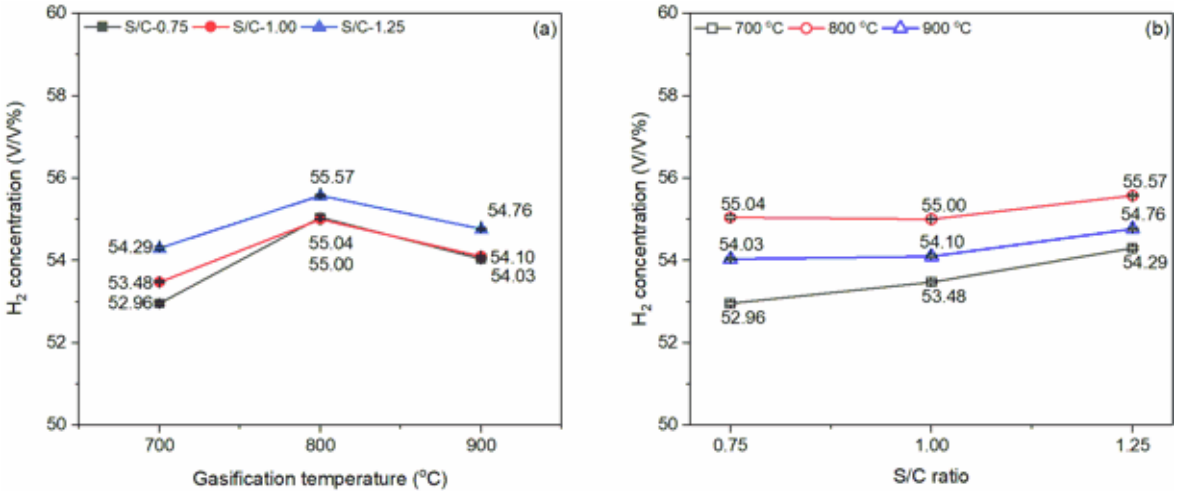

Figure 4-11. H_2 concentration as a function of gasification temperature (a) and S/C ratio (b)

The influence of gasification temperature and S/C ratio on the volume fraction of CO is presented in Figure 4-12. At a constant S/C ratio, the volume fraction of CO increased significantly when the gasification temperature rose from 700 to 900 °C. Moreover, the increase in CO volume fraction was relatively consistent across all S/C ratios with the increasing gasification temperature. For instance, at 0.75 S/C ratio, the CO volume fraction was 8.56 V/V% at 700 °C of gasification temperature, but it increased to 31.38 V/V% at 900 °C, representing around 3.7 times higher. Similarly, in the case of 1.00 and 1.25 S/C ratio, the corresponding increases were 3.85 and 3.87 times higher at 900 °C of gasification temperature, respectively. At all experimental gasification temperatures, the increase in the

S/C ratio resulted in the decline of the CO volume fraction. When the S/C ratio increased from 0.75 to 1.25, the volume fraction of CO dropped from 8.56 to 7.12 V/V% at 700 °C, from 22.32 to 17.52 V/V% at 800 °C, and 31,38 to 27.55 V/V% at 900 °C.

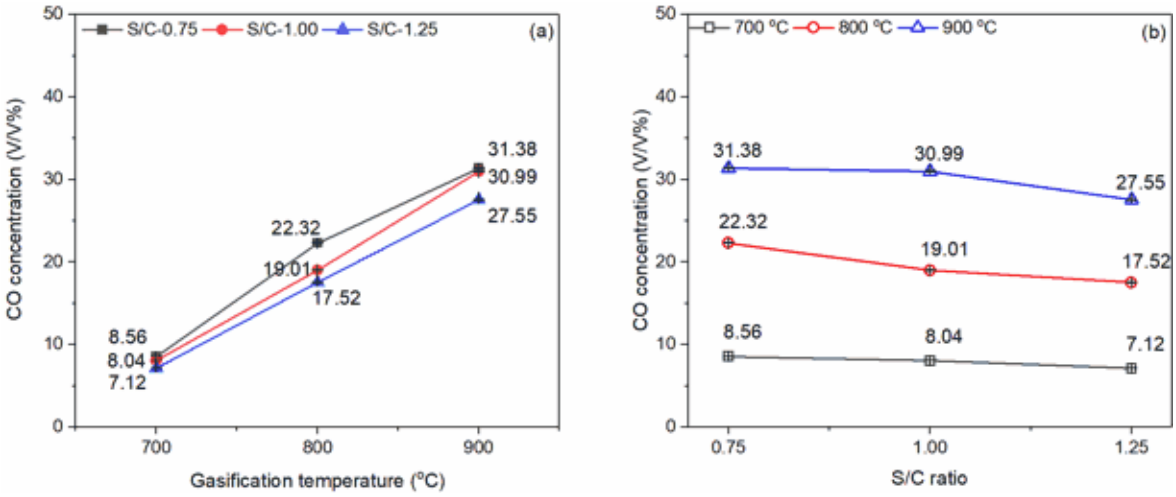

Figure 4-12. CO concentration as a function of gasification temperature (a) and S/C ratio (b)

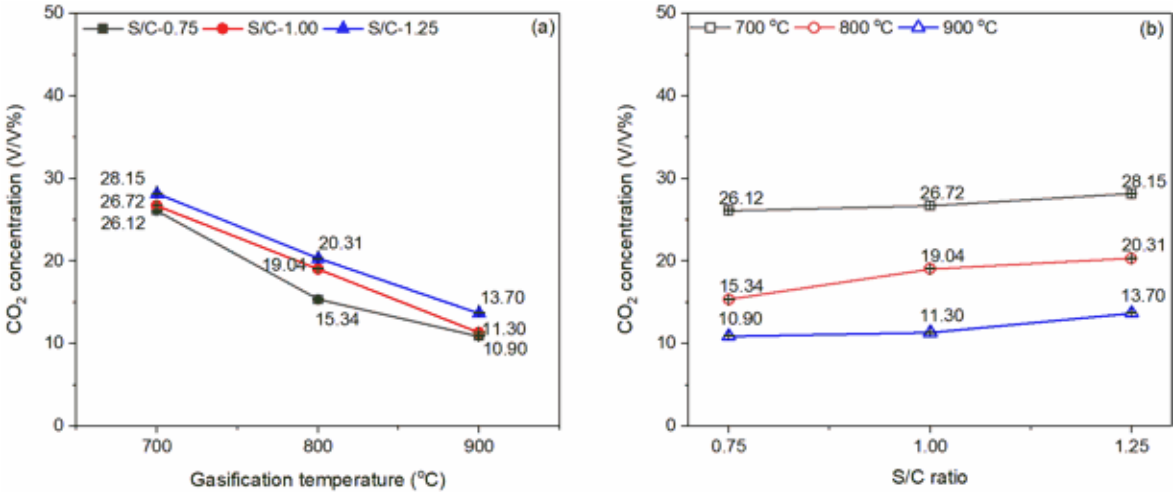

Figure 4-13. CO_2 concentration as a function of gasification temperature (a) and S/C ratio (b)

According to the results shown in Figure 4-13, the behaviour of CO_2 volume fraction was found to be completely opposite to that of CO volume fraction. Specifically, the CO_2 volume fraction exhibited a continuous decrease at all experimental S/C ratio conditions when the gasification temperature increased from 700 to 900 °C. The magnitude of the decrease in CO_2 volume fraction was also analogous across all S/C ratios. At 0.75 S/C ratio, the volume fraction of CO_2 decreased by around 2.4 times within the gasification temperature range of 700 to 900 °C (from 26.12 V/V% to 10.90 V/V%). That numbers were 2.36 and 2.05 times at 1.00 and 1.25 S/C ratios, respectively. In contrast, at a constant gasification temperature, increasing the S/C ratio led to an increase in the volume fraction

of CO_2. Notably, at 700 and 900 °C of gasification temperature, the CO_2 volume fraction visibly increased within the range of 1.00 to 1.25 S/C ratio, while a clear increase in CO_2 volume fraction was observed within the range of 0.75 to 1.00 S/C ratio at 800 °C.

Figure 4-14 reports the effects of gasification temperature and S/C ratio on CH_4 concentration, which did not exceed 8 V/V% in all experiments. As is observed in Figure 4-14, increasing gasification temperature caused a notable decrease in the concentration of CH_4. At 700 °C of gasification temperature, the CH_4 concentration slightly dropped from 7.18 V/V% at 0.75 to 6.61 V/V% at 1.25 S/C ratio. However, at 800 and 900 °C of gasification temperature, the CH_4 concentration was stable as the S/C ratio increased from 0.75 to 1.25. The lowest CH_4 concentration was observed at 900 °C of gasification temperature, approximately 2.5 V/V%.

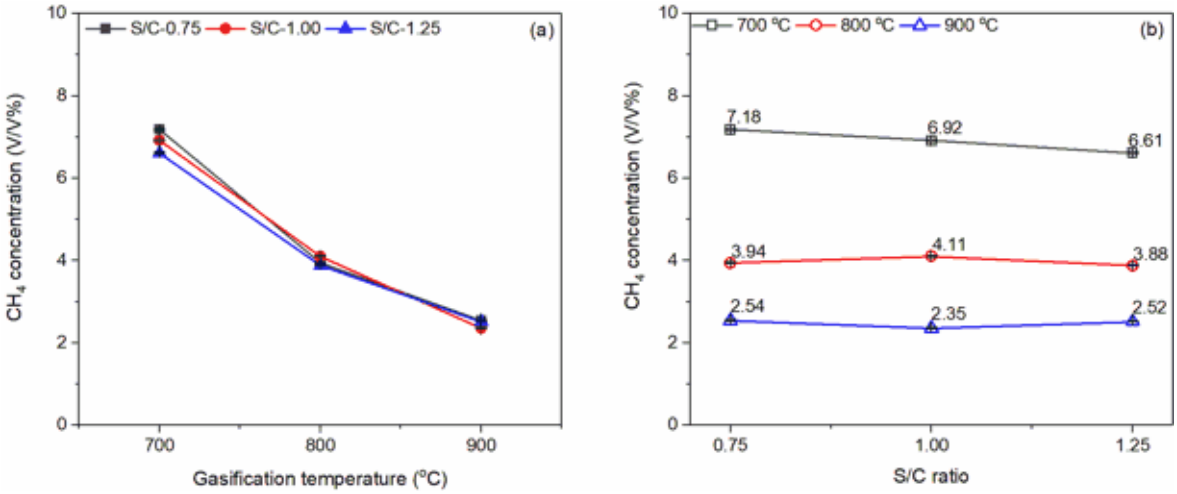

Figure 4-14. CH_4 concentration as a function of gasification temperature (a) and S/C ratio (b)

The variation of syngas concentration could be a result of the strengthening of endothermic reactions (Boudouard reaction-(2-4), water gas reaction-(2-5), methane reforming reaction-(2-8), and tar reforming reaction-(2-10)) by increasing gasification temperature [11,39,41,131]. Therefore, the more CO and H_2 generated and the more CO_2 and CH_4 were consumed during the gasification process.

The water-gas shift reaction-(2-7) is an exothermic reaction, consequently, it was pushed backwards when the gasification temperature was higher than the equilibrium temperature [37,44]. Therefore, it led to a slight drop in the H_2 volume fraction when the gasification temperature increased from 800 to 900 ºC.

The results discussed above indicate that the higher S/C ratio increased the reaction rate of water gas reaction-(2-5), methane reforming reaction-(2-8), and water-gas shift reaction-(2-7) [50,132,133]. Therefore, there were a slight increase in the concentrations of

H_2 and CO_2 and a decrease in the concentrations of CO and CH_4 as increasing in the S/C ratio.

4.5.2. Lower heating value and H_2/CO ratio

The LHV_{syngas} is a key characteristic of syngas from an energetic point of view. The LHV_{syngas} as functions of the gasification temperature and S/C ratio is illustrated in Figure 4-15. The LHV_{syngas} were calculated based on the volume fraction of combustible gases, such as H_2, CO, and CH_4, as mentioned in section 3.3.5.3. Therefore, the tendency of the curves of LHV_{syngas} was sensitive to the changes in the volume fraction of combustible gas. The LHV_{syngas} varied in a range of 9.2 to 10.7 MJ/Nm^3. The volume fraction of CO increased significantly with an increase in the gasification temperature. It led to an increase in the LHV_{syngas}. In addition, when the S/C ratio increased, the volume fraction of CO and CH_4 decreased relatively such that the LHV_{syngas} showed a downward trend when the S/C ratio increased from 0.75 to 1.25. The highest LHV_{syngas} reached 10.69 MJ/Nm^3 at 900 ºC of the gasification temperature and 0.75 S/C ratio.

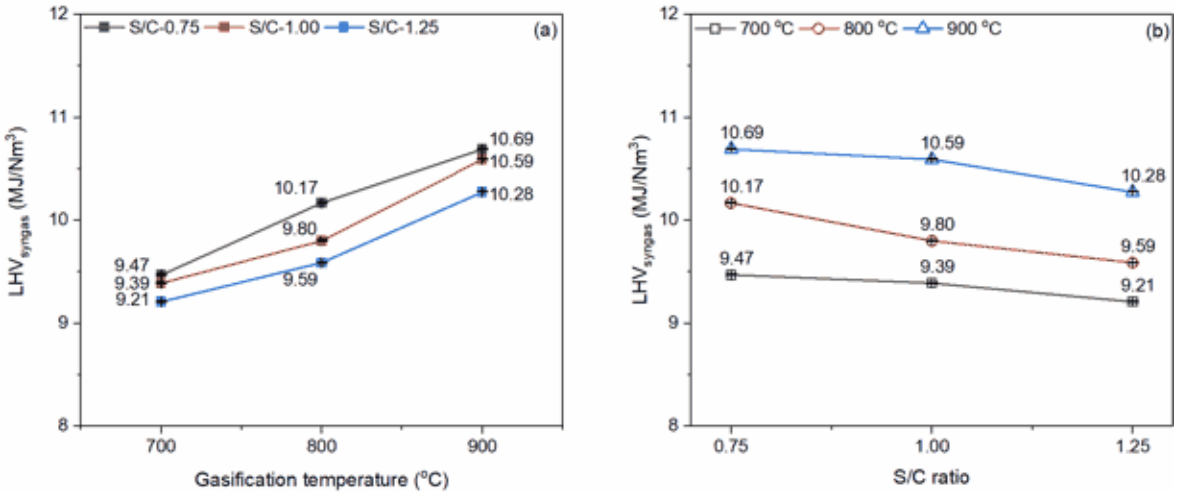

Figure 4-15. The lower heating value of syngas as a function of gasification temperature (a) and S/C ratio (b)

Figure 4-16 depicts the effects of the gasification temperature and S/C ratio on the H_2/CO ratio. As discussed above, the H_2 concentration increased slightly when the gasification temperature increased from 700 to 900 ºC, while the CO concentration increased significantly. Consequently, the H_2/CO ratio decreased with an increase in the gasification temperature. The H_2/CO ratio was above 6 at 700 ºC and then declined to around 2 at 900 ºC of the gasification temperature. In addition, the increase in the S/C ratio resulted in a decrease in CO concentration, with no significant variation in the H_2 concentration. Therefore, the H_2/CO ratio increased with the rising of the S/C ratio from 0.75 to 1.25,

especially at 700 ºC of the gasification temperature. At 700 ºC, the H_2/CO ratio increased from 6.19 at 0.75 S/C ratio to 7.63 at 1.25 S/C ratio. That numbers were 1.72 and 1.99, respectively, at 900 ºC of the gasification temperature.

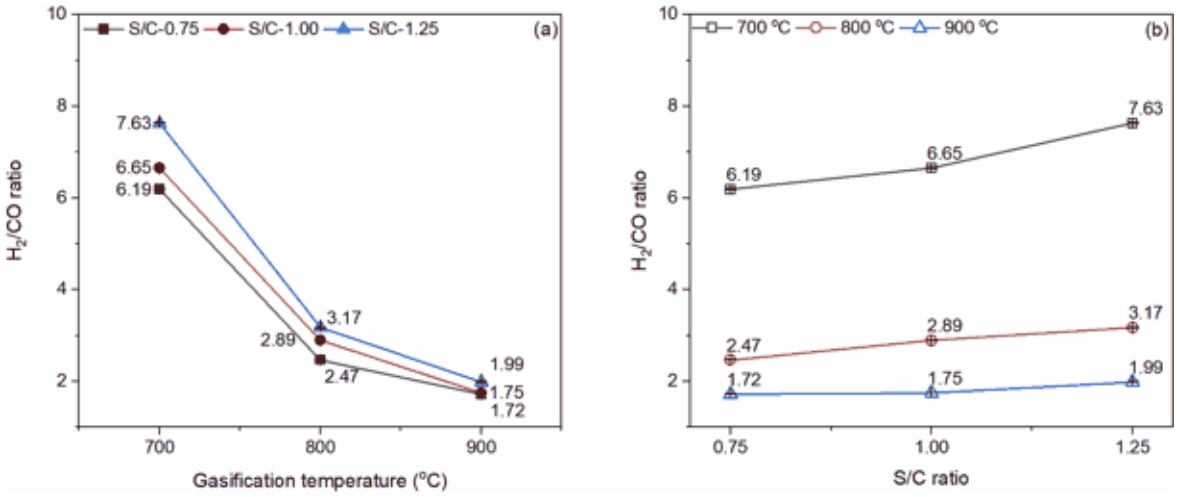

Figure 4-16. H_2/CO ratio as a function of gasification temperature and S/C ratio

4.6. Effects of gasification temperatures and S/C ratio on gasification performance

This section discusses the effects of gasification temperature and S/C ratio on gasification performance, including carbon conversion efficiency, cold gas efficiency, power consumption, and energy balance.

4.6.1. Carbon conversion efficiency and cold gas efficiency

Carbon conversion efficiency-CCE depends on the dry gas yield, as well as the volume fraction of CO, CO_2, and CH_4, as expressed in the equation-(3-3). When the gasification temperature increased from 700 to 900 ºC, the total volume fraction of CO, CO_2, and CH_4 slightly increased only by around 3 V/V% at 0.75 and 1.00 of steam ratio and by around 2 V/V% at 1.205 of steam ratio. Therefore, the dry gas yield played an important role in the change in the CCE when the gasification temperature rose from 700 to 900 ºC. As is observed in Figure 4-17, the increasing gasification temperature increased the CCE. The highest CCE was 75.32 % at 900 ºC of the gasification temperature and 1.00 S/C ratio.

At each temperature condition, the CCE increased significantly as the increasing S/C ratio from 0.75 to 1.00. Then the CCE decreased slightly when the S/C ratio increased to 1.25. At a gasification temperature of 700 ºC, the CCE was found to be 26.06 % at an S/C ratio of 0.75. However, the CCE increased to 30.43 % when the S/C ratio was increased to 1.00 and decreased to 27.94 % when the S/C ratio was further increased to 1.25. Similarly,

at a gasification temperature of 800 ℃, there was a monotonic increase trend in the CCE. the CCE was 32.57 %, which increased to 43.8 % at an S/C ratio of 1.00 and further increased to 50.22 % at an S/C ratio of 1.25 Furthermore, at 900 ℃ of the gasification temperature, the CCE was found to be 57.34 % at an S/C ratio of 0.75 and increased to 75.32 and 75.09 % at 1.00 and 1.25 of the S/C ratios, respectively.

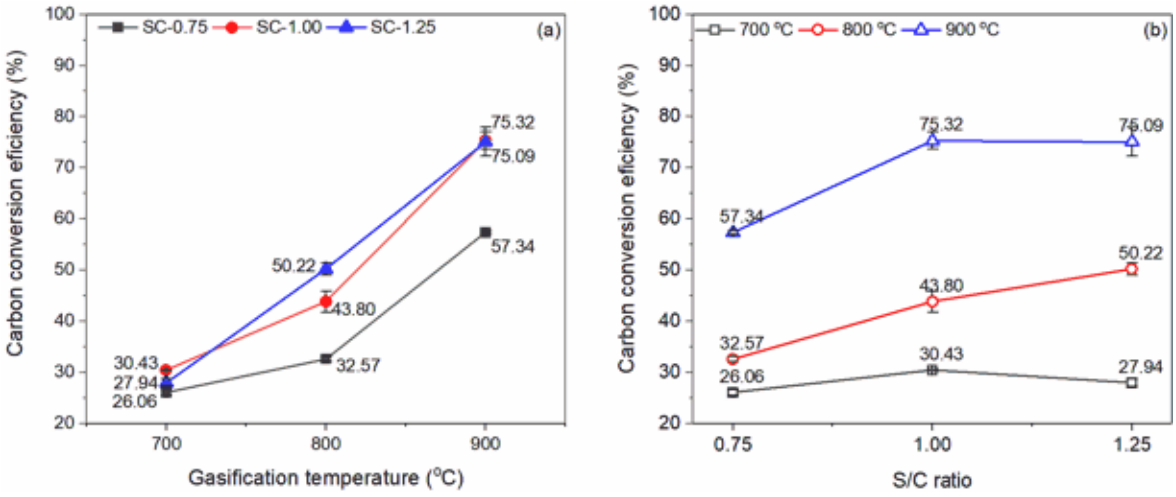

Figure 4-17. Carbon conversion efficiency as a function of gasification temperature (a) and S/C ratio (b)

As described in equation-(3-4), the cold gas efficiency-CGE is affected by the dry syngas yield and LHV_{syngas}. Overall, as is observed in Figure 4-18, increasing both the gasification temperature and S/C ratio led to higher cold gas efficiency. At 0.75 S/C ratio, the CGE increased from 27.57 % at 700 ℃ to 64.8 % at 900 ℃, approximately 2.5 times higher. In the case of 1.00 and 1.25 of the S/C ratio, the corresponding numbers were 2.6 and 2.9 times higher, respectively.

At a gasification temperature of 700 ℃, the increase in the S/C ratio from 0.75 to 1.00 resulted in around a 5% increase in cold gas efficiency, while further increasing the S/C ratio to 1.25 only resulted in a 1% increase in cold gas efficiency. At a gasification temperature of 800 ℃, the cold gas efficiency increased significantly compared to 700 ℃. The increase in S/C ratio from 0.75 to 1.00 resulted in around a 10 % increase in cold gas efficiency while increasing the S/C ratio further to 1.25 resulted in only around a 7 % increase in cold gas efficiency. At a gasification temperature of 900 ℃, the cold gas efficiency was the highest among all the tested conditions. The cold gas efficiency was 64.08, 83.43, and 83.69 % for S/C ratios of 0.75, 1.00, and 1.25, respectively.

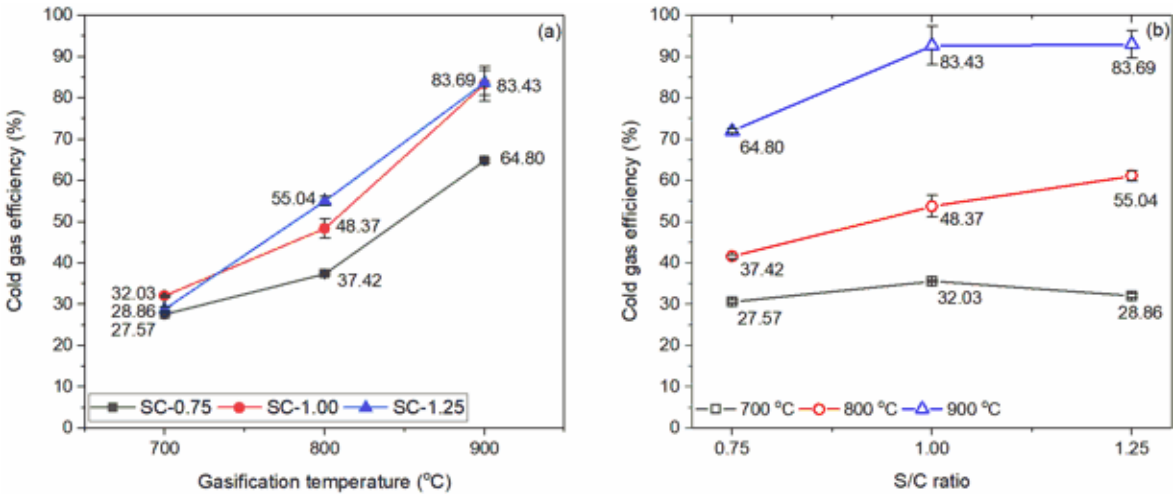

Figure 4-18. Cold gas efficiency as a function of gasification temperature (a) and S/C ratio (b)

4.6.2. Specific power consumption

The effects of the gasification temperature and S/C ratio on power consumption per cubic meter of syngas are illustrated in Figure 4-19.

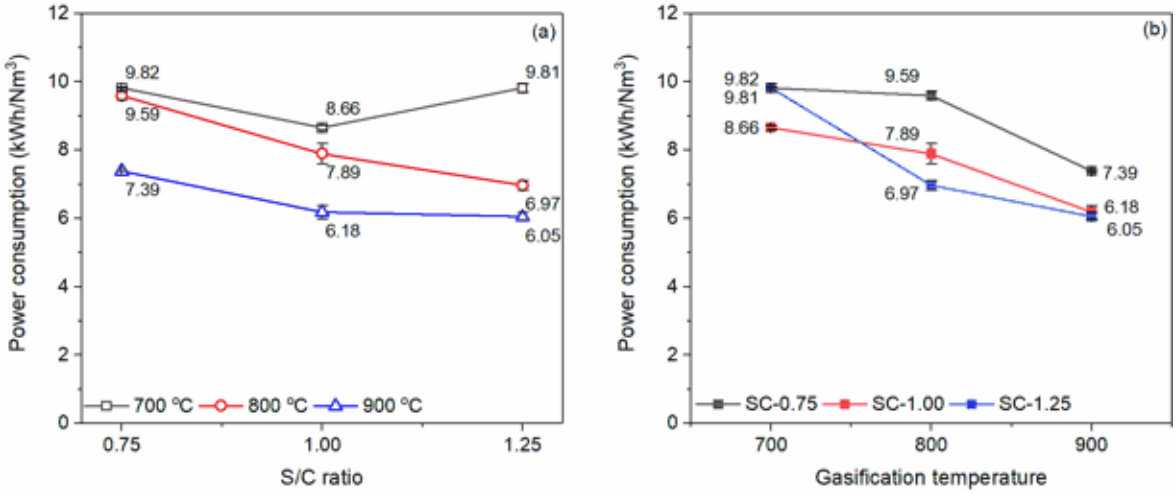

Figure 4-19. Power consumption as a function of gasification temperature (b) and S/C ratio (a)

The higher gasification temperature led to an increase in the dry syngas yield. Therefore, the specific power consumption was lower in the case of the gasification temperature at 900 ºC. As the S/C ratio increased from 0.75 to 1.00, the specific power consumption decreased drastically at all gasification temperature conditions. It can be explained that the higher S/C ratio resulted in a higher syngas flow rate. Although, the steam generator consumed more energy at a higher S/C ratio. When the S/C ratio increased from 1.00 to 1.25, the specific power consumption decreased gradually at 800 ºC of the gasification temperature, from 7.89 to 6.97 kWh/Nm^3, respectively. But the changes in

specific power consumption showed different trends at 700 and 900 ºC. At 700 ºC, the specific power consumption increased significantly when the S/C ratio increased from 1.00 to 1.25, due to a decrease in the dry syngas yield. In the case of 900 ºC, the specific power consumption decreased slightly from 6.18 kWh/Nm^3 at 1.00 S/C ratio to 6.05 kWh/Nm^3 at 1.25 S/C ratio. The lowest specific power consumption was at 900 ºC of the gasification temperature and 1.25 S/C ratio.

4.7. Characteristic of condensate liquid and residual char from the gasification process

4.7.1. Condensate liquid

During the experimental process, the gaseous byproducts leaving the gasifier were subjected to condensation in the heat exchanger and the resulting liquid was collected in a collector located at the bottom of the heat exchanger, as described in Section 3.3.3. The typical volume of condensate liquid obtained for an hour from the experiments conducted on the original coal sample at various experimental conditions is presented in Figure 4-20.

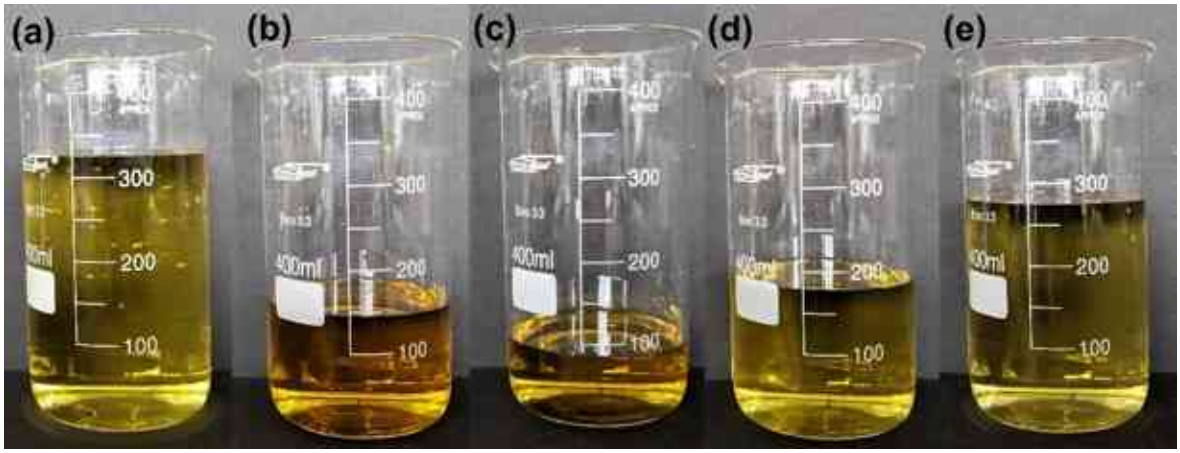

Figure 4-20. Typical condensate liquid volume per hour from the experiments of the original coal sample at the gasification temperature-S/C ratio: 700°C-0.75 (a), 800°C-0.75 (b), 900°C-0.75 (c), 900°C-1.00 (d), 900°C-1.25 (e)

The water content of the condensate liquid was determined using the Standard test method for water in petroleum products and bituminous materials by distillation, which employs toluene as a solvent [134]. However, the water content was found to be higher than 98 V/V%, consequently, further analysis for the condensate liquid was not conducted.

4.7.2. Residual char

The elemental composition, ash content, and heating value of the gasification char samples are shown in Table 4-3. The total weight percentage can exceed 100 %, however, it

can be explained by the uncertainty of measurement equipment, as well as the non-homogeneous char sample.

Table 4-3. General analysis of residual char samples

Gasification temperature	S/C ratio		N	C	H	S	Ash	HHV
℃	(mol/mol)		wt%	wt%	wt%	wt%	wt%	MJ/kg
700	0.75	**Mean**	**0.52**	**38.41**	**0.66**	**3.83**	**60.88**	**13.08**
		SD	0.04	2.95	0.04	0.26		
	1.00	**Mean**	**0.56**	**42.24**	**0.70**	**4.03**	**54.35**	**15.51**
		SD	0.03	1.98	0.05	0.23		
	1.25	**Mean**	**0.47**	**32.58**	**0.61**	**3.71**	**65.47**	**11.54**
		SD	0.04	2.63	0.04	0.45		
800	0.75	**Mean**	**0.36**	**27.04**	**0.34**	**4.95**	**71.20**	**10.23**
		SD	0.05	2.08	0.04	1.00		
	1.00	**Mean**	**0.50**	**29.31**	**0.42**	**3.11**	**71.79**	**9.22**
		SD	0.09	1.95	0.03	0.26		
	1.25	**Mean**	**0.39**	**34.49**	**0.41**	**4.07**	**65.73**	**11.79**
		SD	0.06	3.03	0.07	0.34		
900	0.75	**Mean**	**0.24**	**21.58**	**0.22**	**5.01**	**80.02**	**7.34**
		SD	0.06	1.79	0.03	0.64		
	1.00	**Mean**	**0.02**	**14.86**	**0.11**	**4.42**	**86.32**	**5.29**
		SD	0.01	1.13	0.06	0.27		
	1.25	**Mean**	**0.02**	**12.90**	**0.11**	**4.18**	**90.30**	**4.42**
		SD	0.01	1.34	0.06	0.63		

In comparison with the original coal sample, the char samples obtained at 700 ℃ of gasification temperature and 0.75 and 1.00 of S/C ratio had a higher concentration of C, while there were lower C concentrations in other samples. The N and H concentrations of char samples were lower than those of the original coal sample. On the other hand, the S concentrations increased significantly after the gasification process, ranging from 3.11 to 5.01 wt%. It led to an essential consideration in the use of char samples in secondary processes.

The concentrations of N, C, and H decreased as the gasification temperature increased from 700 to 900 ℃. It indicated that the higher gasification temperature promoted the conversion of these components. A similar trend was observed with the increasing S/C ratio at each experimental gasification temperature.

The ash content increased with both increasing gasification temperature and S/C ratio. At 900 ℃ of gasification temperature, the ash content was higher than 80 wt%, representing a higher conversion at a higher gasification temperature. Notably, there was 90.30 wt% of ash in the char sample obtained at 1.25 of S/C ratio.

From an energetic point of view, the char samples obtained at 700 and 800 ℃ are suitable for power generation processes, with the heating values ranging from 9 to 15 MJ/kg. In the case of the gasification temperature at 900 ℃, the higher heating values of char samples were only 7.34, 5.29, and 4.42 MJ/kg at 0.75, 1.00, and 1.25 of S/C ratio, respectively.

5. Multi-stage gasification of low-rank coal samples from gravity separation process with magnetite suspension media

5.1. Characteristics of materials from the separation process

The TG, DTG, and DTA curves as a function of temperature and time during thermogravimetric analysis are illustrated in Figure 5-1 for the C1 sample and the C2 sample.

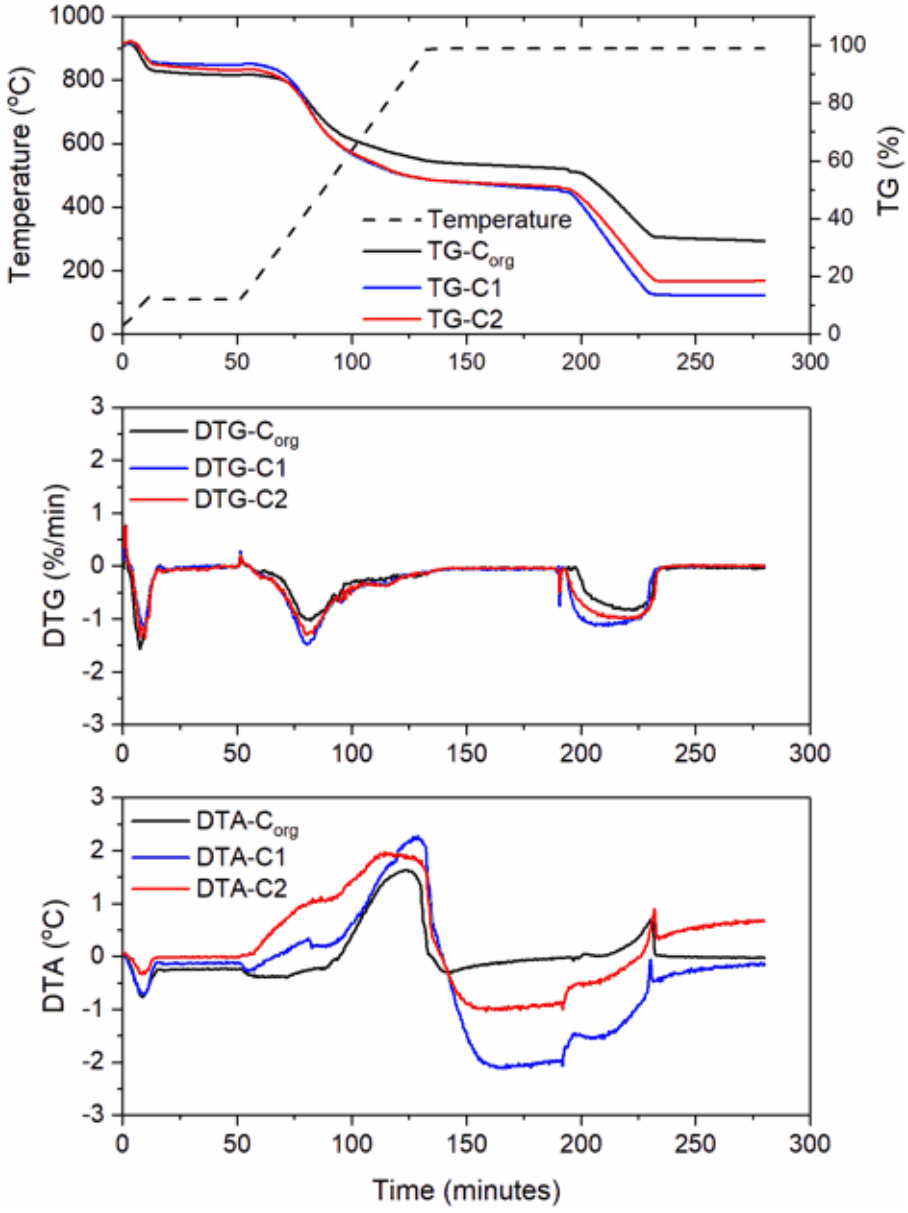

Figure 5-1. TG, DTG, and DTA profiles of C_{org}, C1, and C2 samples

The results of proximate, elemental, and heating value analysis of samples from the separation process are presented in Table 5-1, in which C_{org}-the original coal sample.

Table 5-1. Proximate, elemental, and heating value analysis of samples (as-received basis)

		Fuel name		
		C_{org}	**C1**	**C2**
Proximate analysis-wt%	**Moisture**	10.37	6.97	8.59
	Volatile	32.33	43.93	40.96
	Fixed carbon	25.22	35.80	32.25
	Ash	32.08	13.30	18.20
Elemental analysis-wt%	**N**	0.72	0.83	0.84
	C	35.60	51.95	48.17
	H	3.39	4.68	4.39
	S	3.07	5.14	5.38
	O (by diff.)	25.14	37.40	41.22
Lower heating value (MJ/kg)		14.02	20.62	18.62

The moisture contents of two selected coal samples (C1 and C2) were found to be lower than that of the original coal (C_{org}) sample, with C1 and C2 containing 6.97 and 8.59 wt%, respectively. C1 and C2 samples had higher volatile and fixed carbon contents than the original coal sample. On the other hand, the ash content was higher in the original coal sample, with only 13.3 and 18.02 wt% in C1 and C2, respectively, compared to 32.08 wt% in the original coal sample. The differences among C_{org}, C1, and C2 were most significant in terms of their carbon and sulphur contents. The carbon contents increased in the order of C_{org}, C2, and C1 samples, with 35.60, 48.17, and 51.95 wt%, respectively. The sulphur content of C1 and C2 samples were 5.14 and 5.38 wt%, indicating a critically high sulphur fuel type.

Due to the higher carbon content, C1 and C2 samples had a greater lower heating value compared to the C_{org} sample. The lower heating values were 20.62 and 18.62 MJ/kg for C1 and C2 samples, respectively, while the C_{org} sample had a low heating value of 14.02 MJ/kg.

Table 5-2 displays the results of BET and XRF analyses conducted on C1 and C2 samples. The specific surface area of the C1 and C2 samples was found to be lower than that of the C_{org} sample, with a value of 1.196 m^2/g for the C1 sample and 1.4616 m^2/g for the C2 sample. The ash content of C1 and C2 samples was dominated by SiO_2, accounting for 8.5 and 11.6 wt%, respectively. The Al_2O_3 in C1 and C2 samples was significantly lower than

that of the C_{org} sample, while the weight percentage of Fe_2O_3 was relatively similar across all samples. The group of alkali and alkaline earth metal oxides was higher in the case of the C_{org} sample, although the difference was not significant.

Table 5-2. BET and XRF analysis of C_{org}, C1, and C2 samples

BET analysis				
		Sample name		
		C_{org}	**C1**	**C2**
BET surface area	m^2/g	4.5722	1.196	1.4616
XRF analysis				
Components	**unit**	**Sample name**		
		C_{org}	**C1**	**C2**
SiO_2	wt%	29.70	8.50	11.60
Al_2O_3		11.60	3.10	4.50
MgO		0.96	0.49	0.57
CaO		2.60	3.28	3.39
Na_2O		0.31	0.22	0.21
K_2O		1.36	0.60	0.77
Fe_2O_3		6.83	6.50	7.47
MnO		0.066	0.059	0.063
TiO_2		0.356	0.139	0.188
P_2O_5		0.028	0.026	0.057

5.2. Experimental parameters

The gasification results of the original low-rank coal sample indicated that the highest dry syngas production was achieved at 900 ℃ and 1.25 of S/C ratio. The ratio of H_2/CO at these parameters also reached the desired value of 2. Therefore, the gasification parameters were selected at 900 ℃ and 1.00 and 1.25 of S/C ratio for the samples from the separation process. The detailed experimental parameters are shown in Table 5-3.

Table 5-3. Experimental parameters for the gasification process of C1 and C2 samples

Sample name	**Mass flow rate of coal**	**Gasification temperature**	**S/C ratio**	**Steam flow rate**	**Time of experiment**
	g/h	**℃**	**mol/mol**	**g/min**	**days**
C1	991.70	900	1.00	10.06	3
			1.25	12.87	3
C2	1043.00	900	1.00	9.91	3
			1.25	12.67	3

5.3. Gasification products

The summary of gasification products from the experiments of C1 and C2 samples is shown in Appendix 4- Products from the experiments of C1 and C2 samples.

5.3.1. Char yields

The variations in the char yield as a function of the S/C ratio and type of samples are shown in Figure 5-2. The char yields were lower in the gasification case of C1 and C2 samples at both the S/C ratio of 1.00 and 1.25. In the case of the 1.00 S/C ratio, the decrease in char yield was in the order of C_{org}, C1, and C2 samples, with 407.10, 361.67, and 298.70 g/h, respectively. The corresponding numbers were 373.03, 305.23, and 265.33 g/h in the case of 1.25 S/B ratio. In the case of C1 and C2 samples, with increasing S/C ratio, the decrease in char yield was higher for the gasification process of the C1 sample. The char yield decreased by 56.44 g/h for the gasification process of the C1 sample, while it was by 33.37 g/h for the gasification process of the C2 sample.

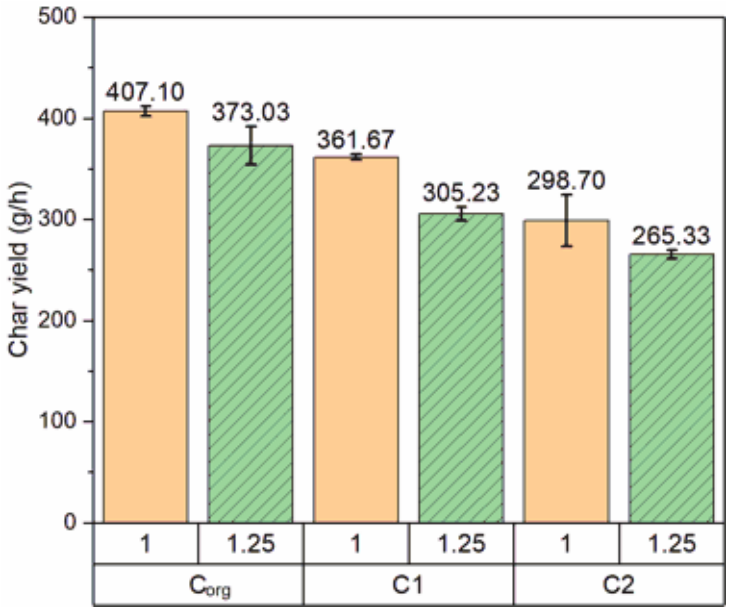

Figure 5-2. Char yield in the gasification of C1 and C2 at 1.00 and 1.25 of S/C ratio

5.3.2. Condensate liquid yield

Figure 5-3 presents the results of liquid yield obtained from the gasification experiments of the C1 and C2 samples at a gasification temperature of 900 °C and 1.00 and 1.25 S/C ratio. The liquid yields were found to be higher in the case of experiments of the C1 and C2 samples compared to that of the C_{org} sample. This could be the result of the larger total quantity of steam in the case of C1 and C2 samples. However, when considering the

percentage of liquid yield in relation to the total steam introduction (Figure 5-4), the percentage of liquid yield was relatively similar between the experiments of C_{org} and C1 samples at 1.25 of the S/C ratio, with 51.58 and 55.28 %, respectively.

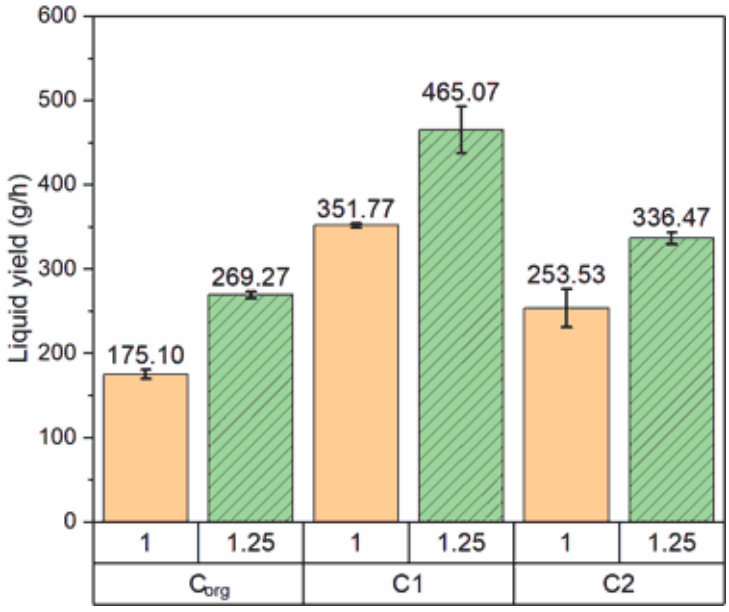

Figure 5-3. Liquid yield in the gasification process of C1 and C2 at 1.00 and 1.25 of the S/C ratio

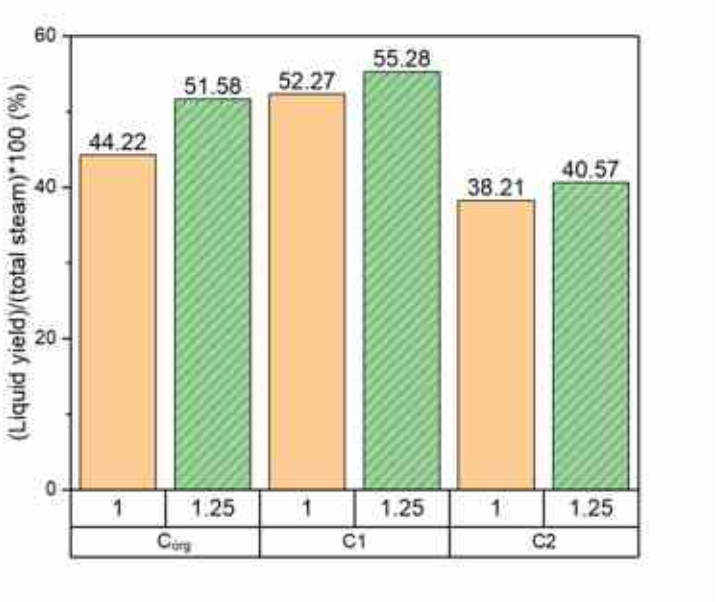

Figure 5-4. Liquid yield by percentage in the gasification process of C1 and C2 at 1.00 and 1.25 of the S/C ratio

As shown in Figure 5-3, the liquid yield in the gasification experiments of the C2 sample was lower than that of the C1 sample at all S/C ratios. At the same S/C ratio, the total quantity of steam introduction was not significantly different between the gasification experiments of the C1 and C2 samples. Consequently, the reaction of steam in the gasification process was greater in the case of the C2 sample at all experimental S/C ratios.

In both gasification experiments of the C1 and C2 samples, a higher S/C ratio generated a higher liquid yield. In the case of the C1 sample, the liquid yields were 351.77 g/h at a 1.00 S/C ratio and 465.07 g/h at a 1.25 S/C ratio. The corresponding numbers were 253.53 and 336.46 g/h at 1.00 and 1.25 of the S/C ratio, respectively, in the case of the C2 sample.

5.3.3. Dry gas yield

Figure 5-5 illustrates the dry gas yield obtained from the gasification experiments conducted on C_{org}, C1, and C2 samples at a temperature of 900 ℃ and S/C ratio of 1.00 and 1.25. Obviously, there was a higher dry gas yield generated in the case of C1 and C2 samples at all S/C ratios, with increasing dry gas yield observed in the order of C_{org}, C1, and C2, respectively. At 1.00 of the S/C ratio, the produced gas yield was only 1.10 Nm^3/kg_{coal} in the case of the C_{org} sample, which increased to 1.4 Nm^3/kg_{coal} for the case of the C1 sample and 1.59 Nm^3/kg_{coal} for the case of C2 sample. At 1.25 of the S/C ratio, the gasification process of the C2 sample produced the highest produced gas yield (1.70 Nm^3/kg_{coal}) and followed by the gasification process of the C1 sample, with 1.52 Nm^3/kg_{coal}.

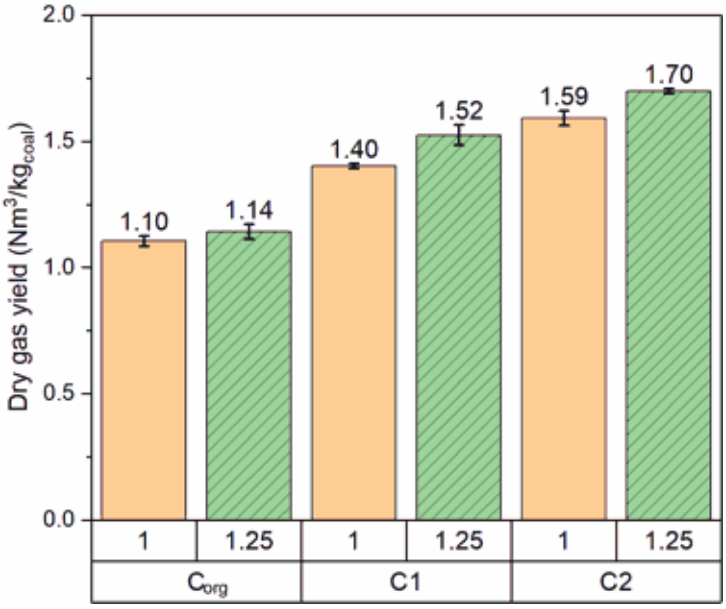

Figure 5-5. Dry gas yield in the gasification process of C1 and C2 samples at 1.00 and 1.25 of the S/C ratio

When the S/C ratio increased from 1.00 to 1.25, the dry gas yield increased in all cases of samples, obviously indicated in the gasification experiment of C1 and C2 samples. The increase in dry gas yield was only by 0.04 Nm^3/kg_{coal} for the gasification experiment of the C_{org} sample. In the case of C1 and C2 samples, the corresponding numbers were 0.12 and 0.11 Nm^3/kg_{coal}, respectively.

The higher dry gas yield observed in the gasification process of the C1 and C2 samples could be attributed to the differences in their chemical composition compared to the C_{org} sample, as follows:

- The C1 and C2 samples had a higher content of volatile matter, 43.93 and 40.96 wt%, respectively, compared to 32.33 wt% in the C_{org} sample. This could result in a higher porous structure of char after the devolatilization process during the pyrolysis process. The higher porous structure of char led to a higher number of active sites [135,136], as well as greater mass transfer properties [137,138]. They helped to promote the reaction between reactants and solid char, thereby producing a higher quantity of syngas.
- Another reason could be the ash content of the samples, the higher ash content of the C_{org} sample could generate a thin layer on the porous carbon surface. Consequently, it inhibited the reaction between the reactants and the carbon surfaces [138]. In contrast, the lower ash content of C1 and C2 samples, allowed easier access of reactants on the surfaces of the char [139,140].
- The presence of SiO_2 and Al_2O_3 can have a negative effect on the gasification process [139,141,142], these components were lower in the case of C1 and C2 samples. It can be a reason for a better gas yield during the gasification process of C1 and C2 samples.
- The higher carbon content of starting materials could improve the reaction between carbon and reactants [143,144], leading to a higher quantity of syngas production during the gasification process of C1 and C2 samples.

5.4. Syngas composition and heating value of syngas

This section discusses the experimental results obtained from the gasification process of the C1 and C2 samples at 900 °C and S/C ratio of 1.00 and 1.25, including the syngas composition, the low heating value of syngas, as well as the H_2/CO ratio. The data of syngas concentration from the experiments of C1 and C2 samples are shown in Appendix 5- Graphs of syngas concentration from the experiments of the C1 and C2 sample and Appendix 6- Average syngas concentration from the experiments of C1 and C2 samples.

5.4.1. Syngas composition

As mentioned in section 4.5.1, the main syngas components were H_2, CO, CO_2, and CH_4. In the case of gasification experiments of C1 and C2 samples, these syngas components accounted for above 98 V/V%. Consequently, the discussion is focused on these syngas components in this section. The details of total syngas composition are exhibited in Appendix 4- Products from the experiments of C1 and C2.

Figure 5-6 presents the concentration (a) and yield (b) of H_2 obtained from the gasification experiments of C1 and C2 samples with the gasification temperature at 900 °C and 1.00 and 1.25 S/C ratios. The H_2 concentration remained relatively constant among the gasification experiments of C_{org}, C1, and C2 samples, ranging from 53.66 to 54.76 V/V%. In addition, the dry syngas yield increased in the order of C_{org}, C1, and C2 at all experimental S/C ratios. Therefore, the H_2 yield followed the same trend, as shown in Figure 5-6-b. At an S/C ratio of 1.00, the gasification experiment of the C_{org} sample produced 0.6 Nm^3/kg_{coal} of H_2 content, while the experiments of C1 and C2 samples generated 0.75 and 0.86 Nm^3/kg_{coal}, respectively. At an S/C ratio of 1.25, the H_2 yields were 0.63, 0.82, and 0.92 Nm^3/kg_{coal} for the C_{org}, C1, and C2 samples, respectively.

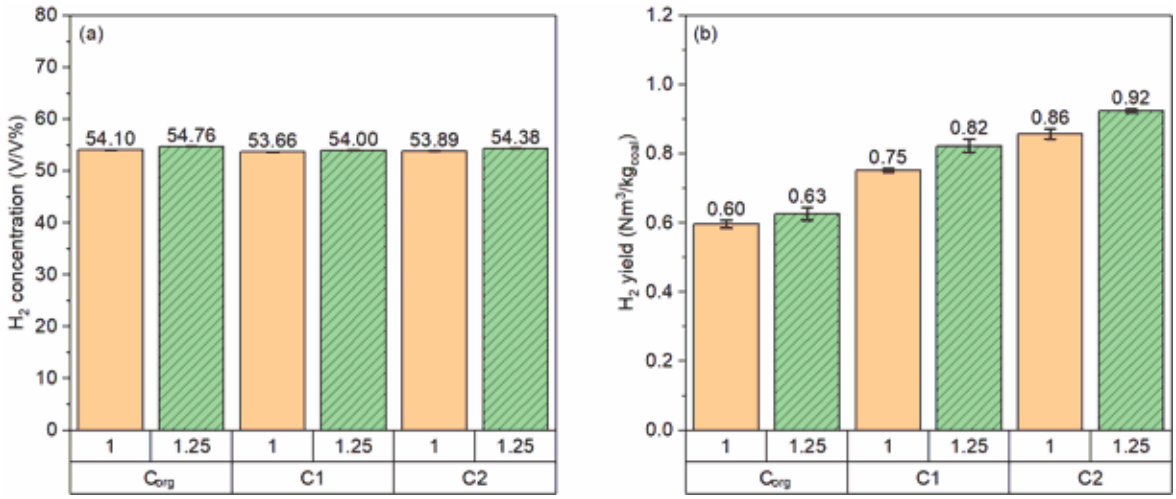

Figure 5-6. H_2 concentration and yield from the gasification process of C1 and C2 samples

It can be observed that an increase in the S/C ratio resulted in a slight increase in H_2 concentration for all samples. When the S/C ratio increased from 1.00 to 1.25, the H_2 concentration increased from 53.66 to 54 V/V% in the case of the experiment of the C1 sample, while from 53.89 to 54.38 V/V% for the C2 sample. In addition, the increasing H_2 yield was significantly observed in the case of the C1 and C2 samples when the S/C ratio changed from 1.00 to 1.25. For the experiment of the C_{org} sample, the H_2 yield increased by

only 0.02 Nm^3/kg_{coal} as an increasing S/C ratio from 1.00 to 1.25. However, the corresponding numbers were 0.07 and 0.06 Nm^3/kg_{coal} for C1 and C2 samples, respectively.

The concentration and yield of CO gained from the gasification process of C1 and C2 samples are illustrated in Figure 5-7. At the same S/C ratios, the CO concentration was lower for the gasification experiments of the C1 and C2 samples compared to that of the C_{org} sample, as shown in Figure 5-7-a. Additionally, the gasification experiment of the C2 sample produced syngas with a higher CO concentration than that from the gasification experiments of the C1 sample. At an S/C ratio of 1.00, the CO concentrations were 25.43 and 28.90 V/V% for the experiments of C1 and C2, respectively. The corresponding numbers were 24.74 and 27.15 V/V% for the experiments of C1 and C2, respectively, at 1.25 of the S/C ratio. Increasing of S/C ratio led to a decrease in the CO concentration for both gasification experiments of C1 and C2 samples but to different extents. When the S/C ratio increased from 1.00 to 1.25, the CO concentration decreased by 0.69 V/V% for the experiment of the C1 sample. In the case of the C2 sample, that number was by 1.75 V/V%.

As shown in Figure 5-7-b, due to an increase in the syngas yield, the CO yields were higher for the experiments of C1 and C2 samples. When the S/C ratio increased from 1.00 to 1.25, the CO yield decreased from 0.34 to 0.31 Nm^3/kg_{coal} in the case of the C_{org} sample, as there was no significant increase in the syngas yield but a significant decrease in the CO concentration. There was an opposite trend in the case of C1 and C2 samples. Although the CO concentration decreased with increasing of S/C ratios, however, the CO yield increased from 0.36 Nm^3/kg_{coal} at 1.00 of S/C ratio to 0.38 Nm^3/kg_{coal} at 1.25 of S/C ratio in the case of C1 sample and remained nearly stable at 0.46 Nm^3/kg_{coal} in the case of C2 sample.

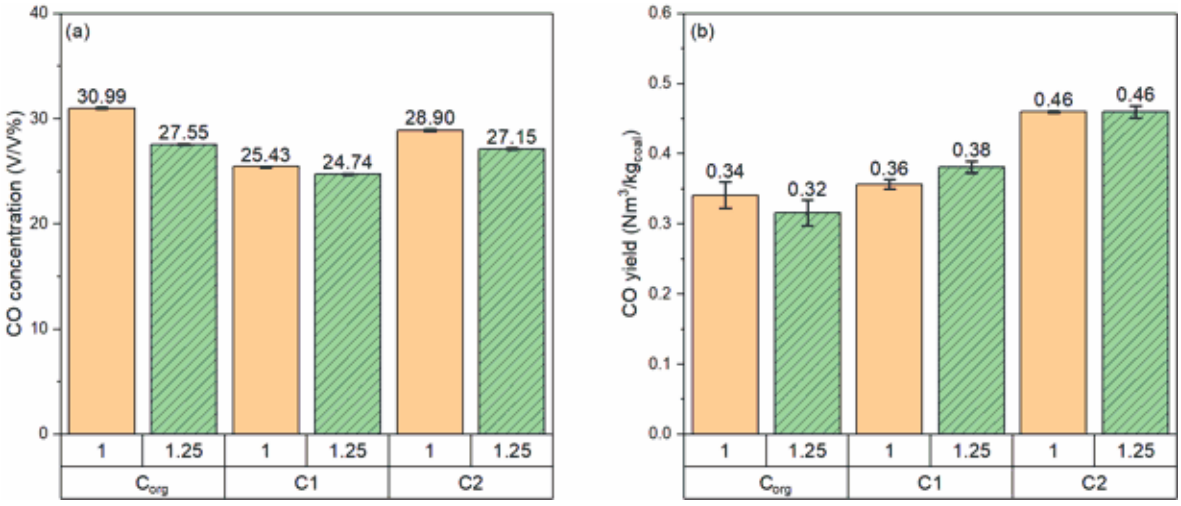

Figure 5-7. CO concentration and yield from the gasification process of C1 and C2 samples

Figure 5-8 presents the volume fraction and yield of CO_2 from the gasification process of C1 and C2 samples. In contrast with the CO volume fraction, the CO_2 volume fraction increased in the order of C, C2, and C1 at all S/C ratios, as shown in Figure 5-8-a. Furthermore, the volume fraction of CO_2 expanded as the S/C ratio increased. In the case of the gasification experiment of the C1 sample, the volume fraction of CO_2 increased from 15.54 to 16.90 V/V% at 1.00 and 1.25 S/C ratios, respectively. These numbers were 12.79 and 14.14 V/V% in the case of the C2 sample.

There was a similar trend in the changes in CO_2 yield, as shown in Figure 5-8-b. At 1.00 of the S/C ratio, the CO_2 yields were 0.13, 0.22, and 0.20 Nm^3/kg_{coal} for the gasification experiments of C_{org}, C1, and C2 samples, respectively. At 1.25 of the S/C ratio, those numbers were 0.16, 0.25, and 0.24 Nm^3/kg_{coal}, respectively.

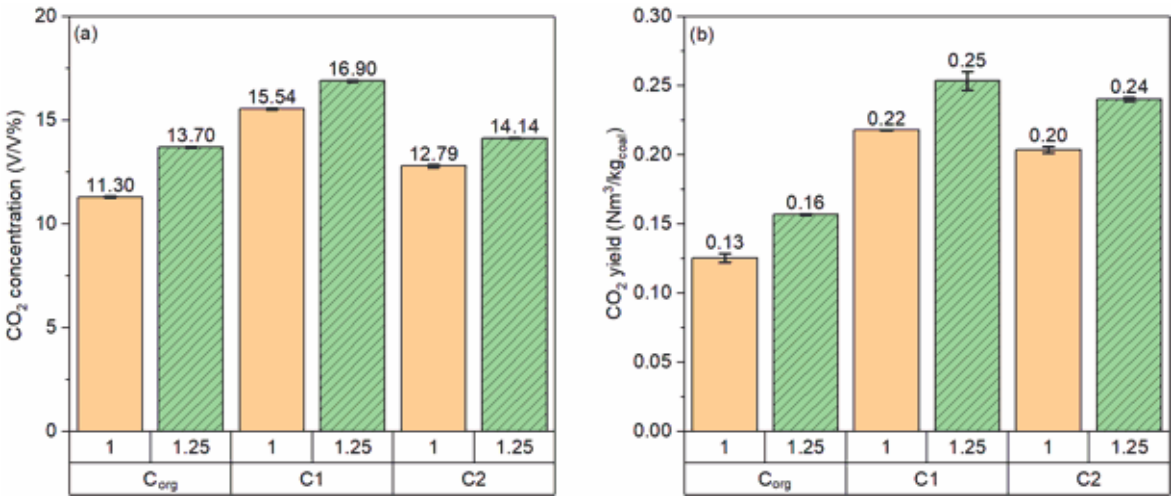

Figure 5-8. CO_2 concentration and yield from the gasification process of C1 and C2 samples

The volume fraction and yield of CH_4 from the gasification experiments of C1 and C2 samples are illustrated in Figure 5-9. At all S/C ratios, the syngas produced from the gasification experiments of C1 and C2 samples had a higher volume fraction of CH_4 than that of the C_{org} sample, as shown in Figure 5-9-a. As increasing of S/C ratio from 1.00 to 1.25, there was an increasing trend in the volume fraction of CH_4 in the case of the C_{org} sample, however, a decreasing trend in the case of C1 and C2 samples. Specifically, the CH_4 volume fraction declined from 3.87 V/V% at 1.00 of the S/C ratio to 3.59 V/V% at 1.25 of the S/C ratio for the experiments of the C1 sample. In the case of the C2 sample, the CH_4 volume fraction nearly kept stable at around 2.83 V/V% when the S/C ratio increased from 1.00 to 1.25.

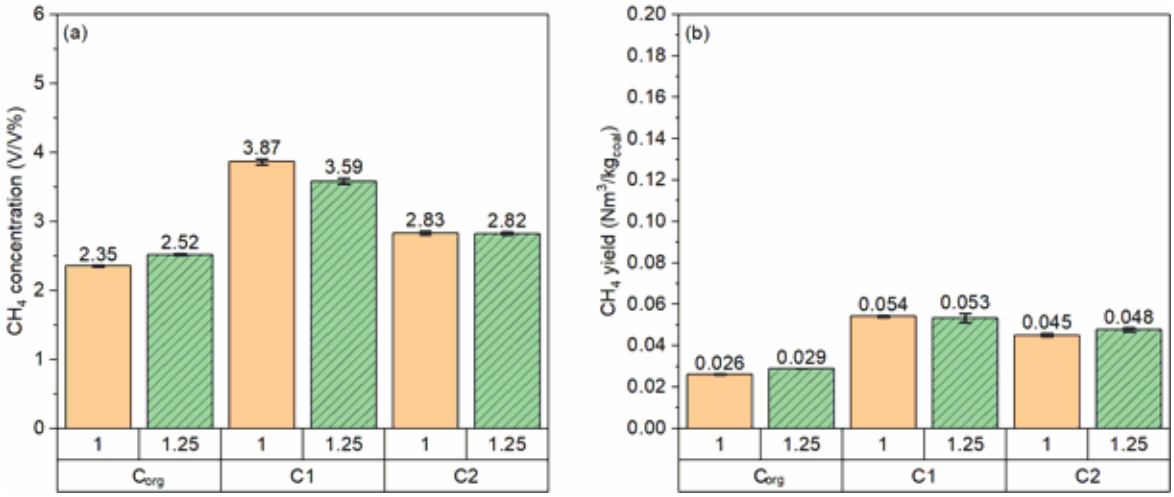

Figure 5-9. CH_4 concentration and yield from the gasification process of C1 and C2 samples

Although the syngas yield increased with the increasing S/C ratio for all coal samples, there was only a slight variation in the volume fraction of CH_4. Consequently, the CH_4 yield did not show significant changes in the experiments of C1 and C2 samples when the S/C ratio increased from 1.00 to 1.25. As shown in Figure 5-9-b, the CH_4 yields were 0.054 Nm^3/kg_{coal} at 1.00 S/C ratio and 0.053 Nm^3/kg_{coal} at 1.25 S/C ratio in the case of the gasification experiment of the C1 sample. In the case of the C2 sample, the corresponding numbers were 0.045 and 0.048 Nm^3/kg_{coal} at 1.00 and 1.25 S/C ratios, respectively.

5.4.2. Lower heating value and H_2/CO ratio of the syngas

Figure 5-10 depicts the lower heating value of the syngas (LHV_{syngas}) obtained from the gasification experiments of the C1 and C2 samples at 900 °C of gasification temperature and S/C ratios of 1.00 and 1.25. It can be observed that there were no significant differences in LHV_{syngas} among the experiments, which can be attributed to the consistent total volume fraction of combustible contents across the experimental conditions. The LHV_{syngas} varied in a slight range of 10.23÷10.59 MJ/Nm^3 across C_{org}, C1, and C2 samples. An increase in the S/C ratio resulted in a slight decrease in the volume fraction of CO, consequently, the LHV_{syngas} showed a slight decrease trend. In the case of the C1 sample, the LHV_{syngas} decreased from 10.38 MJ/Nm^3 at 1.00 S/C ratio to 10.23 MJ/Nm^3 at 1.25 S/C ratio. Similarly, the LHV_{syngas} decreased from 10.47 to 10.29 MJ/Nm^3 in the case of the C2 sample.

The H_2/CO ratio obtained from the gasification experiments of C1 and C2 samples is illustrated in Figure 5-11. It is observed that, with a stable H_2 concentration, the H_2/CO ratio was primarily driven by the CO concentration. Consequently, the H_2/CO ratio was higher in the case of the C1 sample experiment. When the S/C ratio increased from 1.00 to 1.25, the

H_2/CO ratio also increased for all samples, albeit to varying degrees. In the case of the C_{org} sample, the H_2/CO ratio increased from 1.75 at 1.00 of the S/C ratio to 1.99 at 1.25 of the S/C ratio. These numbers were from 2.11 to 2.18 and 1.86 to 2.00 for C1 and C2 samples, respectively, over the same range of S/C ratios.

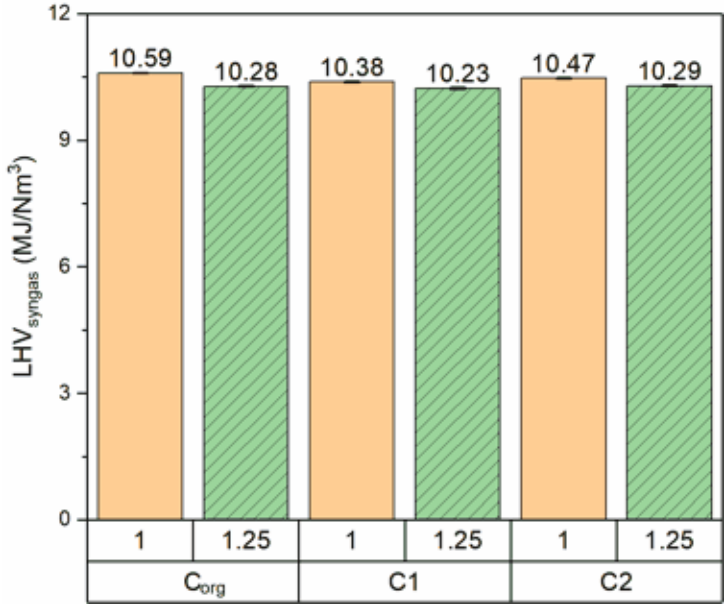

Figure 5-10. The lower heating value of syngas from the gasification process of C1 and C2 samples

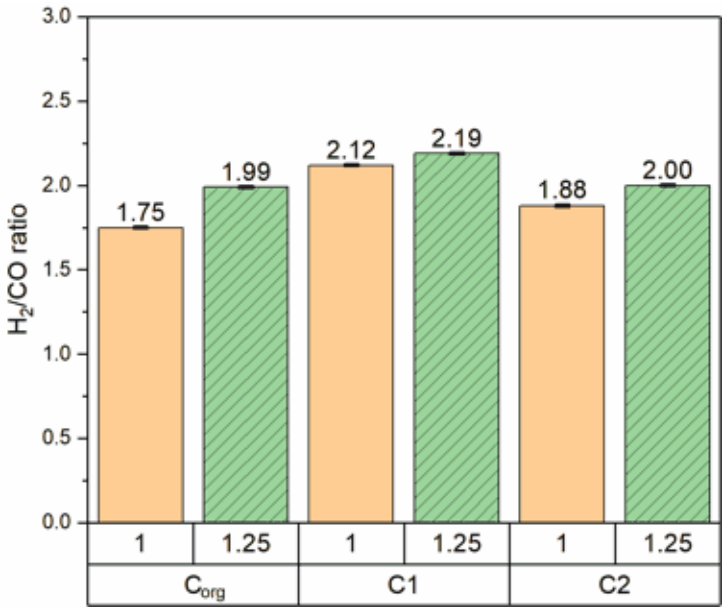

Figure 5-11. H_2/CO ratio from the gasification process of C1 and C2 samples

5.5. Gasification efficiency

The carbon conversion efficiency (CCE) of the gasification experiments conducted on C1 and C2 samples is demonstrated in Figure 5-12. At each S/C ratio, the CCE increased in the order of C1, C_{org}, and C2, respectively. Although the gasification experiment of the

C1 sample produced a higher gas volume compared with the C_{org} sample, the CCE was the lowest among the samples. This phenomenon was associated with the higher carbon content in the C1 sample.

Increasing the S/C ratio led to improving the volume of produced gas for all samples. However, there was a slight decrease in the CCE observed in the case of the C_{org} sample, while increased trends of the CCE were observed in the experiments of the C1 and C2 samples. In the case of the C1 sample, the CCE increased from 64.86 % at the S/C ratio of 1.00 to 71.00 % at the S/C ratio of 1.25. For the experiments of the C2 sample, the CCE increased from 78.82 to 83.15 % at an S/C ratio of 1.00 and 1.25, respectively.

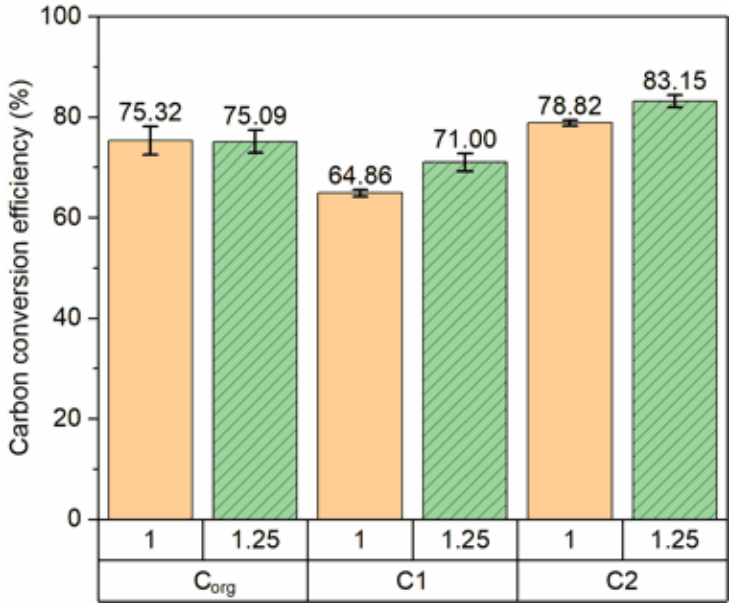

Figure 5-12. The carbon conversion efficiency of the gasification process of C1 and C2 samples

Figure 5-13 shows the cold gas efficiency (CGE) of the gasification process obtained from the experiments of C_{org}, C1 and C2 samples. The cold gas efficiency followed a similar trend as observed in the carbon conversion efficiency, increasing in order of C1, C_{org}, and C2, respectively, at all levels of the S/C ratio.

The CGE is governed by the lower heating value of coal samples, as well as the lower heating value and volume of produced gas, as shown in equation (3-4). As mentioned in section 5.4.2, the LHV_{syngas} nearly kept constant in the range of experimental conditions. Although the experiments of the C1 sample produced a higher volume of gas, the lower heating value of the C1 sample was significantly higher than that of the C_{org} sample. Consequently, the CGE was lower in the case of the C1 sample at all S/C ratios.

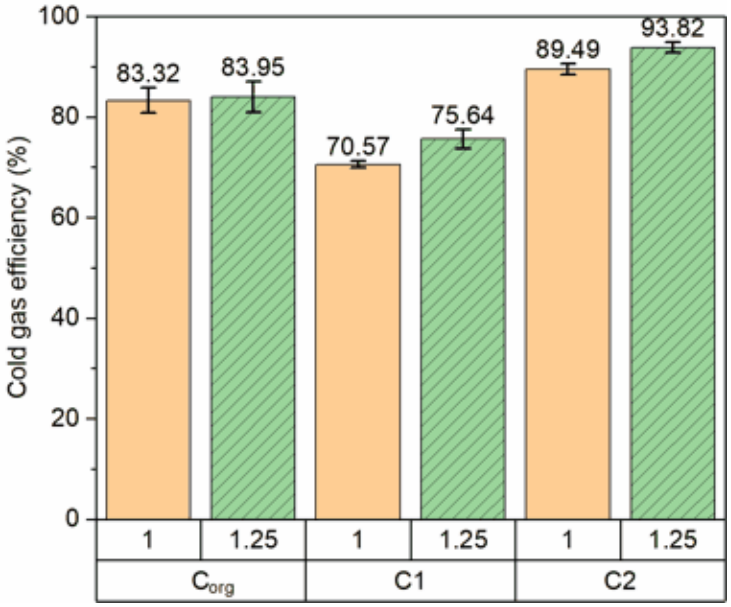

Figure 5-13. Cold gas efficiency of the gasification process of C1 and C2 samples

Increasing the S/C ratio resulted in a minor increase in the volume of produced gas for C_{org} samples but a significant increase in the case of C1 and C2 samples. As a result, the cold gas efficiency remained nearly constant when the S/C ratio increased from 1.00 to 1.25 for the experiments of the C_{org} sample. In the case of the C1 sample, the CGE improved from 70.57 % at an S/C ratio of 1.00 to 75.64 % at an S/C ratio of 1.25. The corresponding numbers were from 89.49 to 93.82 % for the experiments conducted on the C2 sample.

The specific power consumption of the experiments of C1 and C2 samples at 900 °C of gasification temperature and 1.00 and 1.25 of S/C ratios as depicted in Figure 5-14. In general, the specific power consumption decreased in the order of C_{org}, C1, and C2, respectively. This could be attributed to the higher volume of produced gas in the experiments conducted on C1 and C2 samples. Increasing the S/C ratio resulted in an increase in the produced gas, consequently, the specific power consumption was lower at a higher S/C ratio. In the case of experiments of the C1 sample, the specific power consumption was decreased from 5.37 kWh/Nm^3 at an S/C ratio of 1.00 to 5.20 kWh/Nm^3 at an S/C ratio of 1.25. For the experiments of the C2 samples, the specific power consumption decreased from 4.62 to 4.47 kWh/Nm^3 at the same S/C conditions. The lowest specific power consumption was at 900 °C of gasification temperature and 1.25 of S/C ratio in the case of the C2 sample.

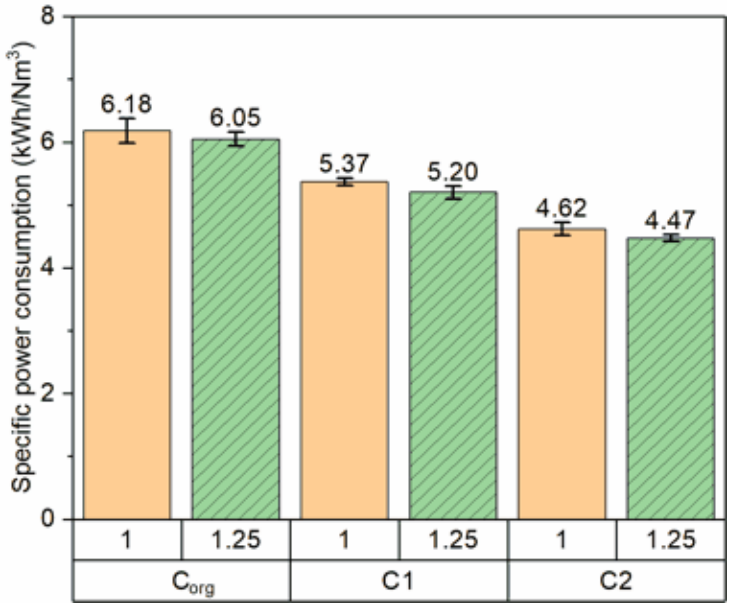

Figure 5-14. Specific power consumption of the gasification process of C1 and C2 samples

5.6. Characteristics of condensate liquid and residual char from the experiments of C1 and C2 samples

The typical volume of condensate liquid obtained for an hour from the experiments conducted on C_{org}, C1, and C2 samples at 900℃ of gasification temperature and S/C ratio of 1.00 and 1.25 is presented in Figure 5-15. As discussed in section 4.7.1, the condensate liquid produced by the gasification process of the C_{org} sample contained a significant amount of water, similar results were observed for the gasification process of the C1 sample (Figure 5-15-c,d) and C2 sample (Figure 5-15-e,f). Therefore, further analysis of the condensate liquid was not conducted.

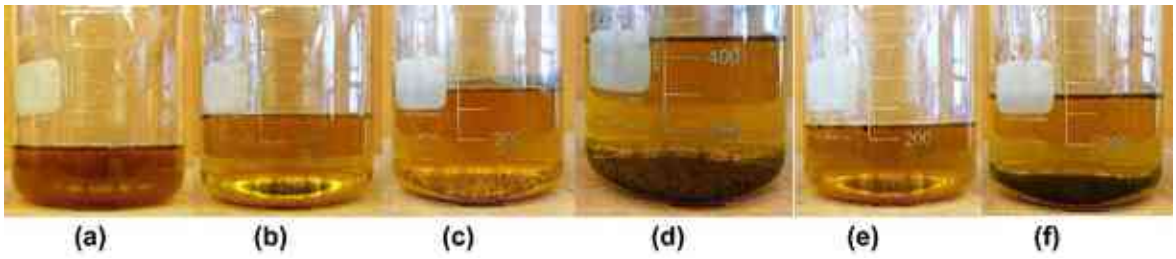

Figure 5-15. Typical condensate liquid volume per hour from the experiments of C_{org} sample at 1.00 and 1.25 of S/C ratio-(a-b), C1 sample at 1.00 and 1.25 of S/C ratio (c-d), and C2 sample at 1.00 and 1.25 of S/C ratio (e-f) and 900 ℃ of gasification temperature

Table 5-4 presents the elemental, ash, and heating value analysis of char samples obtained from the experimental gasification of C1 and C2 samples. The total weight percentage can exceed 100 %, however, it can be explained by the uncertainty of measurement equipment, as well as the non-homogeneous char sample.

The nitrogen and hydrogen contents in char samples were found to be lower than those of the original coal samples, with a significant decrease in hydrogen content. In the case of the C1 sample, the weight percentage of hydrogen content decreased from 4.68 wt% in the original C1 sample to 0.47 and 0.48 wt% in the gasification char obtained at 1.00 and 1.25 of the S/C ratio, respectively. For the experiments of the C2 sample, the weight percentage of hydrogen content decreased from 4.39 to 0.37 and 0.41 wt%, respectively. On the other hand, the weight percentage of carbon and sulphur in the char samples increased at the same experimental conditions, except for the C2-char sample produced at 1.25 of S/C ratio. With a significant S content in char samples, it indicated that there was only a small amount of sulphur left in the produced gas, but the utilisation of char samples in a secondary process has to be considered thoroughly.

Table 5-4. General analysis of char samples from experiments of C1, and C2 at 900 °C

Samples	S/C ratio (mol/mol)		N wt%	C wt%	H wt%	S wt%	Ash wt%	HHV MJ/kg
C1			***0.83***	***51.95***	***4.68***	***5.14***	***13.3***	***21.84***
C1-char	**1.00**	**Mean**	**0.44**	**62.15**	**0.47**	**6.18**	**38.25**	**23.36**
		SD	0.05	2.41	0.24	0.36		
	1.25	**Mean**	**0.38**	**54.35**	**0.40**	**6.94**	**45.81**	**20.62**
		SD	0.04	2.08	0.21	0.40		
C2			***0.84***	***48.17***	***4.39***	***5.38***	***18.2***	***19.81***
C2-char	**1.00**	**Mean**	**0.38**	**48.43**	**0.37**	**8.13**	**53.32**	**18.87**
		SD	0.03	0.85	0.19	0.14		
	1.25	**Mean**	**0.36**	**44.46**	**0.41**	**8.69**	**58.15**	**17.98**
		SD	0.04	0.83	0.21	0.23		

The ash content also increased in all char samples at all experimental conditions. In the case of the C1 sample, the ash content increased from 13.3 wt% in the original C1 sample to 38.25 and 45.81 wt% at 1.00 and 1.25 S/C ratios, respectively. The corresponding numbers were from 18.2 to 53.32 and 58.15 wt% for the C2 sample.

Regarding the energetic perspective, the higher heating value of the original C1 and C2 samples is higher than that of their corresponding char samples, except for the case of the C1 char sample obtained from the gasification process at 1.00 of the S/C ratio. Specifically, the higher heating value increased from 21.84 MJ/kg in the C1 sample to 23.36 MJ/kg in the C1-char sample at 1.00 S/C ratio, but it decreased to 20.62 MJ/kg in the C1-char sample at 1.25 S/C ratio. In the case of experimental gasification of the C2 sample, the higher heating values were 18.87 and 17.98 MJ/kg for char samples at 1.00 and 1.25 S/C ratios, respectively. With a high rate in the heating value of char samples, the residual solid product from the gasification process of the C1 and C2 samples could potentially be used in the further power generation process.

6. Conclusion and recommendations

6.1. Conclusion

Steam gasification in a fixed-bed gasifier is a promising solution in clean coal technologies. The Institute of Energy, Ceramics and Polymer Technology at the University of Miskolc, Hungary has developed and constructed a multi-stage fixed bed gasifier to produce a multi-functional produced gas. This thesis experimentally investigated the performance of the multi-stage fixed bed gasifier for enhanced control of synthesis gas composition using low-rank coal the starting material. Experiments were conducted in a multi-stage fixed bed gasifier with steam as a reactant to investigate the effects of various operating conditions on gasification products, synthesis gas composition, H_2/CO ratio, carbon conversion efficiency, cold gas efficiency, as well as specific power consumption.

Experiments were carried out in a single-line multi-stage fixed bed gasifier arranged in an L shape, with a vertical reactor for the pyrolysis process and a horizontal reactor for the reduction process. Both reactors are made of heat-resistant steel, with an outer diameter of 100 mm and an inner diameter of 80 mm. Each reactor has an effective length of 1600 mm and is covered by electrical heaters.

In the first part of this study, the original low-rank coal sample-C_{org} was examined at gasification temperatures of 700, 800 and 900 ℃ with S/C ratios of 0.75, 1.00, and 1.25, while maintaining the pyrolysis temperature at 600 ℃. The mass flow rate of materials was set at 1.084 kg/h. The low-rank coal-C_{org} is characterized by a low carbon content of 35.6 wt% and a high sulphur content of 3.07 wt%. The volatile and fixed carbon contents accounted for 57.41 wt%, while the ash content was approximately 32.08 wt%. The coal sample has a low higher heating value of 15.03 MJ/kg.

Both increasing gasification temperature and S/C ratio resulted in a higher conversion rate of the gasification process, leading to a decrease in residual char and condensate liquid yields, and an increase in produced gas yield. However, the positive effects of increasing the S/C ratio on char gasification were limited when the S/C ratio exceeded 1.00, as observed in the case of gasification temperature at 700 and 900 ℃. At a gasification temperature of 700 ℃, the produced gas decreased from 0.48 Nm^3/kg_{coal} at an S/C ratio of 1.00 to 0.44 Nm^3/kg_{coal} at an S/C ratio of 1.25. In the case of 900 ℃, the produced gas increased slightly from 1.10 to 1.14 Nm^3/kg_{coal} with similar S/C ratios. Among the experimental conditions, the highest conversion rate was achieved at a gasification temperature of 900 ℃ and an S/C

ratio of 1.25, with an average char yield of 373.03 g/h and an average syngas yield of 1.14 Nm^3/kg_{coal}.

Regarding the syngas composition, the main components of produced gas under all experiments were H_2, CO, CO_2, and CH_4, accounting for at least 94 V/V% of the total volume. Increasing the gasification temperature had a significant effect on the syngas composition. Meanwhile, the volume fraction of syngas varied slightly when the S/C ratio increased from 0.75 to 1.25. The mean volume fraction of CO, CO_2, and CH_4 showed a significant variation when the gasification temperature increased from 700 to 900 ℃ for all S/C ratios. On the other hand, the changes in H_2 concentration did not follow a monotonic trend under the same conditions. From a chemical utilisation point of view, the gasification temperature at 900 ℃ and S/C ratio of 1.25 resulted in the most promising H_2/CO ratio of 1.99 (~2). From an energetic point of view, the highest LHV_{syngas} was observed at 900 ℃ and 0.75 of S/C ratio, approximately 10.69 MJ/Nm^3.

The experimental results showed that the CCE and CGE at 900 ℃ of gasification temperature were significantly higher than that at other gasification temperatures at the same conditions of S/C ratios. However, at 900 ℃ of gasification temperature, the CCE and CGE only showed a minor change when the S/C ratio increased further from 1.00 to 1.25. At 900 ℃ of gasification temperature, The CCE were 75.32 and 75.09 % at 1.00 and 1.25 of S/C ratios, respectively. In the meantime, the CGE were 83.43 and 83.69 % at the same experimental conditions. It was observed that the higher syngas yield at higher gasification temperatures resulted in lower specific power consumption of the gasification process. The lowest specific power consumption was obtained at 900 ℃ of gasification temperature and 1.25 of S/C ratio.

Based on the initial priority of an H_2/CO ratio of 2.00 and the highest syngas yield, the optimal conditions for the original low-rank coal sample were at 900 ℃ of gasification temperature and 1.25 of S/C ratio in our multi-stage gasification process.

In the second part of this study, the original low-rank coal samples were subjected to a gravity separation process using magnetite suspension fluid. The separation process resulted in two types of coal samples, namely C1 and C2. The specific weight of the C1 and C2 samples were ≤ 1.6 g/cm^3 and between 1.6-1.8 g/cm^3, respectively. The experiments were carried out at a gasification temperature of 900 ℃ and S/C ratios of 1.00 and 1.25.

The results indicated that the gasification process of the separated coal samples produced a higher specific volume of syngas compared to the original coal sample. Furthermore, the experiments with the C2 sample showed a higher conversion efficiency

compared to the C1 sample across all experimental settings. Specifically, at a gasification temperature of 900 ℃, the C1 sample experiments generated 1.4 and 1.52 Nm^3/kg_{coal} at S/C ratios of 1.00 and 1.25. In contrast, the C2 sample experiments yielded syngas volumes of 1.59 and 1.70 $Nm3/kg_{coal}$ at the same S/C ratios.

Regarding the H_2/CO ratio, the C1 sample experiments achieved ratios close to the desired value of 2.00, with values of 2.11 and 2.18 at S/C ratios of 1.00 and 1.25, respectively. For the experiments of the C2 sample, the H_2/CO ratio reached 1.88 and 2.00 at S/C ratios of 1.00 and 1.25, respectively. Therefore, the optimal conditions for the C2 sample were identified as a gasification temperature of 900 ℃ and an S/C ratio of 1.25.

6.2. Recommendations for further work

The low-rank coal used in this study has a high sulphur content, resulting in hydrogen sulphide in the produced gas. However, hydrogen sulphide poses a barrier to the application of produced gas in chemical production processes. Therefore, future research efforts should focus on developing efficient and cost-effective methods to remove sulphur-based gases after the gasification process.

Furthermore, it is important to expand the scope of research to include other fuel types such as biomass or refuse-derived fuel. Each fuel type may have different characteristics and requirements, so it is essential to conduct comprehensive investigations to determine the optimal conditions for gasification and produced gas composition based on the specific applications of the produced gas.

7. New scientific results

Thesis 1. The original low-rank coal sample from Hungary with a particle size of 10-30 mm was studied in the steam gasification process. The gasification experiments were carried out in a single-line multi-stage fixed bed configuration, with a mass flow rate of coal of 1084 g/h at the gasification temperatures of 700, 800 and 900 °C, while with S/C ratios were set at 0.75, 1.00, and 1.25.

To establish the relationship between the produced gas yield and the gasification parameters, a linear function and a parabolic were formulated considering the gasification temperatures and S/C ratios. These equations can be expressed as follows:

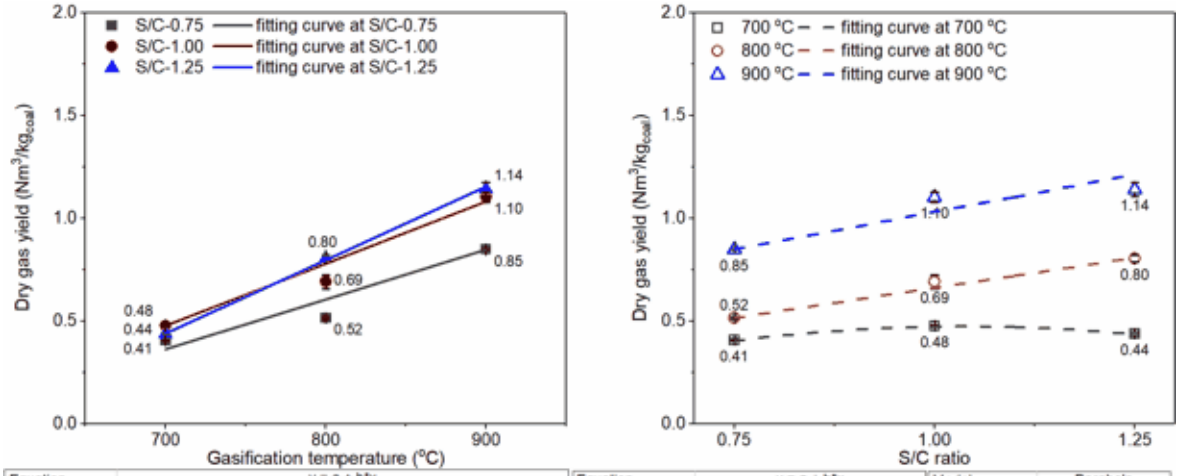

Equation	y = a + b*x		
Plot	Dry gas yield at S/C-0.75	Dry gas yield at S/C-1.00	Dry gas yield at S/C-1.25
Weight	Instrumental		
Intercept	-1.33259 ± 0.4137	-1.63661 ± 0.22277	-2.06137 ± 0.05683
Slope	0.00242 ± 4.64524E-	0.00302 ± 3.16097E-	0.00357 ± 7.82831E-
Pearson's r	0.98211	0.99457	0.99976
R-Square(COD	0.96454	0.98917	0.99952

Equation	y = a + b*x	
Plot	Dry gas yield at 800 °C	Dry gas yield at 900 °C
Weight	Instrumental	
Intercept	0.07711 ± 0.02	0.30346 ± 0.1537
Slope	0.58555 ± 0.03	0.7283 ± 0.2048
Pearson's r	0.99846	0.96266
R-Square(COD)	0.99693	0.92672

Model	Parabola
Equation	y = A + B*x + C*x^2
Plot	Dry gas yield at 700 °C
A	-0.45208 ± 0
B	1.78958 ± 0
C	-0.86397 ± 0
R-Square(COD	0.9787

All linear functions describe well the relations between the dry gas yield, gasification temperature and S/C ratio, with the exception of dry gas yield and S/C ratio at 700 °C, that is best described with a parabolic function.

Thesis 2. Under the same experimental conditions as shown in thesis 1, to investigate the relationship between the H_2/CO ratio and the gasification parameters, an equation was formulated based on the experimental parameters. At a constant S/C ratio, the H_2/CO ratio can be expressed as power functions of the gasification temperatures. The equations describing these relationships are as follows:

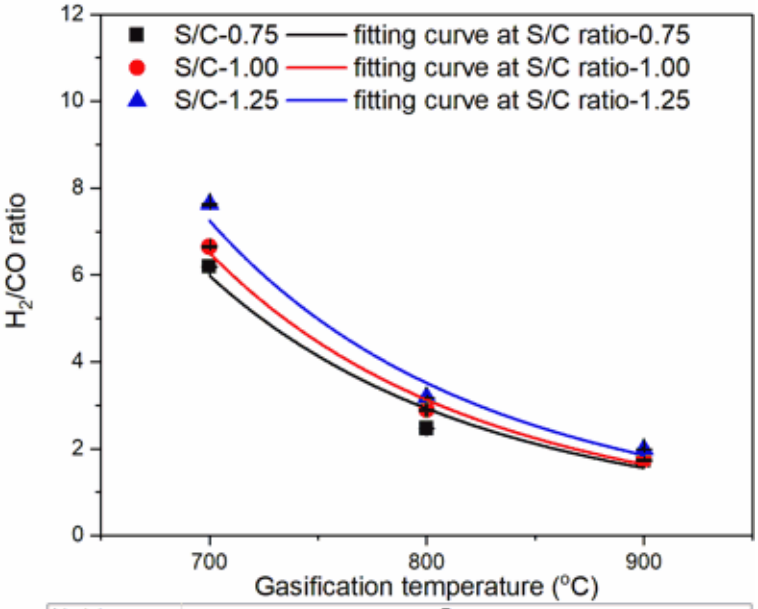

Model	Power		
Equation	y = a*x^b		
Plot	H_2/CO ratio at S/C-0.75	H_2/CO ratio at S/C-1.00	H_2/CO ratio at S/C-1.25
a	1.14621E16 ± 7.25393	2.959E16 ± 1.06058	2.08374E16 ± 1.09469
b	-5.37132 ± 0.95405	-5.5032 ± 0.53999	-5.43328 ± 0.78742
R-Square(CO	0.96523	0.98909	0.97059

Thesis 3. The desired H_2/CO ratio for a specific chemical production process is typically 2.00. The experiments conducted in a single-line multi-stage gasifier demonstrated that an H_2/CO ratio of approximately 2.00 can be achieved at a gasification temperature of 900 °C using an original low-rank coal sample with a particle size of 10-30 mm and a mass flow rate of 1084 g/h. The optimal conditions for achieving an H_2/CO ratio of 2.00 were identified as a gasification temperature of 900 °C and an S/C ratio of 1.25.

Thesis 4. The original low-rank coal sample was subjected to a gravity separation process using a heavy magnetite suspension fluid to obtain two separated coal samples 1) with a specific density of up to 1.6 g/cm^3 (C1) and 2) a specific density between 1.6 - 1.8 g/cm^3 (C2). The heavy suspension-separated coal samples exhibited higher syngas yields compared to the original coal sample, under the same gasification temperature of 900 °C and S/C ratios of 1.00 and 1.25. The produced syngas from the coal sample with a specific density between 1.6 - 1.8 g/cm^3 (C2) can reach an optimal H_2/CO ratio of 2.00 for chemical production processes, while the gas yield can be increased by 50 % compared to the original coal sample, under the same gasification conditions, with an S/C ratio of 1.25 at 900 °C.

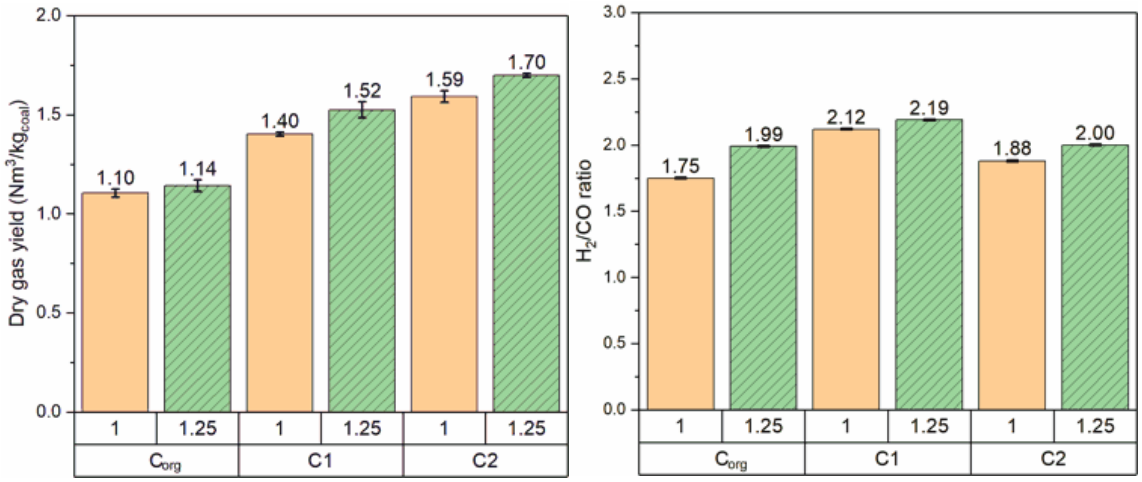
Dry gas yield (Nm³/kg_coal)
2.0
1.5
1.0
0.5
0.0
1.10
1.14
1.40
1.52
1.59
1.70
1
1.25
1
1.25
1
1.25
C_org
C1
C2
H2/CO ratio
3.0
2.5
2.0
1.5
1.0
0.5
0.0
1.75
1.99
2.12
2.19
1.88
2.00
1
1.25
1
1.25
1
1.25
C_org
C1
C2

8. Publications

Journal papers:

1. **Mai, T.D.**; Koós, T.; Sebe, E.; Siménfalvi, Z.; Kállay, A.A. *Efficiency Enhancement of the Single Line Multi-Stage Gasification of Hungarian Low-Rank Coal: Effects of Gasification Temperature and Steam/Carbon (S/C) Ratio*. Energies 2023, 16, 4427. https://doi.org/10.3390/en16114427
2. **Thuan Duc, Mai**; Sebe, Emese; Kallay, Andras Arnold. *The single-stage steam gasification of magnetite heavy suspension separated coal samples from Hungarian brown coal*, Építőanyag: Journal of Silicate Based and Composite Materials 74: 4 pp. 150-155., 6 p. (2022). https://doi.org/ 10.14382_epitoanyag-jsbcm.2022.23.
3. **Mai, Duc Thuan**; Kállay, András Arnold. *Hungarian Low-Rank Coal Gasification and Single Line Multi-Stage Gasification: Short Review*, Materials Science and Engineering: A Publication of The University of Miskolc (2022).
4. **Mai, Duc Thuan**; Kállay, András Arnold. *Development Of Application Tailored Low-Cost Steam Generator for Gasification Process*, Materials Science and Engineering: A Publication of The University of Miskolc (2022).
5. **Mai, Duc Thuan**; Kállay, András Arnold. *Coal Char Steam Gasification of Three Different Hungarian Coal Types,* Materials Science and Engineering: A Publication of The University of Miskolc (2022).

Conference papers:

1. **Mai, Thuan Duc**; Kállay, András Arnold, *Hydrogen production by steam gasification of Hungarian brown coal char*, Multidiszciplináris Tudományok: A Miskolci Egyetem Közleménye 12, 3, pp. 79-88., 10 p. (2022), **DOI: 10.35925/j.multi.2022.3.8**
2. A. A., Kállay; **T. D., Mai**; Zs., Forgács, *The Development of Multi-Stage Gasification at University of Miskolc*, In: Kovács, Helga; Madarász, Tamás; Nagy, Gábor; Nagy, István; Szűcs, Péter; Németh, Norbert; Vadászi, Marianna (szerk.) Fókuszban a hazai felszín alatti természeti erőforrások: Nyersanyagok, energia és technológiák nexusa, Miskolc-Egyetemváros, Magyarország: Miskolci Egyetem (2022) 370 p. pp. 219-231., 13 p.
3. **Mai, Thuan Duc**; Arnold Kállay, András, *Effects of temperature and steam flow rate on Hungarian low-rank coal gasification*, In Scala, Fabrizio; Apicella, Barbara; Chiron, Riccardo; Cimino, Stefano; Commodo, Mario; D'Anna, Andrea; De

Joannon, Mara; Di Benedetto, Almerinda; Fantuzzi, Massimiliano; Faravelli, Tiziano; Fino, Debora; Frassoldati, Alessio; Galletti, Chiara; Giacomazzi, Eugenio; Ragucci, Raffaele; Salatino, Piero; Salzano, Ernesto; Saponaro, Alessandro; Senneca, Osvalda; Vaglieco, Bianca Maria; Valorani, Mauro (szerk.) 10th European Combustion Meeting Proceedings Volume (2021) pp. 497-502. , 6 p.

4. **Mai, Duc Thuan**; Kállay, András, *Heat transfer modelling using waste rubber as starting material in the fluidized bed chamber*, In: Costa, Mário; Rabaçal, Miriam; Fernandes, Edgar; Pires, João; Coelho, Pedro (szerk.) Proceedings of the 9th European Combustion Meeting (2019) Paper: PAPER S1_AIII_39

Poster and oral presentation:

1. **Mai, Thuan Duc**; Kállay, András Arnold, *Hydrogen production by steam gasification of Hungarian brown coal char*, MicroCAD, University of Miskolc, 2022
2. **Mai, Thuan Duc**; Arnold Kállay, András. *The single-stage gasification of magnetite heavy suspension separated coal samples from Hungarian brown coal,* International Conference on Science, Technology, Engineering and Economy –ICOSTEE 2022, 24 March 2022, Szeged, Hungary
3. **Mai, Thuan Duc**; Arnold Kállay, András. *Hydrogen production on the single-stage gasification system from Hungarian brown coal char*, 10th Jubilee Interdisciplinary Doctoral Conference (IDK2021)-the University of Pécs, 12-13th November 2021, Pécs, Hungary.
4. **Mai, Thuan Duc**; Arnold Kállay, András, *Effects of temperature and steam flow rate on Hungarian low-rank coal gasification,* European Combustion Meeting (2021).
5. **Mai, Duc Thuan**; Kállay, András, *Heat transfer modelling using waste rubber as starting material in the fluidized bed chamber,* European Combustion Meeting (2019).
6. **Thuan, Duc Mai**; András, Arnold Kállay, *Model calculation of heat transfer in fluidized bed boiler,* MÉB, Hungary, (2018).

9. References

[1] B. Group, BP Statistical Review of World Energy 2019, 2019.

[2] BP, www.bp.comenglobalcorporateenergy-economicsenergy-outlook.html (dowload 11.Dec.2018), (2018).

[3] M. Melikoglu, Clean coal technologies: A global to local review for Turkey, Energy Strateg. Rev. 22 (2018) 313–319. https://doi.org/10.1016/j.esr.2018.10.011.

[4] IEA, Global energy and CO2 status report - 2018, 2018.

[5] X. Tang, S. Snowden, B.C. McLellan, M. Höök, Clean coal use in China: Challenges and policy implications, Energy Policy. 87 (2015) 517–523. https://doi.org/10.1016/j.enpol.2015.09.041.

[6] G. Yue, S. Li, Clean Coal Technology and Sustainable Development, in: Proc. 8th Int. Symp. Coal Combust. Clean Coal Technol. Sustain. Dev., 2016. https://doi.org/10.1007/978-981-10-2023-0.

[7] D.A. Bell, B.F. Towler, M. Fan, Coal Gasification and Its Application, Elsevier, 2011.

[8] V. Belgiorno, G. De Feo, C. Della Rocca, R.M.A. Napoli, Energy from gasification of solid wastes, Waste Manag. 23 (2003) 1–15. https://doi.org/10.1016/S0956-053X(02)00149-6.

[9] A. Arnold, K. Vivien, G. Nagy, T. Koós, The analysis of the solid and liquid phase products of two-stage pyrolysis, Mater. Sci. Eng. 42 (2017) 46–58.

[10] L. Emami Taba, M.F. Irfan, W.A.M. Wan Daud, M.H. Chakrabarti, The effect of temperature on various parameters in coal, biomass and CO-gasification: A review, Renew. Sustain. Energy Rev. 16 (2012) 5584–5596. https://doi.org/10.1016/J.RSER.2012.06.015.

[11] S. Luo, B. Xiao, Z. Hu, S. Liu, X. Guo, M. He, Hydrogen-rich gas from catalytic steam gasification of biomass in a fixed bed reactor: Influence of temperature and steam on gasification performance, Int. J. Hydrogen Energy. 34 (2009) 2191–2194. https://doi.org/10.1016/j.ijhydene.2008.12.075.

[12] S. Luo, Y. Zhou, C. Yi, Syngas production by catalytic steam gasification of municipal solid waste in fixed-bed reactor, Energy. 44 (2012) 391–395. https://doi.org/10.1016/j.energy.2012.06.016.

[13] L. Peng, Y. Wang, Z. Lei, G. Cheng, Co-gasification of wet sewage sludge and forestry waste in situ steam agent, Bioresour. Technol. 114 (2012) 698–702. https://doi.org/10.1016/j.biortech.2012.03.079.

[14] A. Tavasoli, M.G. Ahangari, C. Soni, A.K. Dalai, Production of hydrogen and syngas via gasification of the corn and wheat dry distiller grains (DDGS) in a fixed-bed micro reactor, Fuel Process. Technol. 90 (2009) 472–482. https://doi.org/10.1016/j.fuproc.2009.02.001.

[15] Y. Niu, F. Han, Y. Chen, Y. Lyu, L. Wang, Experimental study on steam gasification of pine particles for hydrogen-rich gas, J. Energy Inst. 90 (2017) 715–724. https://doi.org/10.1016/j.joei.2016.07.006.

[16] M.A. Hamad, A.M. Radwan, D.A. Heggo, T. Moustafa, Hydrogen rich gas production from catalytic gasification of biomass, Renew. Energy. 85 (2016) 1290–1300. https://doi.org/10.1016/j.renene.2015.07.082.

[17] B. Acharya, A. Dutta, P. Basu, An investigation into steam gasification of biomass for hydrogen enriched gas production in presence of CaO, Int. J. Hydrogen Energy. 35 (2010) 1582–1589. https://doi.org/10.1016/j.ijhydene.2009.11.109.

[18] H. Li, Z. Chen, C. Huo, M. Hu, D. Guo, B. Xiao, Effect of bioleaching on hydrogen-rich gas production by steam gasification of sewage sludge, Energy Convers. Manag. 106 (2015) 1212–1218. https://doi.org/10.1016/j.enconman.2015.10.048.

[19] C.G. Soni, Z. Wang, A.K. Dalai, T. Pugsley, T. Fonstad, Hydrogen production via gasification of meat and bone meal in two-stage fixed bed reactor system, Fuel. 88 (2009) 920–925. https://doi.org/10.1016/j.fuel.2008.10.037.

[20] G. Chen, X. Guo, Z. Cheng, B. Yan, Z. Dan, W. Ma, Air gasification of biogas-derived digestate in a downdraft fixed bed gasifier, Waste Manag. 69 (2017) 162–169. https://doi.org/10.1016/j.wasman.2017.08.001.

[21] N. Gao, A. Li, C. Quan, A novel reforming method for hydrogen production from biomass steam gasification, Bioresour. Technol. 100 (2009) 4271–4277. https://doi.org/10.1016/j.biortech.2009.03.045.

[22] G. Pu, H.P. Zhou, G.T. Hao, Study on pine biomass air and oxygen/steam gasification in the fixed bed gasifier, Int. J. Hydrogen Energy. 38 (2013) 15757–15763. https://doi.org/10.1016/j.ijhydene.2013.04.117.

[23] X. Zheng, C. Chen, Z. Ying, B. Wang, Experimental study on gasification performance of bamboo and PE from municipal solid waste in a bench-scale fixed bed reactor, Energy Convers. Manag. 117 (2016) 393–399. https://doi.org/10.1016/j.enconman.2016.03.044.

[24] X. Yuan, K.B. Lee, H.T. Kim, Investigation of Indonesian low rank coals gasification in a fixed bed reactor with K2CO3 catalyst loading, J. Energy Inst. 92 (2019) 904–

912. https://doi.org/10.1016/j.joei.2018.06.011.

[25] Q. Wang, N. Rong, H. Fan, Y. Meng, M. Fang, L. Cheng, K. Cen, Enhanced hydrogen-rich gas production from steam gasification of coal in a pressurized fluidized bed with CaO as a CO2 sorbent, Int. J. Hydrogen Energy. 39 (2014) 5781–5792. https://doi.org/10.1016/j.ijhydene.2014.01.153.

[26] J. Fermoso, B. Arias, M.G. Plaza, C. Pevida, F. Rubiera, J.J. Pis, F. García-Peña, P. Casero, High-pressure co-gasification of coal with biomass and petroleum coke, Fuel Process. Technol. 90 (2009) 926–932. https://doi.org/10.1016/j.fuproc.2009.02.006.

[27] M. Niu, Y. Huang, B. Jin, X. Wang, Oxygen gasification of municipal solid waste in a fixed-bed gasifier, Chinese J. Chem. Eng. 22 (2014) 1021–1026. https://doi.org/10.1016/j.cjche.2014.06.026.

[28] Q.M.K. Waheed, C. Wu, P.T. Williams, Hydrogen production from high temperature steam catalytic gasification of bio-char, J. Energy Inst. 89 (2016) 222–230. https://doi.org/10.1016/j.joei.2015.02.001.

[29] W. Li, Q. Li, R. Chen, Y. Wu, Y. Zhang, Investigation of hydrogen production using wood pellets gasification with steam at high temperature over 800 °c to 1435 °c, Int. J. Hydrogen Energy. 39 (2014) 5580–5588. https://doi.org/10.1016/j.ijhydene.2014.01.102.

[30] N. Gao, A. Li, C. Quan, F. Gao, Hydrogen-rich gas production from biomass steam gasification in an updraft fixed-bed gasifier combined with a porous ceramic reformer, Int. J. Hydrogen Energy. 33 (2008) 5430–5438. https://doi.org/10.1016/j.ijhydene.2008.07.033.

[31] M. Niu, Y. Huang, B. Jin, X. Wang, Oxygen gasification of municipal solid waste in a fixed-bed gasifier, Chinese J. Chem. Eng. 22 (2014) 1021–1026. https://doi.org/10.1016/j.cjche.2014.06.026.

[32] J. Huang, Y. Fang, H. Chen, Y. Wang, Coal Gasification Characteristic in a Pressurized Fluidized Bed, Energy and Fuels. 17 (2003) 1474–1479. https://doi.org/10.1021/ef030052k.

[33] C. Fushimi, M. Goto, A. Tsutsumi, J.I. Hayashi, T. Chiba, Steam gasification characteristics of coal with rapid heating, J. Anal. Appl. Pyrolysis. 70 (2003) 185–197. https://doi.org/10.1016/S0165-2370(02)00131-6.

[34] M.H. Sedghkerdar, E. Mostafavi, N. Mahinpey, Sorbent enhanced hydrogen production from steam gasification of coal integrated with CO2 capture, Int. J. Hydrogen Energy. 39 (2014) 17001–17008.

https://doi.org/10.1016/j.ijhydene.2014.08.062.

[35] F. Zhang, F.M. Hong, HuangXin, M. D.Argyle, ZhangBo, B. Towler, ZhangYulong, Catalytic gasification of a Powder River Basin coal with CO2andH2Omixtures.pdf, (n.d.).

[36] Y. Kong, J. Kim, D. Chun, S. Lee, Y. Rhim, J. Lim, H. Choi, S. Kim, J. Yoo, Comparative studies on steam gasification of ash-free coals and their original raw coals, Int. J. Hydrogen Energy. 39 (2014) 9212–9220. https://doi.org/10.1016/j.ijhydene.2014.04.054.

[37] S. Fan, X. Yuan, L. Zhao, L.H. Xu, T.J. Kang, H.T. Kim, Experimental and kinetic study of catalytic steam gasification of low rank coal with an environmentally friendly, inexpensive composite K2CO3-eggshell derived CaO catalyst, Fuel. 165 (2016) 397–404. https://doi.org/10.1016/j.fuel.2015.10.084.

[38] X. Zhou, J. Zhao, S. Guo, J. Li, Z. Yu, S.S. Song, J. Li, Y. Fang, High quality syngas production from pressurized K2CO3 catalytic coal gasification with in-situ CO2 capture, Int. J. Hydrogen Energy. 43 (2018) 17091–17099. https://doi.org/10.1016/j.ijhydene.2018.07.062.

[39] Y. Xiao, S. Xu, Y. Song, C. Wang, S. Ouyang, Gasification of low-rank coal for hydrogen-rich gas production in a dual loop gasification system, Fuel Process. Technol. 171 (2018) 110–116. https://doi.org/10.1016/j.fuproc.2017.11.014.

[40] Z.H. Chen, D.G. Lai, L.Q. Bai, Y. Tian, S.Q. Gao, G.W. Xu, A. Tsutsumi, Methane-rich syngas production in an integrated fluidized bed by coupling pyrolysis and gasification of low-rank coal, Fuel Process. Technol. 140 (2015) 88–95. https://doi.org/10.1016/j.fuproc.2015.08.028.

[41] X. Yuan, H. Namkung, T.-J. Kang, H.-T. Kim, K2CO3-Catalyzed Steam Gasification of Indonesian Low-Rank Coal for H2-Rich Gas Production in a Fixed Bed Reactor, Energy Technol. 3 (2015) 527–534. https://doi.org/10.1002/ente.201402198.

[42] A. Smoliński, K. Stańczyk, N. Howaniec, Steam gasification of selected energy crops in a fixed bed reactor, Renew. Energy. 35 (2010) 397–404. https://doi.org/10.1016/j.renene.2009.06.005.

[43] S. Fan, L.H. Xu, T.J. Kang, H.T. Kim, Application of eggshell as catalyst for low rank coal gasification: Experimental and kinetic studies, J. Energy Inst. 90 (2017) 696–703. https://doi.org/10.1016/j.joei.2016.07.008.

[44] Z. Chen, Q. Dun, Y. Shi, D. Lai, Y. Zhou, S. Gao, G. Xu, High quality syngas production from catalytic coal gasification using disposable Ca(OH)2 catalyst, Chem.

Eng. J. 316 (2017) 842–849. https://doi.org/10.1016/j.cej.2017.02.025.

[45] H. Yang, H. Chen, Biomass gasification for synthetic liquid fuel production, © 2015 Woodhead Publishing Limited. All rights reserved., 2015. https://doi.org/10.1016/B978-0-85709-802-3.00011-4.

[46] T. Valliyappan, D. Ferdous, N.N. Bakhshi, A.K. Dalai, Production of hydrogen and syngas via steam gasification of glycerol in a fixed-bed reactor, Top. Catal. 49 (2008) 59–67. https://doi.org/10.1007/s11244-008-9062-7.

[47] J. Li, S. Liao, W. Dan, K. Jia, X. Zhou, Experimental study on catalytic steam gasification of municipal solid waste for bioenergy production in a combined fixed bed reactor, Biomass and Bioenergy. 46 (2012) 174–180. https://doi.org/10.1016/j.biombioe.2012.08.026.

[48] J. Li, J. Liu, S. Liao, R. Yan, Hydrogen-rich gas production by air–steam gasification of rice husk using supported nano-NiOγ-Al2O3 catalyst.pdf, Int. J. Hydrogen Energy. 35 (2010) 7399–7404.

[49] J. Wang, B. Xiao, S. Liu, Z. Hu, P. He, D. Guo, M. Hu, F. Qi, S. Luo, Catalytic steam gasification of pig compost for hydrogen-rich gas production in a fixed bed reactor, Bioresour. Technol. 133 (2013) 127–133. https://doi.org/10.1016/j.biortech.2013.01.092.

[50] K. Li, R. Zhang, J. Bi, Experimental study on syngas production by co-gasification of coal and biomass in a fluidized bed, Int. J. Hydrogen Energy. 35 (2010) 2722–2726. https://doi.org/10.1016/j.ijhydene.2009.04.046.

[51] R. Zhang, D. Liu, Q. Wang, Z. Luo, M. Fang, K. Cen, Coal Char Gasification on a Circulating Fluidized Bed for Hydrogen Generation: Experiments and Simulation, Energy Technol. 3 (2015) 1059–1067. https://doi.org/10.1002/ente.201500135.

[52] Y.J. Kim, S.H. Lee, S.D. Kim, Coal gasification characteristics in a downer reactor, Fuel. 80 (2001) 1915–1922. https://doi.org/10.1016/S0016-2361(01)00052-7.

[53] J.G. Speight, Handbook of Gasification Technology, Wiley, 2020. https://doi.org/10.1002/9781118773970.

[54] R.W. Breault, Gasification processes old and new: A basic review of the major technologies, Energies. 3 (2010) 216–240. https://doi.org/10.3390/en3020216.

[55] P. Basu, Biomass Gasification, Pyrolysis, and Torrefaction, 2013. http://search.ebscohost.com/login.aspx?direct=true&db=f5h&AN=19565935&site=ehost-live.

[56] C. García Cortés, E. Tzimas, S.D. Peteves, Technologies for Coal based Hydrogen

and Electricity Co-production Power Plants with CO 2 Capture. EUR 23661 EN, 2009. https://doi.org/10.2790/23969.

[57] J.A. Ruiz, M.C. Juárez, M.P. Morales, P. Muñoz, M.A. Mendívil, Biomass gasification for electricity generation: Review of current technology barriers, Renew. Sustain. Energy Rev. 18 (2013) 174–183. https://doi.org/10.1016/j.rser.2012.10.021.

[58] X. Zhang, K. Li, C. Zhang, A. Wang, Performance analysis of biomass gasification coupled with a coal-fired boiler system at various loads, Waste Manag. 105 (2020) 84–91. https://doi.org/10.1016/j.wasman.2020.01.039.

[59] D. Sofia, P. Coca Llano, A. Giuliano, M. Iborra Hernández, F. García Peña, D. Barletta, Co-gasification of coal-petcoke and biomass in the Puertollano IGCC power plant, Chem. Eng. Res. Des. 92 (2014) 1428–1440. https://doi.org/10.1016/j.cherd.2013.11.019.

[60] O. Shinada, A. Yamada, Y. Koyama, The development of advanced energy technologies in Japan: IGCC - A key technology for the 21st century, Energy Convers. Manag. 43 (2002) 1221–1233. https://doi.org/10.1016/S0196-8904(02)00009-2.

[61] P. Hofmann, K.D. Panopoulos, L.E. Fryda, A. Schweiger, J.P. Ouweltjes, J. Karl, Integrating biomass gasification with solid oxide fuel cells: Effect of real product gas tars, fluctuations and particulates on Ni-GDC anode, Int. J. Hydrogen Energy. 33 (2008) 2834–2844. https://doi.org/10.1016/j.ijhydene.2008.03.020.

[62] P. Hofmann, A. Schweiger, L. Fryda, K.D. Panopoulos, U. Hohenwarter, J.D. Bentzen, J.P. Ouweltjes, J. Ahrenfeldt, U. Henriksen, E. Kakaras, High temperature electrolyte supported Ni-GDC/YSZ/LSM SOFC operation on two-stage Viking gasifier product gas, J. Power Sources. 173 (2007) 357–366. https://doi.org/10.1016/j.jpowsour.2007.04.073.

[63] G. Balan, C.; Dey, D.; Eker, S.; Peter, M.; Sokolov, P.; Wotzak, Coal Integrated Gasification Fuel Cell System Study, 2004. https://www.osti.gov/servlets/purl/897864.

[64] A. Arnold, K. Vivien, V. Gábor, Two-stage pyrolysis of Hungarian brown coal to reduce hydrocarbons within synthesis gas, Mater. Sci. Eng. 42 (2017) 65–75.

[65] D.-Y. Lee, M.T. Mehran, J. Kim, S. Kim, S.-B. Lee, R.-H. Song, E.-Y. Ko, J.-E. Hong, J.-Y. Huh, T.-H. Lim, Scaling up syngas production with controllable H2/CO ratio in a highly efficient, compact, and durable solid oxide coelectrolysis cell unit-bundle, Appl. Energy. 257 (2020) 114036. https://doi.org/10.1016/j.apenergy.2019.114036.

[66] X. Song, Z. Guo, Technologies for direct production of flexible H2/CO synthesis gas, Energy Convers. Manag. 47 (2006) 560–569. https://doi.org/10.1016/j.enconman.2005.05.012.

[67] K. Aasberg-Petersen, J.-H. Bak Hansen, T.. Christensen, I. Dybkjaer, P.S. Christensen, C. Stub Nielsen, S.E.. Winter Madsen, J.. Rostrup-Nielsen, Technologies for large-scale gas conversion, Appl. Catal. A Gen. 221 (2001) 379–387. https://doi.org/10.1016/S0926-860X(01)00811-0.

[68] K. Liu, C. Song, V. Subramani, Hydrogen and syngas production and purification technologies, John Wiley & Sons, 2010.

[69] J. Rezaiyan, N. P.Cheremisinoff, Gasification technologies: A primer for engineers and scientists, Taylor & Francis Group, 2005.

[70] R.J. Evans, T.A. Milne, Biomass Gasifier "Tars": Their Nature, Formation, and Conversion T.A., 1998.

[71] P. Hasler, T. Nussbaumer, Gas cleaning for IC engine applications from fixed bed biomass gasification, Biomass and Bioenergy. 16 (1999) 385–395. https://doi.org/10.1016/S0961-9534(99)00018-5.

[72] L.C. Laurence, D. Ashenafi, Syngas treatment unit for small scale gasification - Application to IC engine gas quality requirement, J. Appl. Fluid Mech. 5 (2012) 95–103.

[73] M. Baratieri, P. Baggio, B. Bosio, M. Grigiante, G.A. Longo, The use of biomass syngas in IC engines and CCGT plants: A comparative analysis, Appl. Therm. Eng. 29 (2009) 3309–3318. https://doi.org/10.1016/j.applthermaleng.2009.05.003.

[74] A. V. Bridgwater, The technical and economic feasibility of biomass gasification for power generation, Fuel. 74 (1995) 631–653. https://doi.org/10.1016/0016-2361(95)00001-L.

[75] A. Faaij, R. Van Ree, L. Waldheim, E. Olsson, A. Oudhuis, A. Van Wijk, C. Daey-Ouwens, W. Turkenburg, Gasification of biomass wastes and residues for electricity production, Biomass and Bioenergy. 12 (1997) 387–407. https://doi.org/10.1016/S0961-9534(97)00010-X.

[76] GE, Specification for Fuel Gases for Combustion in Heavy-Duty Gas Turbines, 2002. http://citeseerx.ist.psu.edu/viewdoc/download?doi=10.1.1.143.6392&rep=rep1&type=pdf.

[77] H. Boerrigter, H. den Uil, H.-P. Calis, Green Diesel from Biomass via Fischer-Tropsch synthesis: New Insights in Gas Cleaning and Process Design, in: Pyrolysis

Gasif. Biomass Waste, Expert Meet., 2002: pp. 1–13.

[78] M.J.A. Tijmensen, A.P.C. Faaij, C.N. Hamelinck, M.R.M. Van Hardeveld, Exploration of the possibilities for production of Fischer Tropsch liquids and power via biomass gasification, Biomass and Bioenergy. 23 (2002) 129–152. https://doi.org/10.1016/S0961-9534(02)00037-5.

[79] C.N. Hamelinck, A.P.C. Faaij, H. den Uil, H. Boerrigter, Production of FT transportation fuels from biomass; technical options, process analysis and optimisation, and development potential, Energy. 29 (2004) 1743–1771. https://doi.org/10.1016/j.energy.2004.01.002.

[80] M. Asadullah, Biomass gasification gas cleaning for downstream applications: A comparative critical review, Renew. Sustain. Energy Rev. 40 (2014) 118–132. https://doi.org/10.1016/j.rser.2014.07.132.

[81] Prabhansu, M.K. Karmakar, P. Chandra, P.K. Chatterjee, A review on the fuel gas cleaning technologies in gasification process, J. Environ. Chem. Eng. 3 (2015) 689–702. https://doi.org/10.1016/j.jece.2015.02.011.

[82] X. Zeng, Y. Ueki, R. Yoshiie, I. Naruse, F. Wang, Z. Han, G. Xu, Recent progress in tar removal by char and the applications: A comprehensive analysis, Carbon Resour. Convers. 3 (2020) 1–18. https://doi.org/10.1016/j.crcon.2019.12.001.

[83] Z.A. El-rub, Biomass Char As an in-Situ Catalyst for Tar Removal in Gasification Systems, Twente University, 2008.

[84] Y. Feng, J. Lu, J. Wang, J. Mi, M. Zhang, M. Ge, Y. Li, Z. Zhang, W. Wang, Desulfurization sorbents for green and clean coal utilization and downstream toxics reduction: A review and perspectives, J. Clean. Prod. 273 (2020) 123080. https://doi.org/10.1016/j.jclepro.2020.123080.

[85] P.J. Woolcock, R.C. Brown, A review of cleaning technologies for biomass-derived syngas, Biomass and Bioenergy. 52 (2013) 54–84. https://doi.org/10.1016/j.biombioe.2013.02.036.

[86] S. Hamel, H. Hasselbach, S. Weil, W. Krumm, Autothermal two-stage gasification of low-density waste-derived fuels, Energy. 32 (2007) 95–107. https://doi.org/10.1016/j.energy.2006.03.017.

[87] C. Borgianni, P. De Filippis, F. Pochetti, M. Paolucci, Gasification process of wastes containing PVC, Fuel. 81 (2002) 1827–1833. https://doi.org/10.1016/S0016-2361(02)00097-2.

[88] Y. Wang, K. Yoshikawa, T. Namioka, Y. Hashimoto, Performance optimization of

two-staged gasification system for woody biomass, Fuel Process. Technol. 88 (2007) 243–250. https://doi.org/10.1016/j.fuproc.2006.10.002.

[89] C. Wu, Q. Huang, M. Sui, Y. Yan, F. Wang, Hydrogen production via catalytic pyrolysis of biooil in a two-stage fixed bed reactor system, Fuel Process. Technol. 89 (2008) 1306–1316.

[90] J. Li, Y. Yin, X. Zhang, J. Liu, R. Yan, Hydrogen-rich gas production by steam gasification of palm oil wastes over supported tri-metallic catalyst, Int. J. Hydrogen Energy. 34 (2009) 9108–9115. https://doi.org/10.1016/j.ijhydene.2009.09.030.

[91] Y. Xiao, S. Xu, Y. Song, Y. Shan, C. Wang, G. Wang, Biomass steam gasification for hydrogen-rich gas production in a decoupled dual loop gasification system, Fuel Process. Technol. J. 165 (2017) 54–61. https://doi.org/10.1016/j.fuproc.2017.05.013 0378-3820/©.

[92] Y. Pan, A. Abulizi, D. Talifu, Y. Tursun, S. Xu, Catalytic gasification of biomass and coal blend with Fe2O3/olivine in a decoupled triple bed, Fuel Process. Technol. 194 (2019) 106121. https://doi.org/10.1016/j.fuproc.2019.106121.

[93] T. Bui, R. Loof, S.C. Bhattacharya, Multi-stage reactor for thermal gasification of wood, Energy. 19 (1994) 397–404. https://doi.org/10.1016/0360-5442(94)90118-X.

[94] S.C. Bhattacharya, A.H.M.M.R. Siddique, H.-L. Pham, A study on wood gasification for low-tar gas production, Energy. 24 (1999) 285–296.

[95] C.A.V.B. de Sales, D.M.Y. Maya, E.E.S. Lora, R.L. Jaén, A.M.M. Reyes, A.M. González, R.V. Andrade, J.D. Martínez, Experimental study on biomass (eucalyptus spp.) gasification in a two-stage downdraft reactor by using mixtures of air, saturated steam and oxygen as gasifying agents, Energy Convers. Manag. 145 (2017) 314–323. https://doi.org/10.1016/j.enconman.2017.04.101.

[96] A.L. Galindo, E.S. Lora, R.V. Andrade, S.Y. Giraldo, R.L. Jaén, V.M. Cobas, Biomass gasification in a downdraft gasifier with a two-stage air supply: Effect of operating conditions on gas quality, Biomass and Bioenergy. 61 (2014) 236–244. https://doi.org/10.1016/j.biombioe.2013.12.017.

[97] N.K. Ram, N.R. Singh, P. Raman, A. Kumar, P. Kaushal, A detailed experimental analysis of air–steam gasification in a dual fired downdraft biomass gasifier enabling hydrogen enrichment in the producer gas, Energy. 187 (2019) 1–16. https://doi.org/10.1016/j.energy.2019.115937.

[98] A.R. Saleh, B. Sudarmanta, Experimental investigation on multi-stage downdraft gasification: Influence of air ratio and equivalent ratio to the gasifier performance, in:

2018: p. 020026. https://doi.org/10.1063/1.5046222.

[99] J.D. Martínez, E.E. Silva Lora, R.V. Andrade, R.L. Jaén, Experimental study on biomass gasification in a double air stage downdraft reactor, Biomass and Bioenergy. 35 (2011) 3465–3480. https://doi.org/10.1016/j.biombioe.2011.04.049.

[100] A.R. Saleh, B. Sudarmanta, H. Fansuri, O. Muraza, Syngas production from municipal solid waste with a reduced tar yield by three-stages of air inlet to a downdraft gasifier, Fuel. 263 (2020) 116509. https://doi.org/10.1016/j.fuel.2019.116509.

[101] U. Brandt, Peder; Larson, Elfinn; Henriksen, High Tar Reduction in a Two Stage Gasifier, Energy & Fuels. 14 (2000) 816–819.

[102] J. Ahrenfeldt, U. Henriksen, T.K. Jensen, B. Gøbel, L. Wiese, A. Kather, H. Egsgaard, Validation of a Continuous Combined Heat and Power (CHP) Operation of a Two-Stage Biomass Gasifier, Energy & Fuels. 20 (2006) 2672–2680. https://doi.org/10.1021/ef0503616.

[103] Z. Wang, T. He, J. Qin, J. Wu, J. Li, Z. Zi, G. Liu, J. Wu, L. Sun, Gasification of biomass with oxygen-enriched air in a pilot scale two-stage gasifier, Fuel. 150 (2015) 386–393. https://doi.org/10.1016/j.fuel.2015.02.056.

[104] R.Ø. Gadsbøll, Z. Sárossy, L. Jørgensen, J. Ahrenfeldt, U.B. Henriksen, Oxygen-blown operation of the TwoStage Viking gasifier, Energy. 158 (2018) 495–503. https://doi.org/10.1016/j.energy.2018.06.071.

[105] J. Brynda, S. Skoblia, M. Pohořelý, Z. Beňo, K. Soukup, M. Jeremiáš, J. Moško, B. Zach, L. Trakal, M. Šyc, K. Svoboda, Wood chips gasification in a fixed-bed multi-stage gasifier for decentralized high-efficiency CHP and biochar production: Long-term commercial operation, Fuel. 281 (2020) 118637. https://doi.org/10.1016/j.fuel.2020.118637.

[106] Bruce G. Miller, Coal Energy Systems, 2001. https://shop.elsevier.com/books/coal-energy-systems/miller/978-0-12-497451-7.

[107] BP, Statistical Review of World Energy 2020, 2020.

[108] C. Gaedicke, D. Franke, S. Ladage, R. Lutz, M. Pein, D. Rebscher, M. Schauer, S. Schmidt, G. von Goerne, BGR Energy Study - Data and developments concerning German and Global energy supplies, 2019. https://www.bgr.bund.de/EN/Themen/Energie/Downloads/energiestudie_2017_en.pdf?__blob=publicationFile&v=2.

[109] Z. Luo, M. Agraniotis, Low-Rank Coals for Power Generation, Fuel and Chemical

Production, 2017.

[110] M. Aziz, Y. Kansha, A. Kishimoto, Y. Kotani, Y. Liu, A. Tsutsumi, Advanced energy saving in low rank coal drying based on self-heat recuperation technology, Fuel Process. Technol. 104 (2012) 16–22. https://doi.org/10.1016/j.fuproc.2012.06.020.

[111] Z. Peng, X. Lin, Z. Li, J.Y. Hwang, B.G. Kim, Y. Zhang, G. Li, T. Jiang, Dielectric characterization of Indonesian low-rank coal for microwave processing, Fuel Process. Technol. 156 (2017) 171–177. https://doi.org/10.1016/j.fuproc.2016.11.001.

[112] I.S. Gwak, Y.R. Gwak, Y. Bin Kim, S.H. Lee, Drying characteristics of low rank coals in a pressurized flash drying system, J. Ind. Eng. Chem. 57 (2018) 154–159. https://doi.org/10.1016/j.jiec.2017.08.017.

[113] H. Osman, S. V. Jangam, J.D. Lease, A.S. Mujumdar, Drying of low-rank coal (LRC)-A Review of recent patents and innovations, Dry. Technol. 29 (2011) 1763–1783. https://doi.org/10.1080/07373937.2011.616443.

[114] L. Dingcheng, X. Qiang, L. Guangsheng, C. Junya, Z. Jun, Influence of heating rate on reactivity and surface chemistry of chars derived from pyrolysis of two Chinese low rank coals, Int. J. Min. Sci. Technol. 28 (2018) 613–619. https://doi.org/10.1016/j.ijmst.2018.05.001.

[115] H. Song, G. Liu, J. Wu, Pyrolysis characteristics and kinetics of low rank coals by distributed activation energy model, Energy Convers. Manag. 126 (2016) 1037–1046. https://doi.org/10.1016/j.enconman.2016.08.082.

[116] H. Ullah, G. Liu, B. Yousaf, M.U. Ali, Q. Abbas, C. Zhou, A. Rashid, Hydrothermal dewatering of low-rank coals: Influence on the properties and combustion characteristics of the solid products, Energy. 158 (2018) 1192–1203. https://doi.org/10.1016/j.energy.2018.06.052.

[117] X. Lu, T. Wang, Investigation of Low Rank Coal Gasification in a Two-Stage Downdraft Entrained-Flow Gasifier, 2014 (2014) 1–12.

[118] Q. You, S.Y. Wu, Y.Q. Wu, S. Huang, J.S. Gao, J.X. Shang, X.J. Min, H.A. Zheng, Product distributions and characterizations for integrated mild-liquefaction and carbonization of low rank coals, Fuel Process. Technol. 156 (2017) 54–61. https://doi.org/10.1016/j.fuproc.2016.09.022.

[119] A. Setiawan, Z. Arifin, Low rank coal drying technology for decreasing electricity cost production: Case study of Nagan Raya power plant, E3S Web Conf. 181 (2020). https://doi.org/10.1051/e3sconf/202018103003.

[120] A. Masudi, N.W. Che Jusoh, O. Muraza, Recent progress on low rank coal conversion

to dimethyl ether as clean fuel: A critical review, J. Clean. Prod. 277 (2020) 124024. https://doi.org/10.1016/j.jclepro.2020.124024.

[121] L. Bokányi, Á. Pintér-Móricz, Potential methanol-ethanol synthesis from Hungarian sub-bituminous coal via plasma gasification and Fischer-Tropsch synthesis, Int. J. Oil, Gas Coal Technol. 18 (2018) 55–73.

[122] A. Pettinau, Z. Dobó, Z. Köntös, A. Zsemberi, Experimental characterization of a high sulfur Hungarian brown coal for its potential industrial applications, Fuel Process. Technol. 122 (2014) 1–11. https://doi.org/10.1016/j.fuproc.2014.01.018.

[123] J. Morales Pedraza, Electrical Energy Generation in Europe, Springer International Publishing, Cham, 2015. https://doi.org/10.1007/978-3-319-08401-5.

[124] D.A. Bell, B.F. Towler, M. Fan, Coal gasification and its applications, 1st ed., Elsevier, 2011.

[125] International Organization for Standardization-ISO 1928:2019, Solid mineral fuels — Determination of gross calorific value by the bomb calorimetric method and calculation of net calorific value, 2009. https://www.iso.org/standard/41592.html.

[126] P. Grammelis, N. Margaritis, E. Karampinis, Solid fuel types for energy generation: Coal and fossil carbon-derivative solid fuels, Elsevier Ltd, 2015. https://doi.org/10.1016/B978-1-78242-378-2.00002-X.

[127] International Organization for Standardization-ISO 29541:2010, Solid biofuels — Determination of total content of carbon , hydrogen and nitrogen — Instrumental methods, 2010. https://www.iso.org/standard/45546.html.

[128] International Organization for Standardization-ISO 540:2008, Hard coal and coke — Determination of ash fusibility, 2008. https://www.iso.org/standard/41484.html.

[129] T. Phengsaart, P. Srichonphaisan, C. Kertbundit, N. Soonthornwiphat, S. Sinthugoot, N. Phumkokrux, O. Juntarasakul, K. Maneeintr, A. Numprasanthai, I. Park, C.B. Tabelin, N. Hiroyoshi, M. Ito, Conventional and recent advances in gravity separation technologies for coal cleaning: A systematic and critical review, Heliyon. 9 (2023) e13083. https://doi.org/10.1016/j.heliyon.2023.e13083.

[130] M. Mureddu, F. Dessì, A. Orsini, F. Ferrara, A. Pettinau, Air- and oxygen-blown characterization of coal and biomass by thermogravimetric analysis, Fuel. 212 (2018) 626–637. https://doi.org/10.1016/j.fuel.2017.10.005.

[131] S. Chang, Z. Zhang, L. Cao, L. Ma, S. You, W. Li, Co-gasification of digestate and lignite in a downdraft fixed bed gasifier: Effect of temperature, Energy Convers. Manag. 213 (2020) 112798. https://doi.org/10.1016/j.enconman.2020.112798.

[132] C.-L. Lin, W.-C. Weng, Effects of different operating parameters on the syngas composition in a two-stage gasification process, Renew. Energy. 109 (2017) 135–143. https://doi.org/10.1016/j.renene.2017.03.019.

[133] K. Mondal, K. Piotrowski, D. Dasgupta, E. Hippo, T. Wiltowski, Hydrogen from Coal in a Single Step, Ind. Eng. Chem. Res. 44 (2005) 5508–5517. https://doi.org/10.1021/ie048974d.

[134] A. International, Standard Test Method for Water in Petroleum Products and Bituminous Materials by Distillation, 2018. https://doi.org/10.1520/D0095-13R18.

[135] A. Molina, F. Mondragón, Reactivity of coal gasification with steam and CO2, Fuel. 77 (1998) 1831–1839. https://doi.org/10.1016/S0016-2361(98)00123-9.

[136] Y.T. Kim, D.K. Seo, J. Hwang, Study of the Effect of Coal Type and Particle Size on Char–CO 2 Gasification via Gas Analysis, Energy & Fuels. 25 (2011) 5044–5054. https://doi.org/10.1021/ef200745x.

[137] S. Su, Y. Song, Y. Wang, T. Li, S. Hu, J. Xiang, C.-Z. Li, Effects of CO2 and heating rate on the characteristics of chars prepared in CO2 and N2 atmospheres, Fuel. 142 (2015) 243–249. https://doi.org/10.1016/j.fuel.2014.11.025.

[138] C. Ellison, V. Abdelsayed, M. Smith, D. Shekhawat, Comparative evaluation of microwave and conventional gasification of different coal types: Experimental reaction studies, Fuel. 321 (2022) 124055. https://doi.org/10.1016/j.fuel.2022.124055.

[139] K. Śpiewak, P. Soprych, G. Czerski, Influence of dry coal deshaling by pneumatic vibrating FGX separator on steam gasification of coal, Thermochim. Acta. 713 (2022) 179233. https://doi.org/10.1016/j.tca.2022.179233.

[140] A. Martinez-Alonso, J.M.D. Tascon, The Determining Role of Mineral Matter on Gasification Reactivities of Brown Coal Chars, in: Fundam. Issues Control Carbon Gasif. React., Springer Netherlands, Dordrecht, 1991: pp. 435–460. https://doi.org/10.1007/978-94-011-3310-4_22.

[141] C. Choi, U.P.M. Ashik, S. Kudo, K. Uebo, K. Norinaga, J. Hayashi, Effect of SiO2 on loss of catalysis of inherent metallic species in CO2 gasification of coke from lignite, Carbon Resour. Convers. 2 (2019) 13–22. https://doi.org/10.1016/j.crcon.2018.09.002.

[142] C. Hognon, C. Dupont, M. Grateau, F. Delrue, Comparison of steam gasification reactivity of algal and lignocellulosic biomass: Influence of inorganic elements, Bioresour. Technol. 164 (2014) 347–353.

https://doi.org/10.1016/j.biortech.2014.04.111.

[143] Z. He, Y. Sun, S. Cheng, Z. Jia, R. Tu, Y. Wu, X. Shen, F. Zhang, E. Jiang, X. Xu, The enhanced rich H2 from co-gasification of torrefied biomass and low rank coal: The comparison of dry/wet torrefaction, synergetic effect and prediction, Fuel. 287 (2021) 119473. https://doi.org/10.1016/j.fuel.2020.119473.

[144] J. Fermoso, B. Arias, M. V. Gil, M.G. Plaza, C. Pevida, J.J. Pis, F. Rubiera, Co-gasification of different rank coals with biomass and petroleum coke in a high-pressure reactor for H2-rich gas production, Bioresour. Technol. 101 (2010) 3230–3235. https://doi.org/10.1016/j.biortech.2009.12.035.

Appendix

Appendix 1-Graphs of syngas concentration

Appendix 1.1. Gasification temperature: 700 ℃ and S/C ratio: 0.75

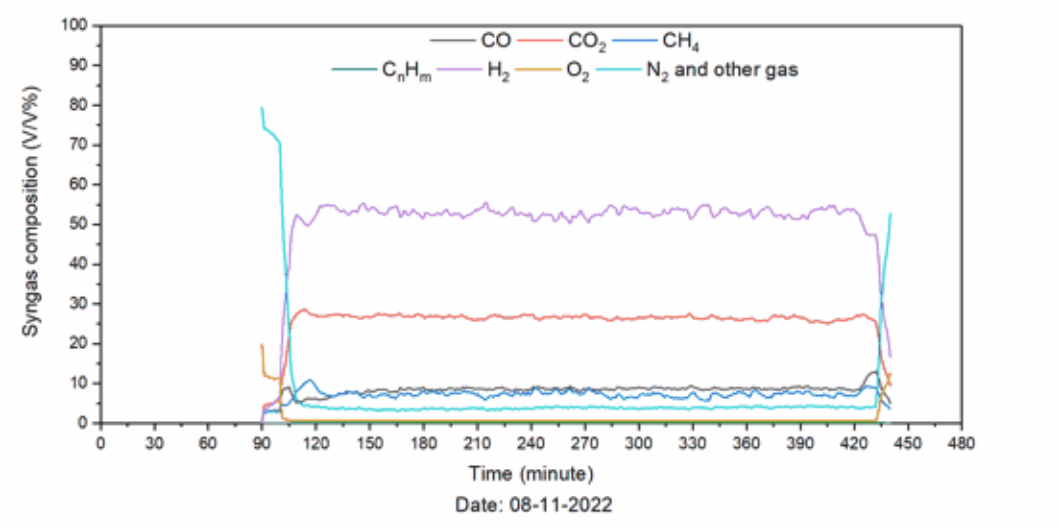

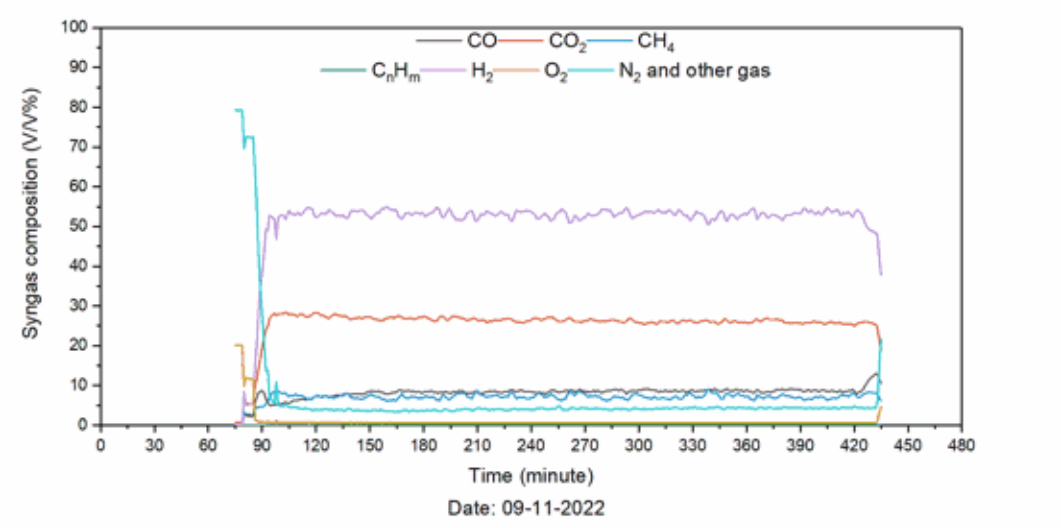

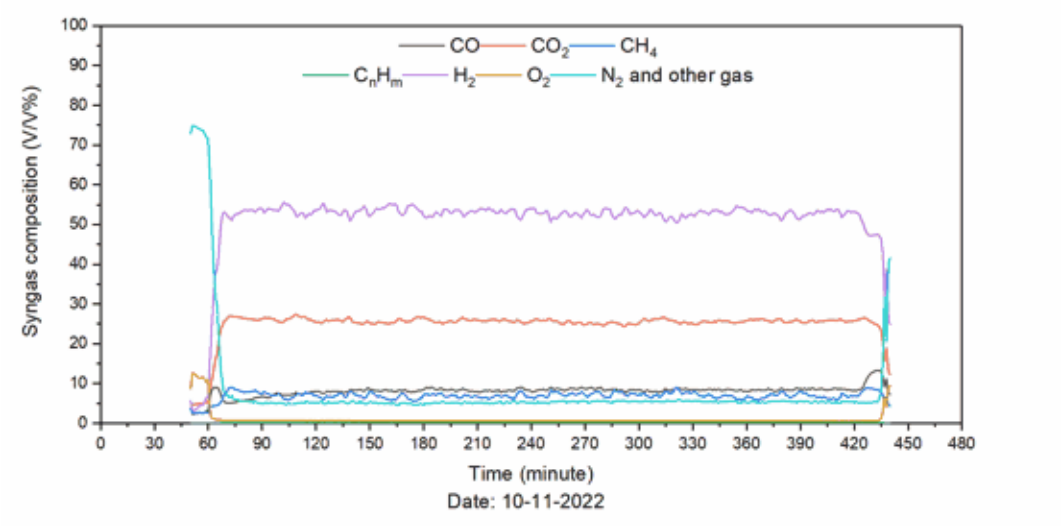

Appendix 1.2. Gasification temperature: 700 ℃ and S/C ratio: 1.00

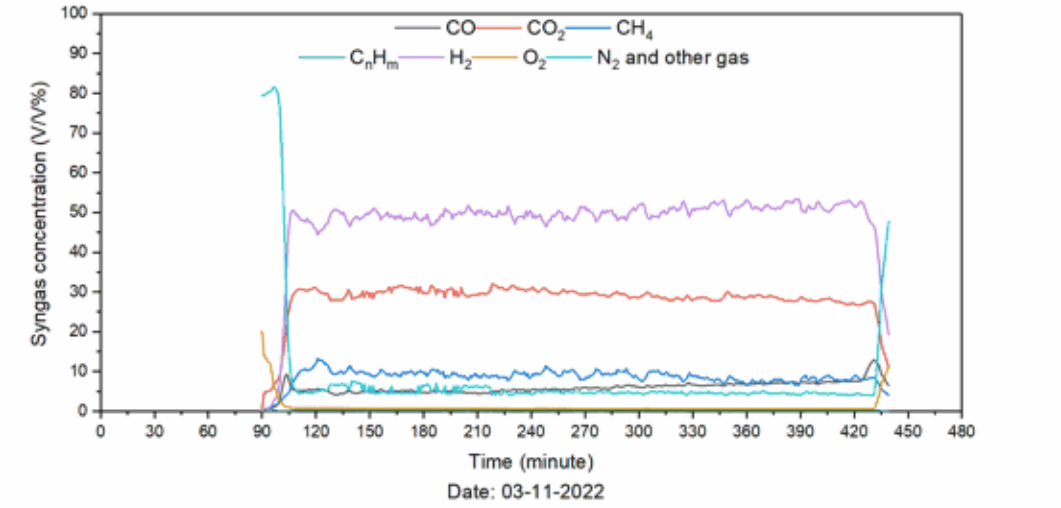

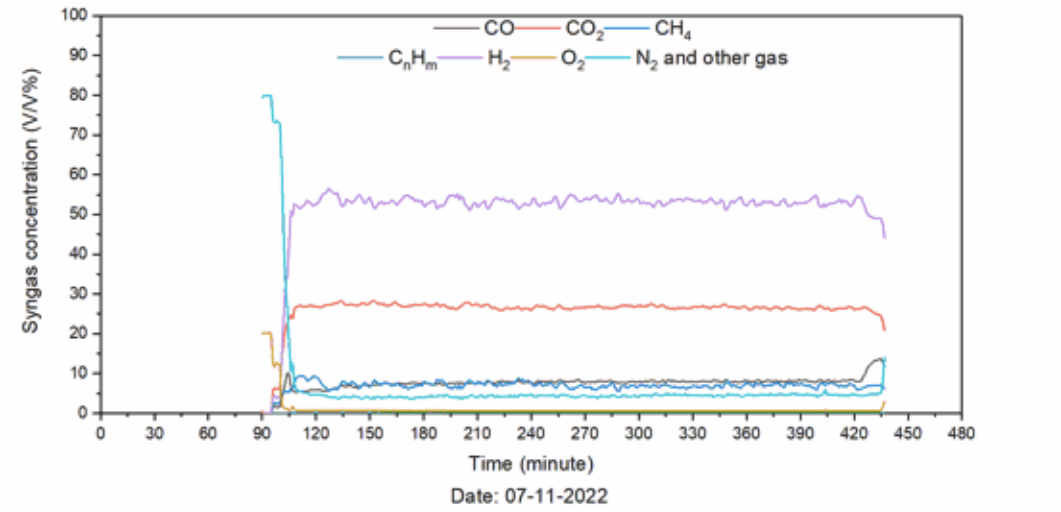

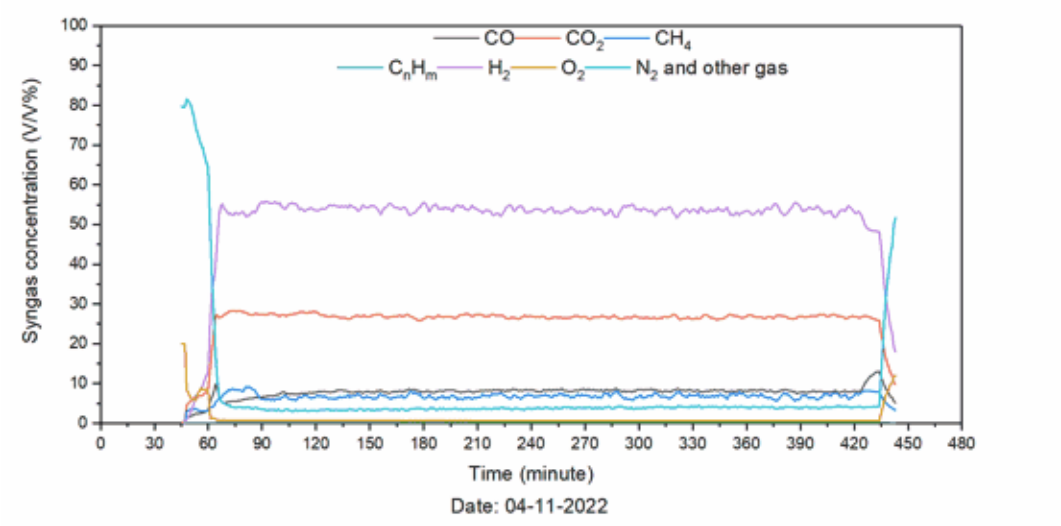

Appendix 1.3. Gasification temperature: 700 ℃ and S/C ratio: 1.25

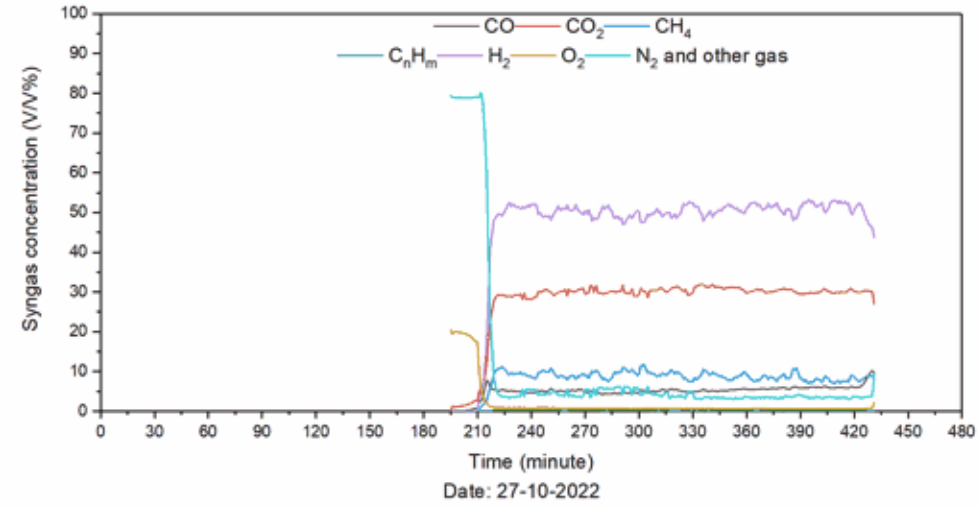

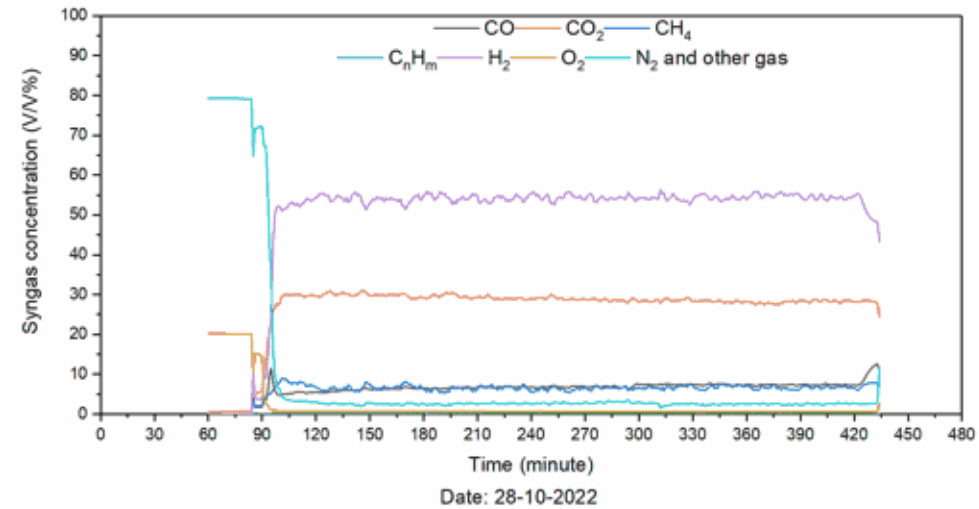

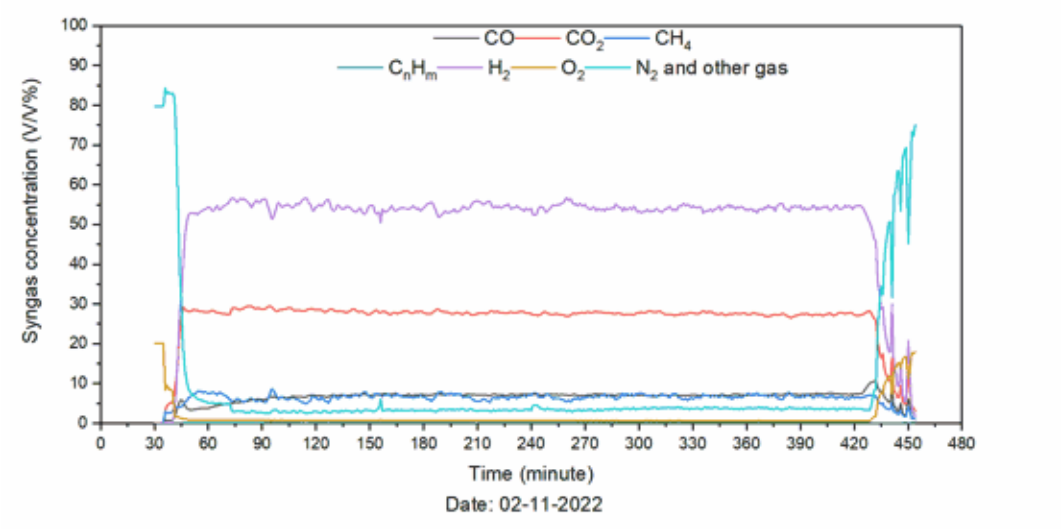

Appendix 1.4. Gasification temperature: 800 ℃ and S/C ratio: 0.75

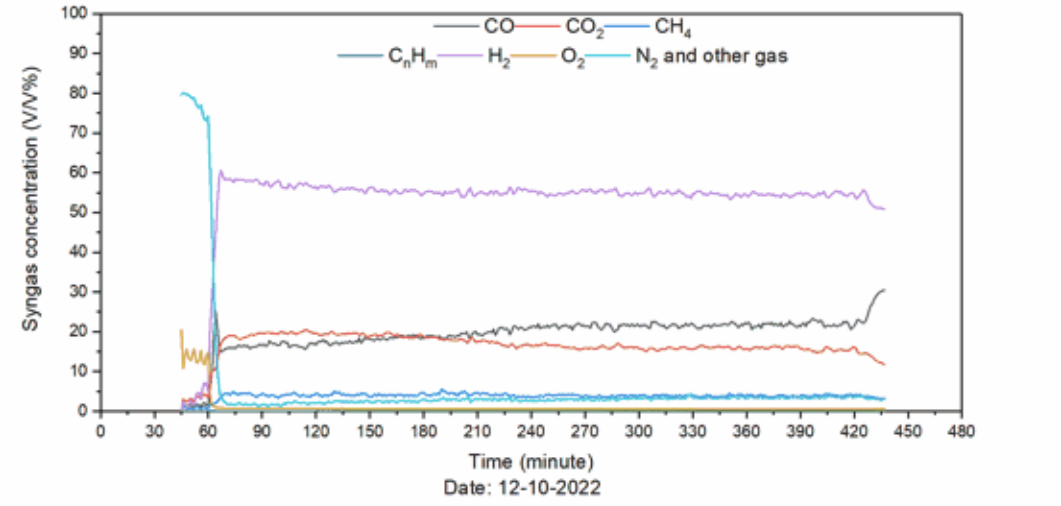

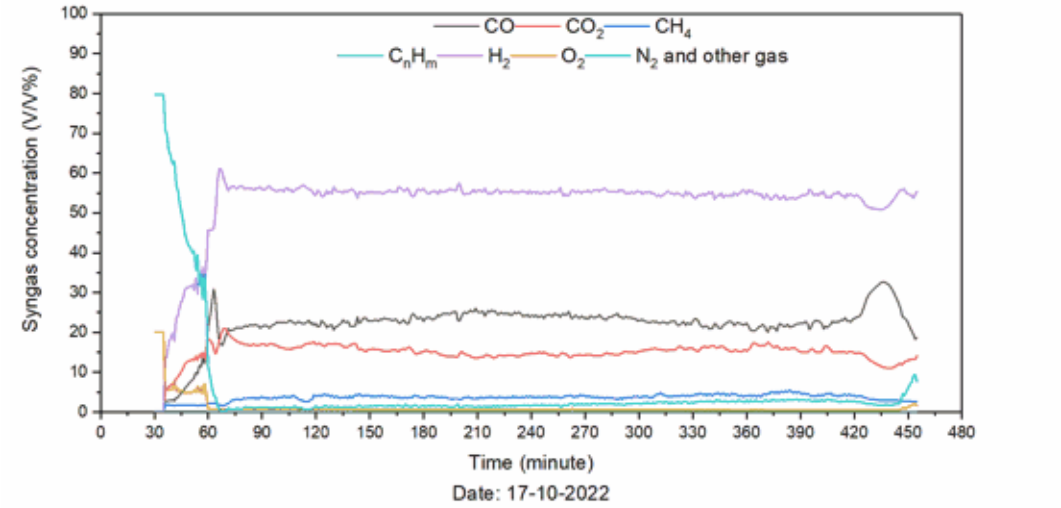

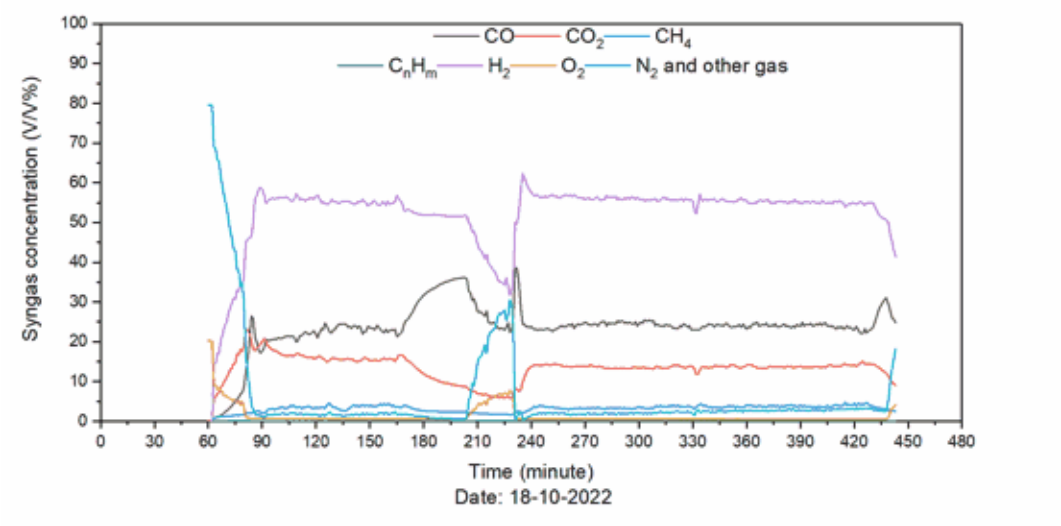

Appendix 1.5. Gasification temperature: 800 °C and S/C ratio: 1.00

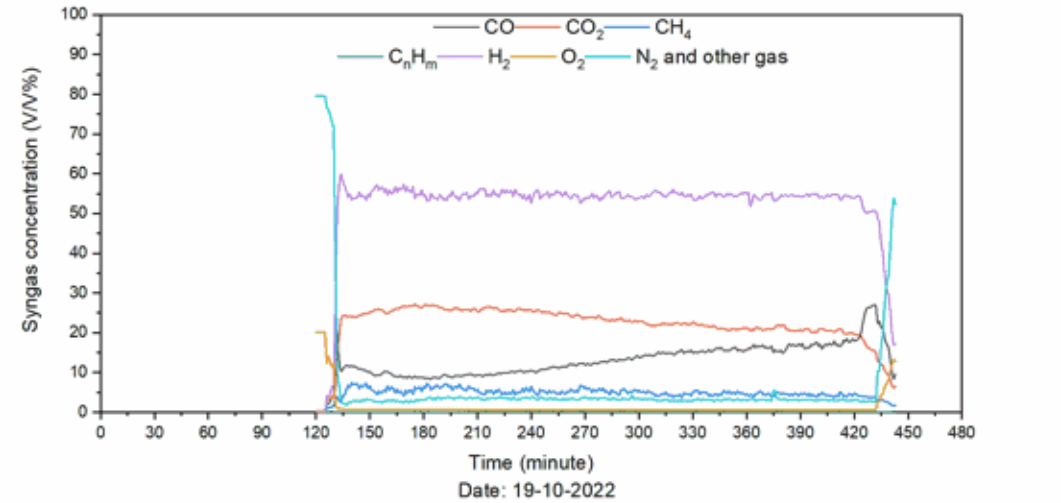

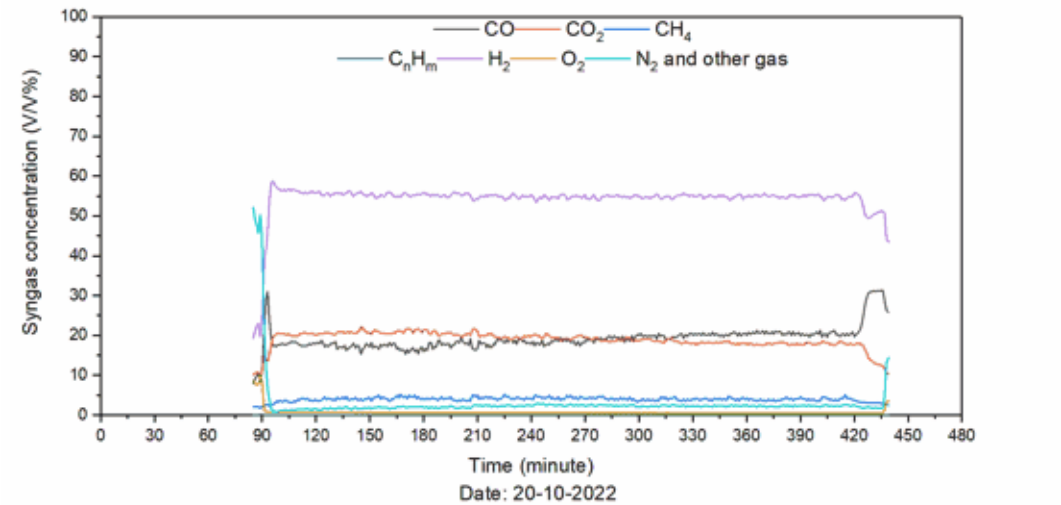

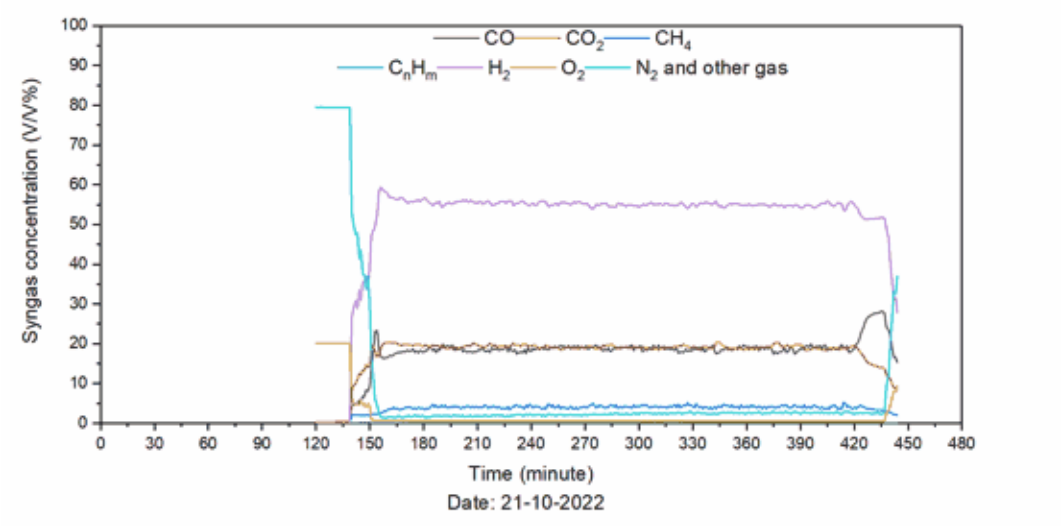

Appendix 1.6. Gasification temperature: 800 ℃ and S/C ratio: 1.25

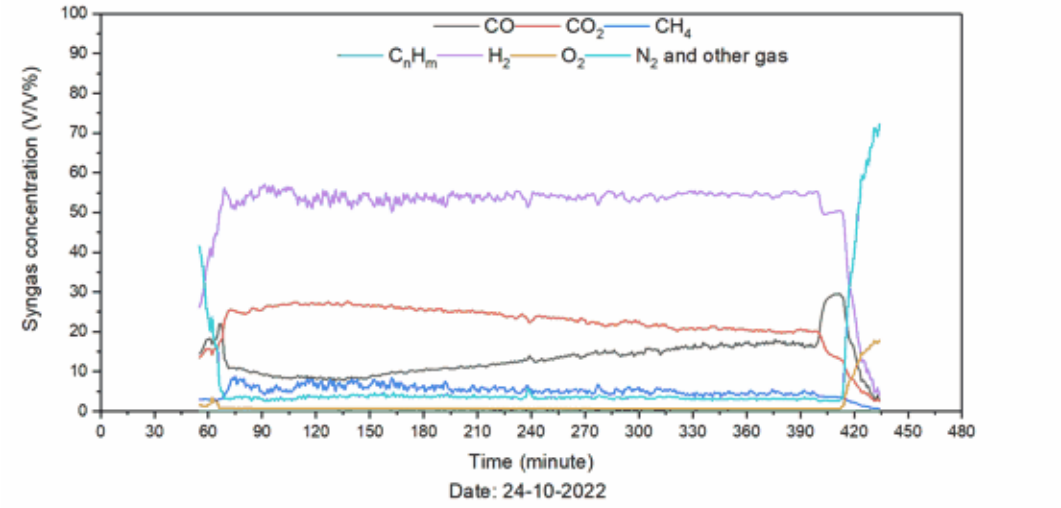

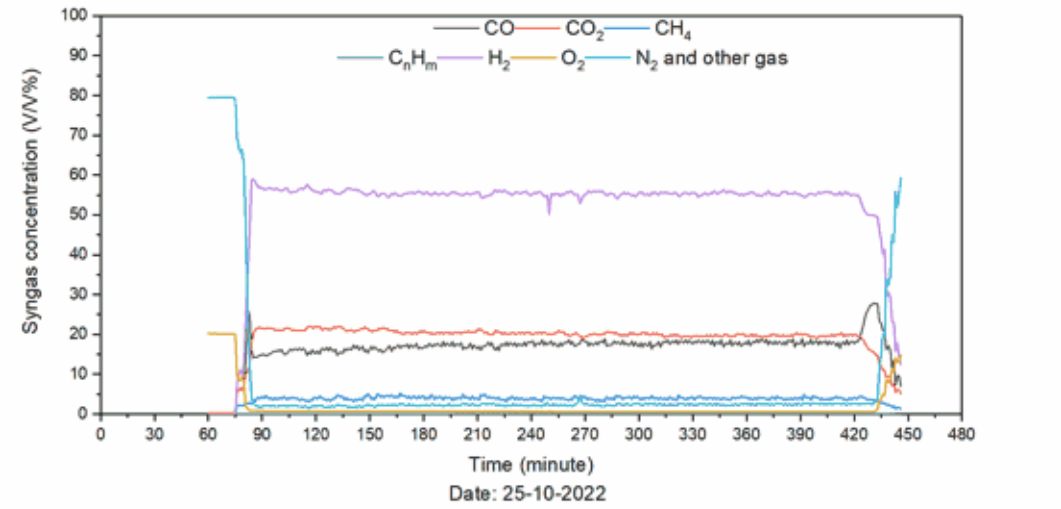

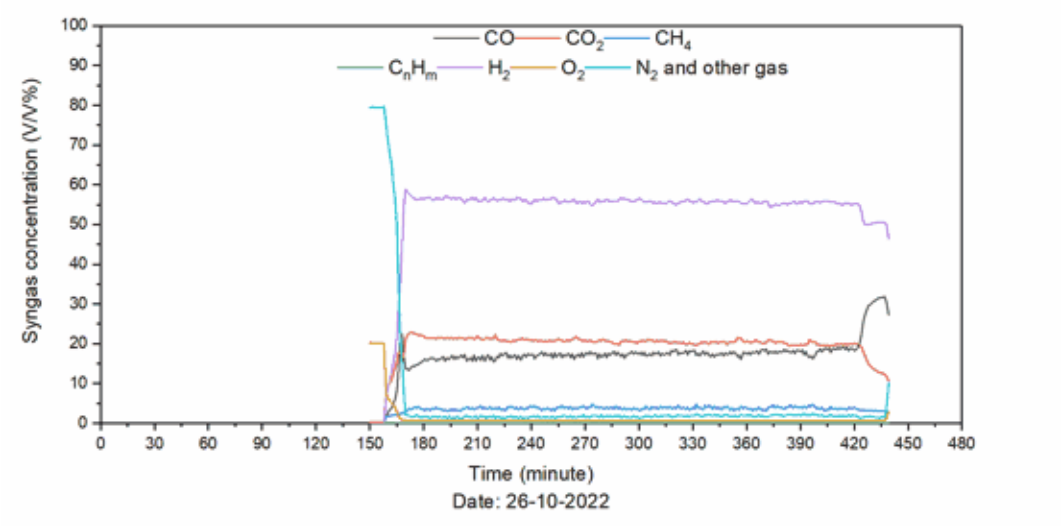

Appendix 1.7. Gasification temperature: 900 ℃ and S/C ratio: 0.75

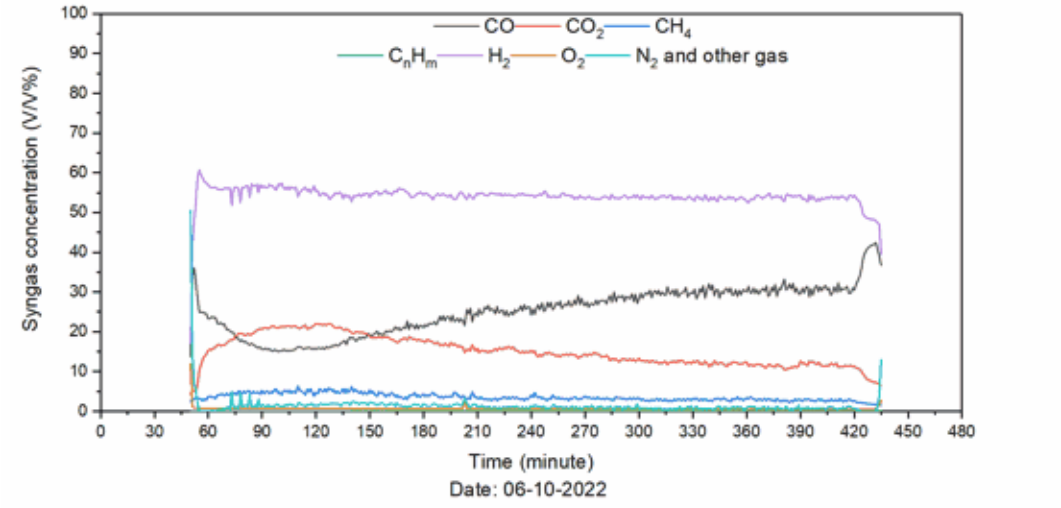

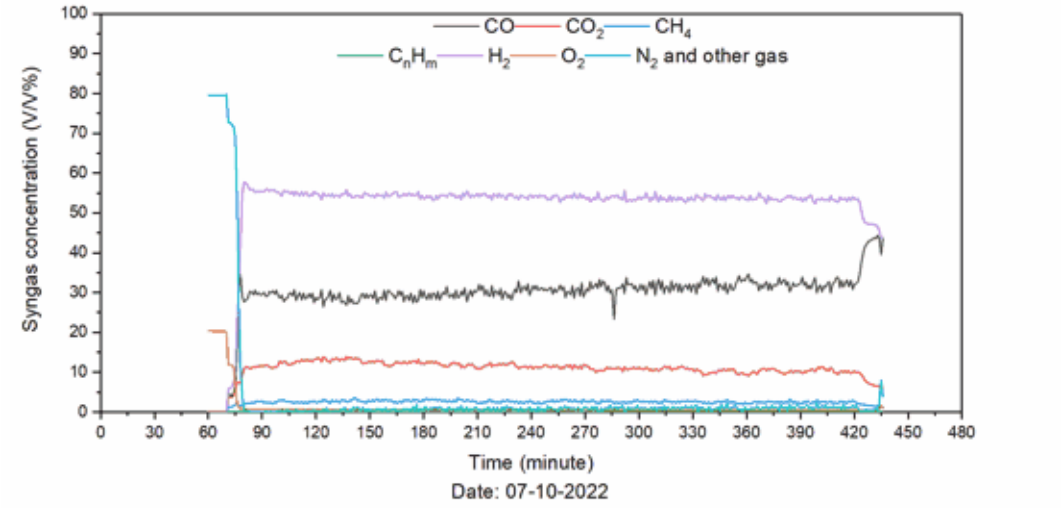

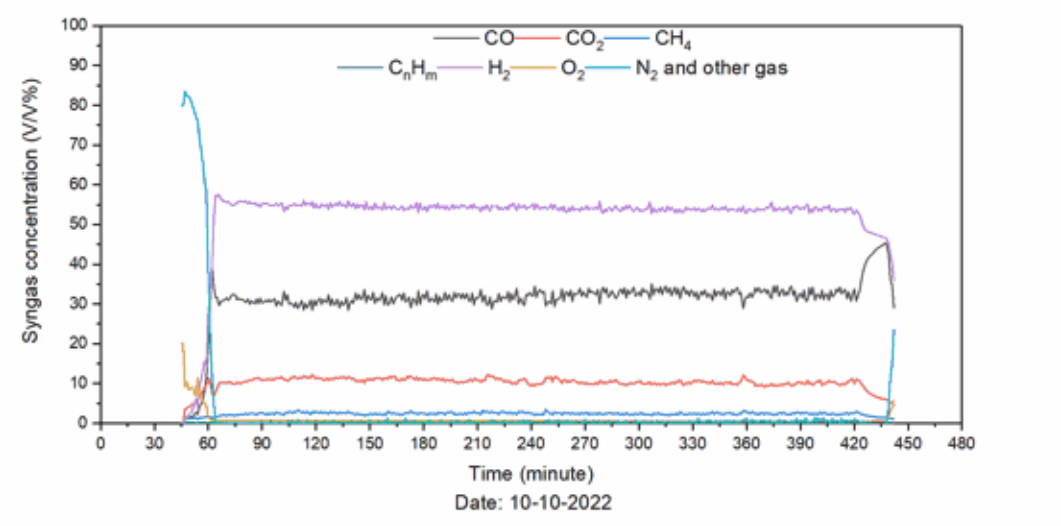

Appendix 1.8. Gasification temperature: 900 ℃ and S/C ratio: 1.00

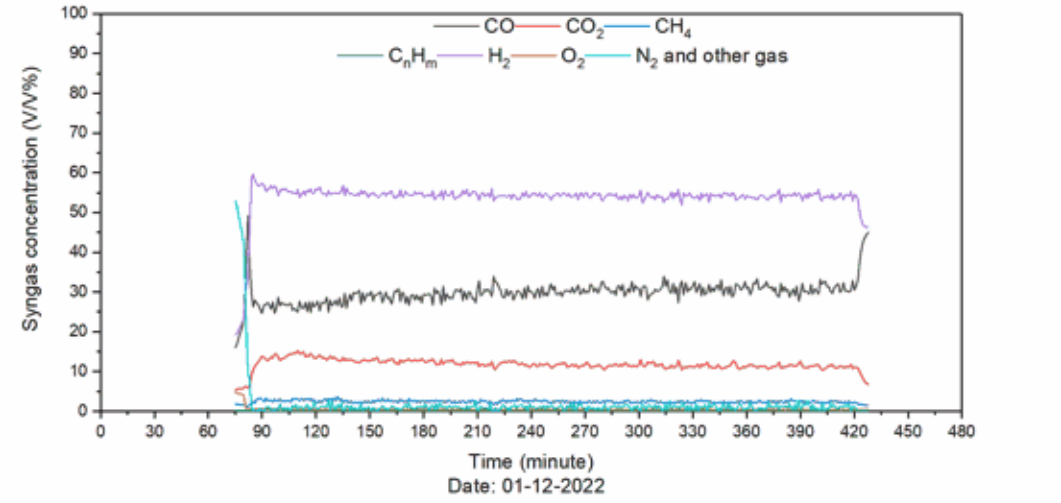

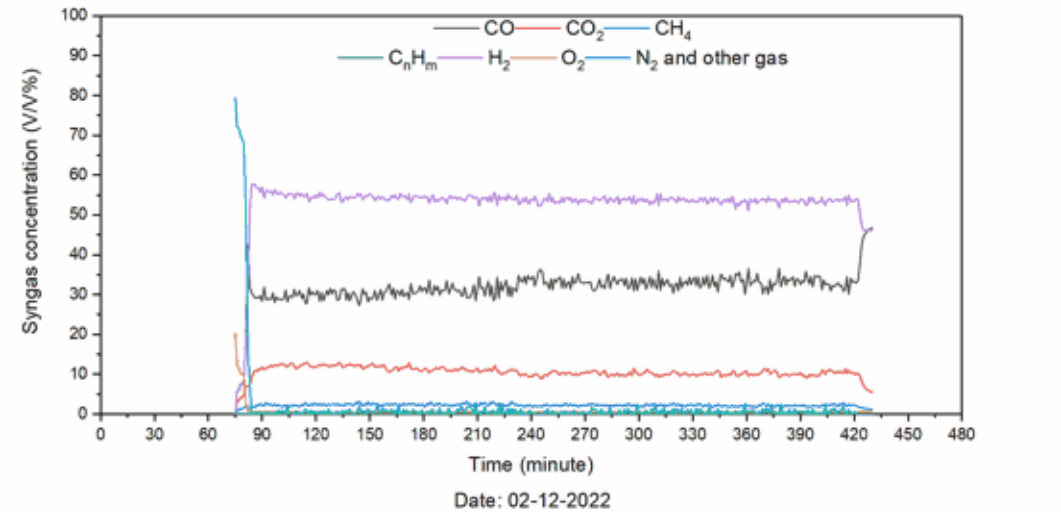

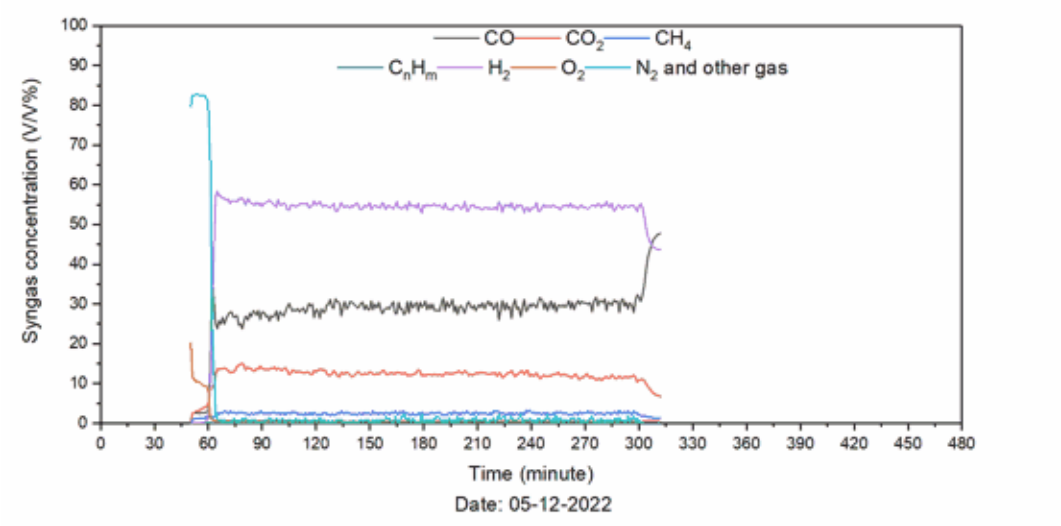

Appendix 1.9. Gasification temperature: 900 ℃ and S/C ratio: 1.25

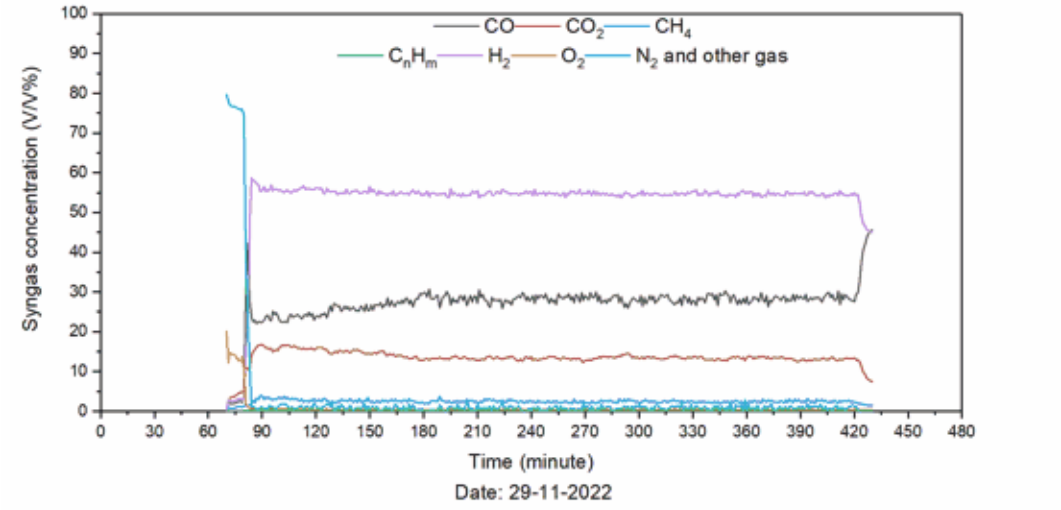

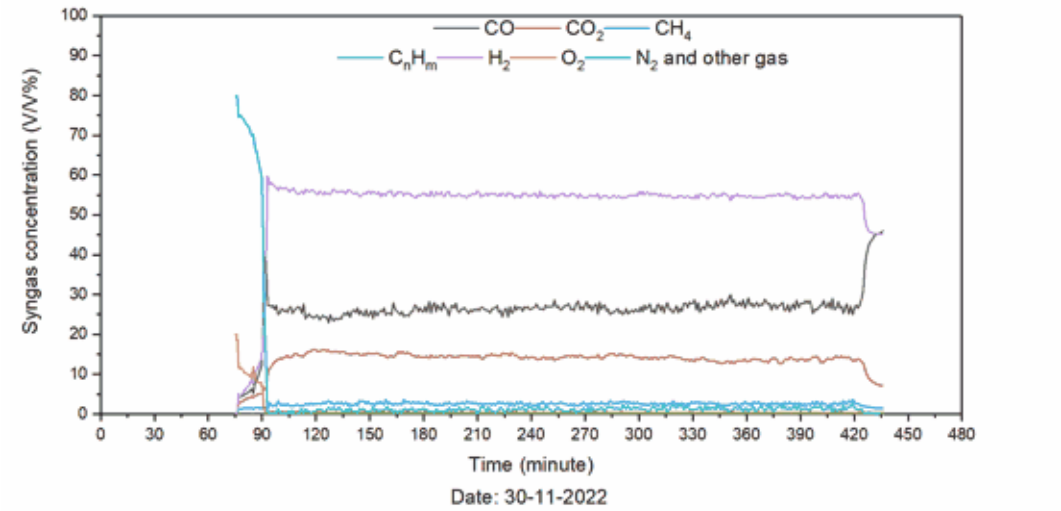

Appendix 2- Products of the experiments of the original coal sample

		Gasification temperture					
		700		800		900	
S/C ratio		Char (g/h)	Liquid (g/h)	Char (g/h)	Liquid (g/h)	Char (g/h)	Liquid (g/h)
0.75	1	625.70	329.50	547.30	141.10	470.00	90.60
	2	629.80	326.30	621.05	151.50	502.90	83.40
	3	612.70	327.90	630.60	132.30	491.90	81.30
	Mean value	**622.73**	**327.90**	**599.65**	**141.90**	**488.27**	**85.10**
1.00	1	568.00	410.80	568.90	260.40	417.00	169.10
	2	588.80	409.60	584.50	273.60	401.60	185.60
	3	585.80	417.10	550.50	273.50	402.70	170.60
	Mean value	**580.87**	**412.50**	**567.97**	**269.17**	**407.10**	**175.10**
1.25	1	593.60	431.30	499.70	359.90	409.00	277.40
	2	596.30	435.00	484.00	338.00	363.60	263.50
	3	613.40	431.40	490.00	310.70	346.50	266.90
	Mean value	**601.10**	**432.57**	**491.23**	**336.20**	**373.03**	**269.27**

Appendix 3- Average syngas concentration from the experiments of the original coal sample

Gasification temperature	S/C ratio		Syngas composition (V/V%)							LHV_{syngas}
°C	mol/mol		**CO**	**CO_2**	**CH_4**	**C_nH_m**	**H_2**	**O_2**	**N_2**	MJ/Nm^3
700	**0.75**	Mean	8.56	26.12	7.18	0.13	52.96	0.57	4.48	9.47
		Max	9.47	27.53	9.04	0.23	55.49	0.66	5.91	9.99
		Min	7.70	24.38	5.68	0.05	50.32	0.50	3.26	9.00
		SD	0.30	0.59	0.61	0.03	0.90	0.03	0.68	0.17
	1.00	Mean	8.04	26.72	6.92	0.15	53.48	0.61	4.08	9.39
		Max	8.81	27.91	8.87	0.25	55.54	0.84	5.92	9.92
		Min	7.15	25.87	5.53	0.08	51.21	0.53	3.02	8.99
		SD	0.27	0.37	0.55	0.03	0.85	0.05	0.43	0.15
	1.25	Mean	7.12	28.15	6.61	0.11	54.29	0.63	3.08	9.21
		Max	7.68	30.39	7.82	0.19	56.68	0.76	4.56	9.59
		Min	6.19	26.48	5.19	0.02	51.95	0.55	1.44	8.70
		SD	0.28	0.72	0.52	0.03	0.76	0.04	0.55	0.15
			CO	**CO_2**	**CH_4**	**C_nH_m**	**H_2**	**O_2**	**N_2**	
800	**0.75**	Mean	22.32	15.34	3.94	0.01	55.04	0.52	2.79	10.17
		Max	25.51	18.78	5.52	0.06	57.53	0.60	4.35	10.62
		Min	18.18	11.75	2.93	0.00	52.18	0.47	1.30	9.71
		SD	1.56	1.37	0.44	0.01	0.77	0.03	0.52	0.17
	1.00	Mean	19.01	19.04	4.11	0.01	55.00	0.53	2.30	9.80
		Max	21.26	21.77	5.26	0.07	56.65	0.65	2.96	10.15
		Min	15.88	17.46	3.26	0.00	53.33	0.46	1.38	9.47
		SD	0.98	0.77	0.37	0.01	0.47	0.05	0.30	0.11
	1.25	Mean	17.52	20.31	3.88	0.00	55.57	0.64	2.06	9.59
		Max	19.23	22.37	5.04	0.06	57.05	0.78	4.73	9.87
		Min	15.47	18.91	3.04	0.00	50.08	0.58	1.10	9.10
		SD	0.74	0.60	0.37	0.01	0.60	0.04	0.42	0.10
900	**0.75**		**CO**	**CO_2**	**CH_4**	**C_nH_m**	**H_2**	**O_2**	**N_2**	
		Mean	31.38	10.90	2.54	0.00	54.03	0.52	0.59	10.69
		Max	35.19	14.00	3.56	0.15	56.00	0.66	2.51	10.93
		Min	23.39	8.99	1.82	0.00	52.27	0.43	0.00	10.32
		SD	1.70	0.96	0.31	0.02	0.66	0.06	0.51	0.11
	1.00	Mean	30.99	11.30	2.35	0.01	54.10	0.43	0.79	10.59
		Max	36.55	13.54	3.21	0.16	56.17	0.59	2.75	10.98
		Min	26.01	8.95	1.65	0.00	51.01	0.36	0.00	10.20
		SD	1.92	0.99	0.31	0.04	0.75	0.03	0.64	0.14
	1.25	Mean	27.55	13.70	2.52	0.00	54.76	0.40	1.06	10.28
		Max	30.79	15.47	3.74	0.13	56.15	0.47	2.85	10.51
		Min	24.34	12.29	1.86	0.00	53.57	0.35	0.00	9.96
		SD	1.23	0.61	0.32	0.01	0.46	0.03	0.58	0.10

Appendix 4- Products from the experiments of C1 and C2 samples

	Gasification temperature	S/C ratio	Samples		Char	Liquid
	℃	mol/mol			(g)	(g)
C1	900	1.25		1	295.70	519.70
				2	318.10	440.80
				3	301.90	434.70
			Mean		**305.23**	**465.07**
		1		1	356.00	347.40
				2	366.00	354.90
				3	363.00	353.00
			Mean		**361.67**	**351.77**
C2	900	1.25		1	257.10	340.60
				2	271.70	346.40
				3	267.20	322.40
			Mean		**265.33**	**336.47**
		1		1	345.90	299.10
				2	292.10	231.50
				3	258.10	230.00
			Mean		**298.70**	**253.53**

Appendix 5- Graphs of syngas concentration from the experiments of the C1 and C2 sample

Appendix 5.1. C1 sample gasification at 900 ℃ and S/C ratio: 1.00

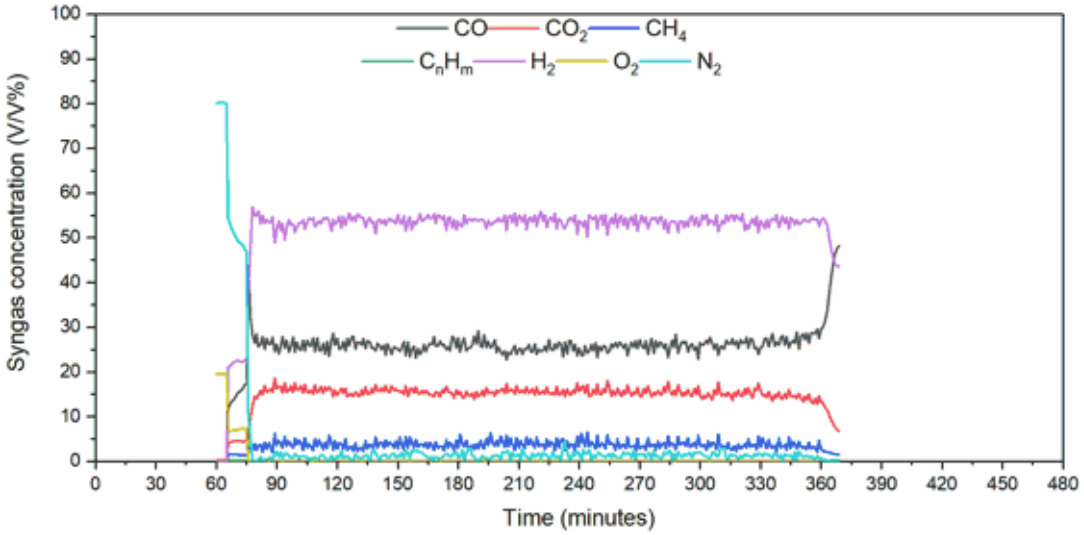

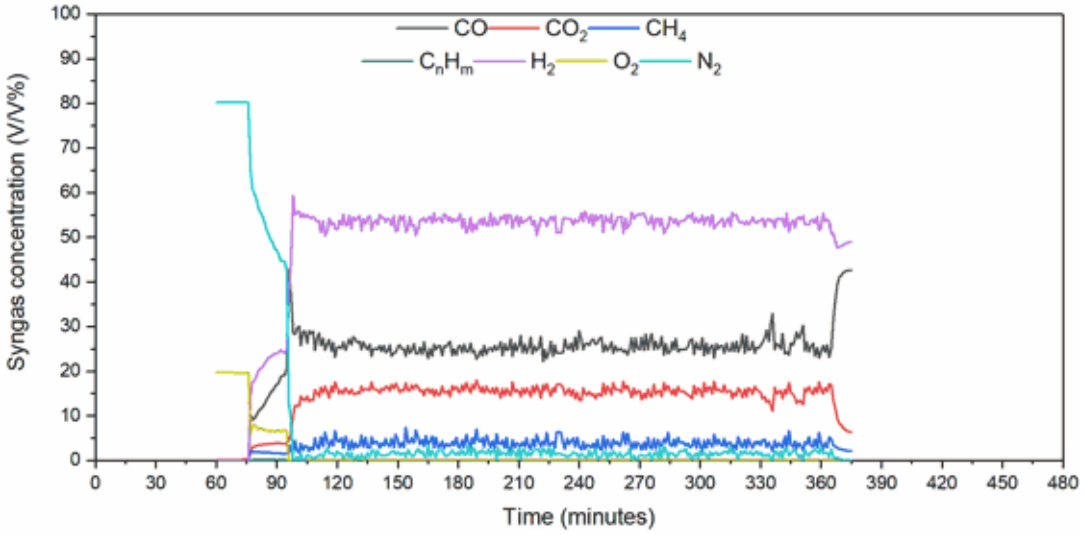

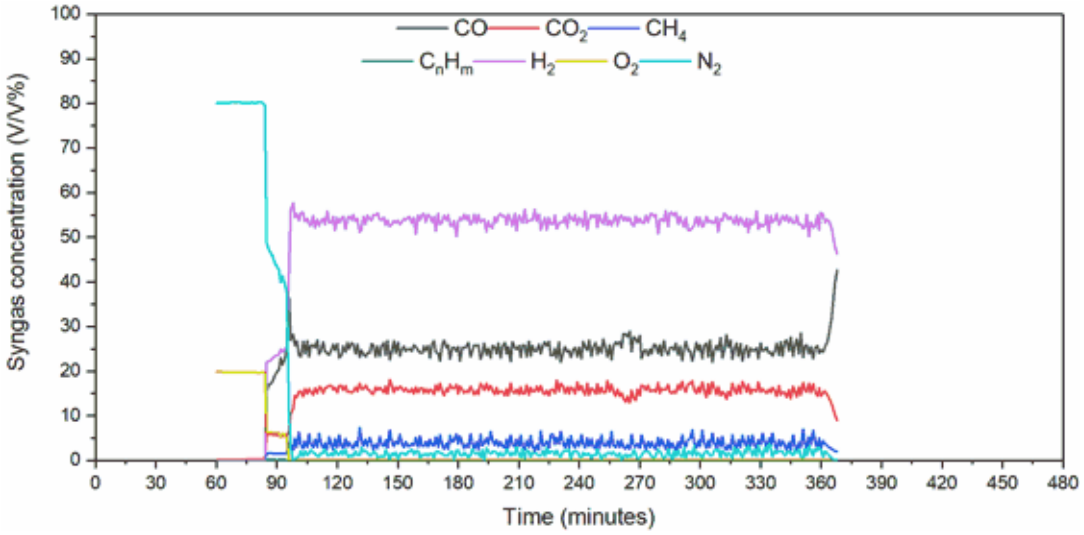

Appendix 5.2. C1 sample gasification at 900 ℃ and S/C ratio: 1.25

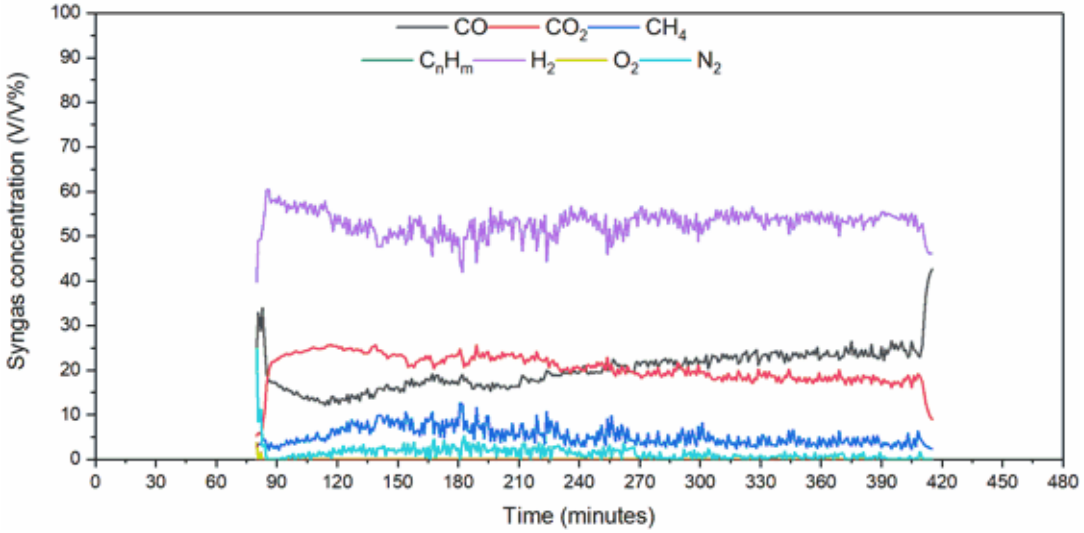

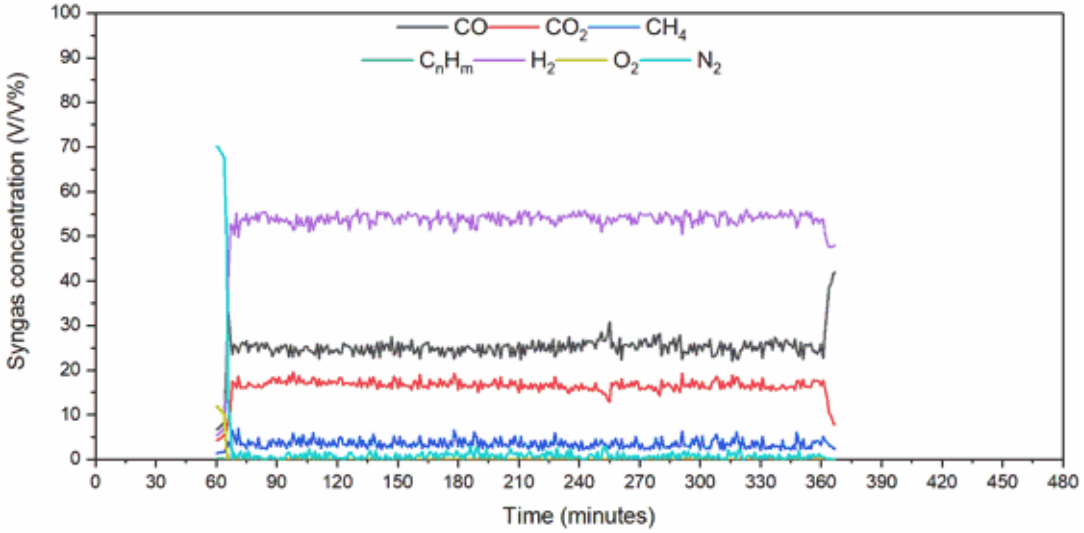

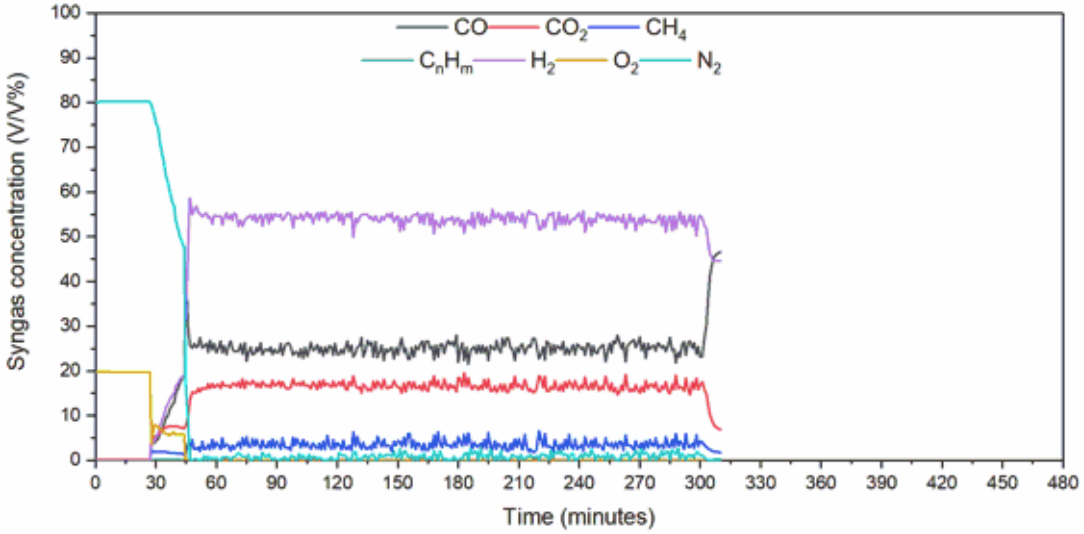

Appendix 5.3. C2 sample gasification at 900 ℃ and S/C ratio: 1.00

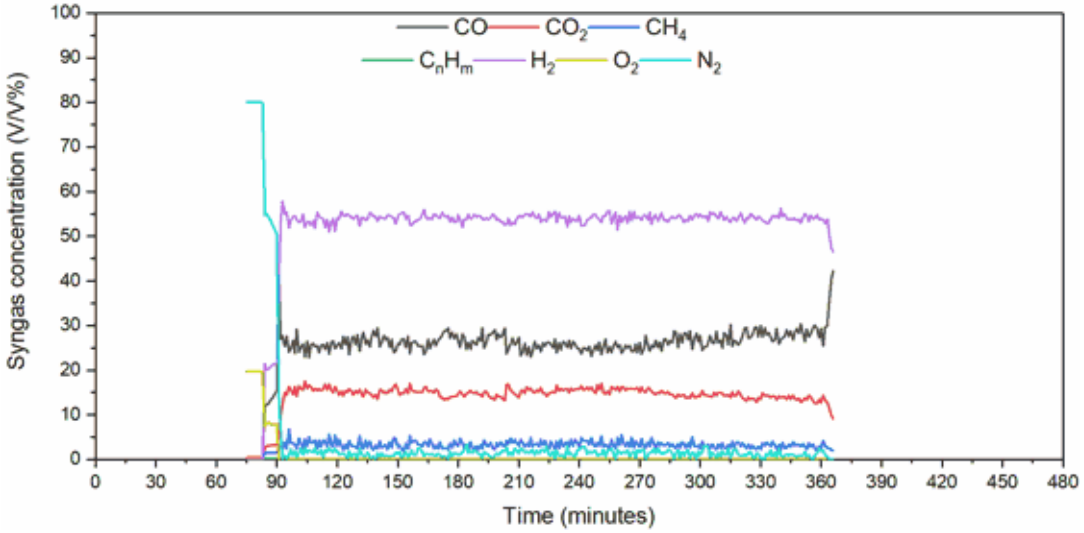

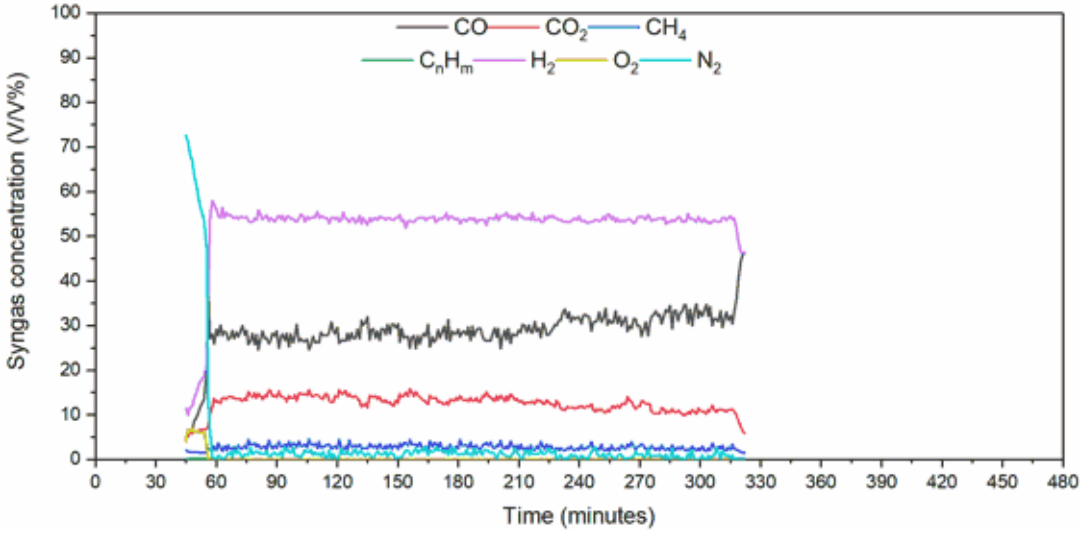

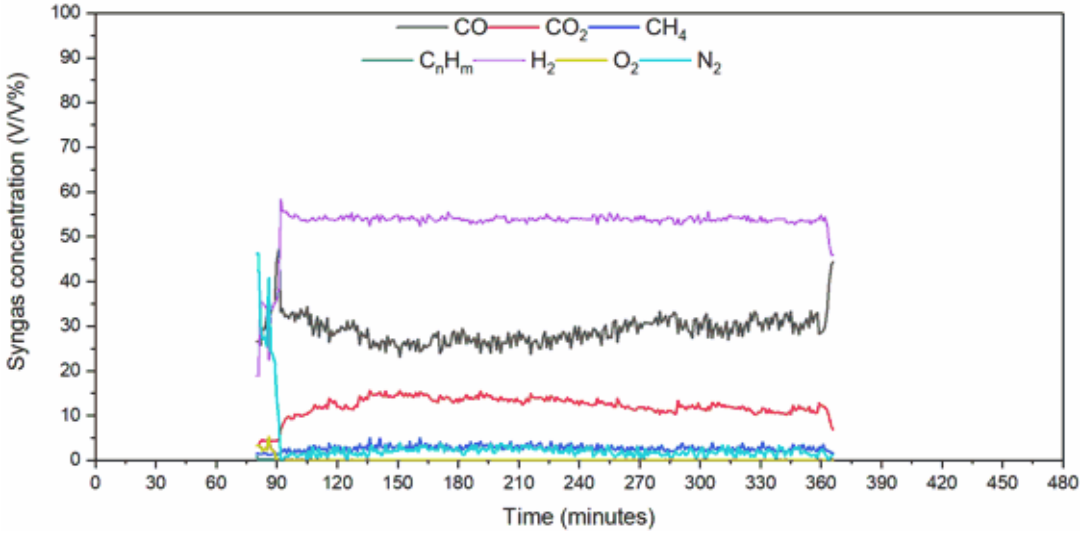

Appendix 5.4. C2 sample gasification at 900 ℃ and S/C ratio: 1.00

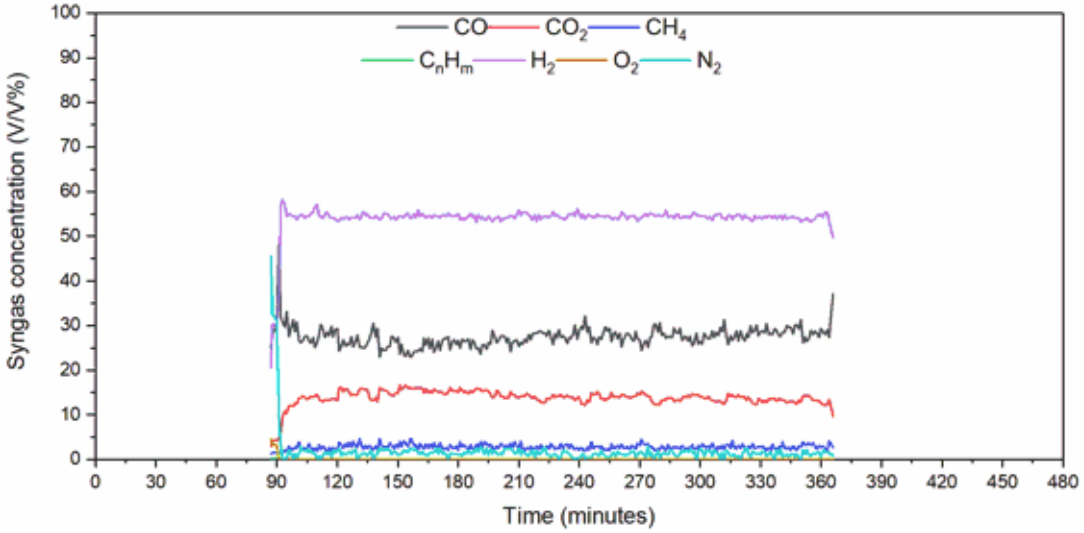

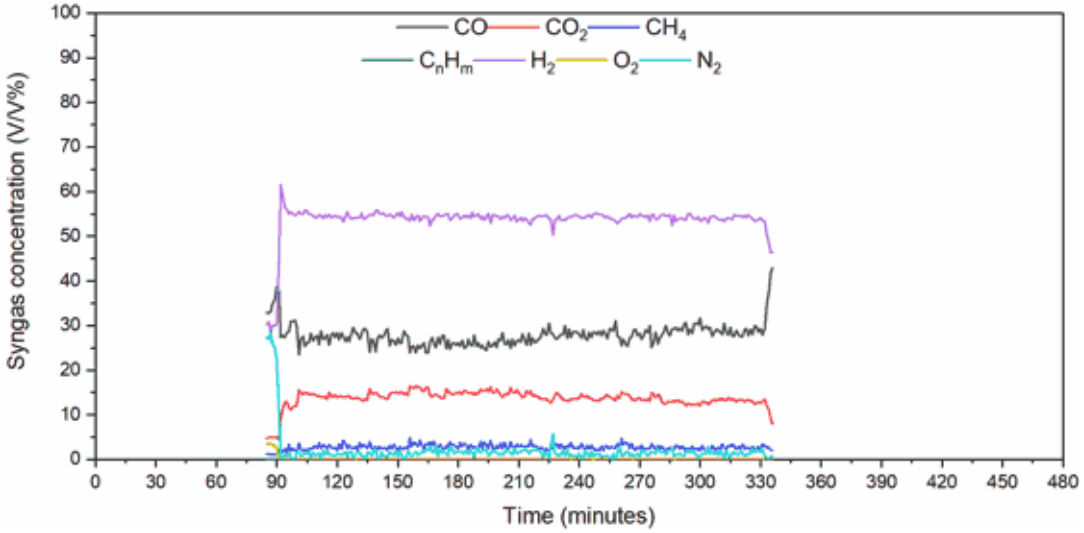

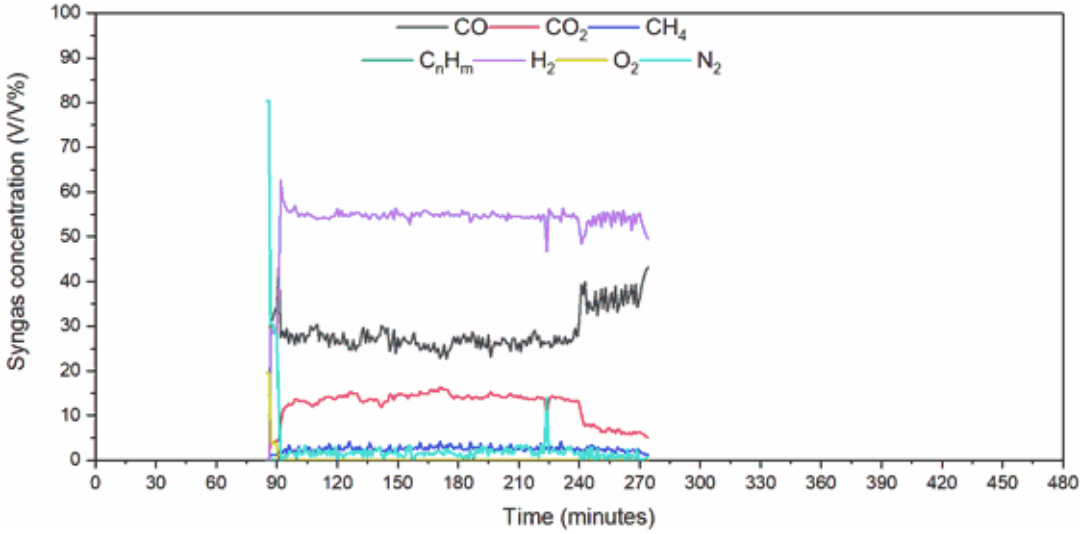

Appendix 6- Average syngas concentration from the experiments of C1 and C2 samples

	S/C ratio		Syngas composition (V/V%)							LHV_{syngas}
	mol/mol		**CO**	**CO_2**	**CH_4**	**C_nH_m**	**H_2**	**O_2**	**N_2**	MJ/Nm^3
C1	**1.00**	Mean	25.43	15.54	3.87	0.01	53.66	0.00	1.48	10.38
		Max	32.90	18.07	7.44	0.09	56.24	0.00	15.05	11.17
		Min	22.00	11.08	2.08	0.00	42.33	0.00	0.00	9.67
		SD	1.51	1.03	1.09	0.02	1.23	0.00	0.89	0.23
	1.25	Mean	24.74	16.90	3.59	0.01	54.00	0.00	0.76	10.23
		Max	30.79	20.20	8.16	0.16	56.58	0.01	2.95	11.11
		Min	20.34	12.92	1.88	0.00	49.98	0.00	0.00	9.80
		SD	1.44	1.11	1.06	0.02	1.17	0.00	0.68	0.21
			CO	**CO_2**	**CH_4**	**C_nH_m**	**H_2**	**O_2**	**N_2**	
C2	**1.00**	Mean	28.90	12.79	2.83	0.01	53.89	0.00	1.59	10.47
		Max	34.80	15.77	4.97	0.16	55.80	0.00	3.95	10.98
		Min	23.13	9.93	1.70	0.00	51.83	0.00	0.00	9.96
		SD	2.40	1.40	0.63	0.03	0.57	0.00	0.87	0.19
	1.25	Mean	27.15	14.14	2.82	0.00	54.38	0.00	1.50	10.29
		Max	32.08	16.67	4.85	0.14	56.38	0.01	14.05	10.77
		Min	22.68	10.05	1.90	0.00	43.07	0.00	0.00	9.05
		SD	1.67	0.98	0.58	0.01	0.85	0.00	1.01	0.17